Integral field spectroscopy of the GQ Lup companion

Dissertation

zur Erlangung des akademischen Grades
doctor rerum naturalium (Dr. rer. nat.)

vorgelegt dem Rat der Physikalisch-Astronomischen Fakultät
der Friedrich-Schiller-Universität Jena

von Dipl.-Phys. Andreas Seifahrt
geboren am 12.02.1978 in Gotha

Gutachter

1. Prof. Dr. Ralph Neuhäuser
   Friedrich Schiller Universität Jena

2. Prof. Dr. Artie Hatzes
   Thüringer Landessternwarte Tautenburg

3. Prof. Dr. Rolf Chini
   Ruhr-Universität Bochum

Tag der letzten Rigorosumsprüfung: 30.01.2008

Tag der öffentlichen Verteidigung: 07.02.2008

Meinen Eltern

Zusammenfassung

Nur wenige sehr junge und extrem massearme substellare Objekte sind zur Zeit bekannt. Ihr Entstehungsmechanismus ist nur unzureichend verstanden und umstritten. Gängige Entwicklungsmodelle vereinfachen die Anfangsbedingungen für diese Objekte zu stark und ihre Vorhersagen im Altersbereich unter einigen Millionen Jahren sind recht spekulativ.

Die Spektren dieser jungen und massearmen Objekte sind nur schwer zu modellieren. Niedrige Temperaturen und Obenflächenschwerkräfte führen zu komplexen chemischen Reaktionen und zu Staubbildung in ihren Atmosphären, Prozesse deren adäquate theoretische Beschreibung durch synthetische Spektren eine große Herausforderung darstellt.

Hinzu kommt, dass nur extrem wenige Ankerpunkte im Bereich niedriger Massen und niedrigen Alters bekannt sind. Solche Ankerpunkte, Objekte deren Massen und Radien durch direkte Messungen bestimmt werden, sind jedoch dringend notwendig um die theoretischen Modelle zu eichen und ihre Gültigkeit zu überprüfen.

Wenn extrem massearme substellare Objekte als Begleiter von jungen T-Tauri Sternen entdeckt und bestätigt werden, gewinnt man zusätzliche Informationen über das substellare Objekt (wie beispielsweise Entfernung und Alter) durch die physikalische Bindung beider Objekte. Allerdings sind die Begleiter junger Sterne, welche oft Mitglieder von Sternentstehungsregionen sind, meist mehr als ca. 100 pc entfernt und damit recht leuchtschwach. Hinzu kommt die scheinbare Nähe zum hellen Mutterstern, die eine Beobachtung erschwert. In den meisten Fällen sind deshalb nur Spektren niedriger Auflösung und mäßiger Qualität von solchen Objekten verfügbar, selbst wenn diese mit den welt-größten Teleskopen der 8- und 10-m Klasse gewonnen wurden.

Mit dem Aufkommen neuer Infrarotspektrographen für mittlere und hohe spektrale Auflösung hat sich diese Situation deutlich verbessert. In dieser Arbeit beschreibe ich die Beobachtung, Datenauswertung und Analyse von neuen Spektren des massearmen Begleiters zu GQ Lupus, einem jungen T-Tauri Stern. Diese Spektren sind in Chile mit dem neuen integral-field Spektrographen SINFONI am Very Large Telescope (Cerro Paranal) aufgenommen worden. Zum ersten mal steht damit ein komplettes JHK Spektrum eines jungen massearmen Objekts mit einer Auflösung von R=2500–4000 und hohem Signal-zu-Rausch Verhältnis zur Verfügung. Dieses Spektrum wurde im Rahmen der vorliegenden Arbeit analysiert.

Im Vergleich zu Spektren von Standardobjekten der, zur Zeit noch eindimensionalen, Spektralklassen M und L sowie zu synthetischen Spektren zweier Gruppen (Lyon und Tokio) habe ich in dieser Arbeit die Effektivtemperatur (T_{eff}= 2650±100 K) und Oberflächenschwerkraft ($\log(g)$=3.7±0.5) des Begleiters zu GQ Lupus neu bestimmt. In Verbindung mit einer leicht veränderten Leuchtkraft ($\log(L/L_\odot)$= −2.21±0.15) ergibt sich so ein Radius von $R = 3.63\,^{+0.75}_{-0.53}$ R$_{\mathrm{Jup}}$ und damit eine Masse von $M \simeq 27$ M$_{\mathrm{Jup}}$ für den GQ Lup Begleiter. Diese neuen Werte weichen substantiell von den bisherigen Schätzwerten ab, insbesondere hinsichtlich der Effektivtemperatur. Ich habe deshalb frühere Spektren des Objekts neu analysiert und zeige, dass diese mit den neuen SINFONI Spektren konsistent sind.

Effektivtemperatur und Leuchtkraft liefern nun intrinsisch konsistente Massen im Vergleich zu Entwicklungsmodellen. Diese Massenvorhersagen sind ebenfalls voll konsistent mit der aus Radius und Oberflächenschwerkraft berechneten Masse von ca. 27 M$_{\mathrm{Jup}}$.

Am Ende der Arbeit wird der GQ Lup Begleiter mit anderen jungen und massearmen Objekten verglichen. Hierzu zählen sowohl einzelne Mitglieder von Sternentstehungsregionen als auch Begleiter junger Sterne und Brauner Zwerge. Ich stelle fest, dass der Begleiter von GQ Lupus scheinbar zu der bis jetzt kleinen aber wachsenden Klasse junger, extrem massearmer substellarer Objekte gehört, deren Massenschätzung (unabhängig von deren endgültiger Genauigkeit) unser Verständnis des Entstehungsprozesses solcher Objekte in Frage stellt und ein neues Klassifikationsschema für Braune Zwerge und extrasolare Planeten nötig machen wird.

Abstract

Only few ultra low mass substellar objects are currently observed in their earliest stages of formation. Their exact formation process is only poorly understood and a matter of debate. Evolutionary models oversimplify the initial conditions and are highly speculative for objects up to a few Myr of age.

The spectral properties of such objects are hard to model. At extremely low temperatures and low surface gravities complex molecular chemistry and dust formation challenges theoreticians to compute synthetic spectra of high reliability. The extreme scarcity of anchor points – objects whose mass and radius can be measured directly – enhances the difficulties in properly describing and classifying such objects.

When ultra low mass substellar objects are common proper motion companions to young (T-Tauri) stars, we gain information (distance, age) from the primary. Very close companions to young stars, which have typically distances larger than 100 pc, are however hard to observe due to their intrinsic faintness and adjacence to the much brighter primary. Thus, ususally only low resolution spectra of poor quality were obtained of these objects, even at the world leading 8 and 10 m class telescopes.

With the onset of new infrared spectrographs, both, for medium (SINFONI) and high resolution (CRIRES), the situation in regard to the availability of higher quality spectroscopic data has significantly improved. In this thesis I present new data and a much enhanced spectral analysis for the ultra low mass companion to the young T-Tauri star GQ Lup, based on near-infrared spectra obtained with the new integral-field spectrograph SINFONI at the Very Large Telescope, Paranal, Chile. For the first time a complete JHK near infrared spectrum of the GQ Lup companion at a spectral resolution of R=2500–4000 was be taken and is analysed here.

Spectral templates of a yet one-dimensional spectral classification scheme as well as synthetic spectra provided by two groups (Lyon and Tokyo) were used to compute a reliable estimate for the effective temperature (T_{eff}= 2650±100 K) and surface gravity ($\log(g)$=3.7±0.5) of the GQ Lup companion. A radius of $R = 3.63\,^{+0.75}_{-0.53}$ $\mathrm{R_{Jup}}$ and a mass of $M \simeq 27$ $\mathrm{M_{Jup}}$ was derived for the GQ Lup companion, using a revised value for the luminosity ($\log(L/L_{\odot})$= −2.21±0.15), adopting a distance of $d = 150 \pm 20$ pc.

The new parameters for the GQ Lup companion are substantially different from previous estimates based on a lower resolution spectrum. A detailed re-analysis of these earlier data revealed, however, consistent results with the data presented here.

The new suite of parameters for the GQ Lup companion yield mass predictions from *hot start* evolutionary models that are fully consistent with the mass $M \simeq 27$ $\mathrm{M_{Jup}}$, derived directly from radius and surface gravity.

The GQ Lup companion is further put into context of other very young and ultra low mass objects, either being free floating members of star forming regions or companions to young brown dwarfs and T-Tauri stars. I find that the GQ Lup companion belongs to a small but slowly growing class of objects whose mass estimate (regardless of its challengeable accuracy) is low enough to question our understanding of brown dwarf formation and our current classification scheme for brown dwarfs and extrasolar planets.

"... Sir, do *you* read a book *through*?'

Samuel Johnson

Contents

Introduction

1

1.1   Motivation

Neuhäuser et al. (2005) announced the discovery of faint, low mass object $0.''7$ west of the young (≤ 2 Myr) nearby ($d = 140 \pm 50$ pc) classical T-Tauri star GQ Lup. The object appears about 6 magnitudes fainter in the near infrared (NIR) K-band than GQ Lup. Based on multi-epoch imaging, using archival data of the space-based WFPC/HST[1] and of the ground-based adaptive optics (AO) imagers CIAO/SUBARU[2] and NACO/VLT[3] the authors demonstrate the common proper motion of this faint object with the bright star GQ Lup at a significance level of more than 7σ against a background hypothesis.

A low resolution K-band spectrum ($R \sim 700$) was used for the determination of the spectral type (M9 to L4), effective temperature ($T_{\text{eff}} = 2050 \pm 450$ K) and surface gravity ($\log(g)$=2–3) of the GQ Lup companion. With these information on hand the authors employ different evolutionary models to constrain the mass of the companion. The result from the widely used models of Baraffe et al. (2002) and Burrows et al. (1997) give a spread of 3–42 M_{Jup}, depending which physical parameters (luminosity or effective temperature) are used to determine the mass. The models of Wuchterl & Tscharnuter (2003) give a mass of 1–2 M_{Jup} deduced from luminosity and effective temperature. Given the wide spread and the apparent inconsistencies of the deduced masses from the very same model but by using different parameters, the authors refrain from further commenting on the precise taxonomy of the object.

---

[1] *Wide Field Planetary Camera* onboard the *Hubble Space Telescope*

[2] *Coronagraphic Imager with Adaptive Optics* at the Japanese SUBARU telescope atop Mauna Kea, Hawai'i

[3] NACO, itself an abbreviation for NAOS-CONICA, stands for *Nasmyth Adaptive Optics System* - attached to the NIR camera and spectrograph *COudé Near Infrared CAmera* and is mounted to the *Very Large Telescope* atop Cerro Paranal in Chile.

At this point the reader was faced with an important finding but also left with a number of questions, like:

1. *Which uncertainties and assumptions limit the usefulness of the evolutionary models, thus, limiting the validity of the determined mass?*

The principle difficulty in the mass determination for low mass substellar objects is that, unlike stars, substellar objects are not massive enough to sustain stable hydrogen fusion as their main source of energy. Below a certain mass limit of about 75 M_{Jup} (depending on the metallicity of the object, see e.g. Baraffe et al., 2003) the object continuously collapses during its formation process until electron degeneracy supports the internal structure and the collapse is dramatically slowed down (see e.g. Burrows et al., 2001, Fig. 3). Such objects radiate away the gravitational energy they gain from the collaps without a substantial source of energy replenishment[4]. Hence, such objects continuously cool out. They never reach a stable configuration on the main sequence but rather move along a track in the Hertzsprung-Russell-Diagram (HRD) just above an artificially prolonged main sequence at its lower end. See e.g. Kirkpatrick (2005) for a more comprehensive overview about substellar objects and their respective classification into spectral types L and T.

Eventually one has to employ theoretical models to derive the mass of such objects from other observables. The theoretical models are basically cooling curves that take the internal structure and atmospheric radiation profiles into account. Such models are generally degenerate in their parameter space, since without a pinned down age the mass of a substellar object is not unambiguously defined by its observational parameters alone (such as luminosity, effective temperature, surface gravity, etc.).

The calibration of the models with objects of known mass and age is a difficult and an ongoing process. Only substellar objects in short term binary and multiple systems (e.g. GJ569Bab, see Zapatero Osorio et al., 2004) or eclipsing binary systems (e.g. 2M0535, see Stassun et al., 2006) can provide anchor points to which the models can be attached. Only the latter also add important information on the radius of the objects. Other than for nearby M dwarfs, interferometric radius measurements of brown dwarfs are currently out of reach.

This situation is even worse for the very early phases of formation of substellar objects, since all standard evolutionary models (Baraffe et al., 1998; Chabrier et al., 2000; Burrows et al., 1997; D'Antona & Mazzitelli, 1994, 1997) do not calculate the initial collapse phase but start from ad-hoc initial conditions. The models assume fully convective and adiabatic objects of spherical symmetry that have previously contracted on a Hayashi track starting from an arbitrarily large radius – the so called *hot start* scenario. There has been a long standing dispute about the importance of this oversimplified description. Baraffe et al. (2002) address this issue regarding their COND and DUSTY models (Baraffe

---

[4]Objects above $\sim$13 M_{Jup} fuse Deuterium for a short period during their early development, however, without ever reaching a fully stable configuration

et al., 1998; Chabrier et al., 2000, hereafter BCAH98 and CBAH00) and conclude that assigning masses to objects younger than ≤ 1 Myr from observable quantities "[...] must be considered with highly limited – if any – validity."

Baraffe et al. (2002) show that depending on the initial surface gravity, the efficiency of convection and the resulting opacity are strongly affected by the actual mixing length parameter α_m. For a range of effective temperatures of T_{eff}=2200–3500 K the mixing length plays in important role for objects with surface gravities of $\log{(g)} \leq 3.5$, at ages up to 1 Myr. Beyond that age (thus for higher surface gravity) the convection and opacity become more insensitive for the mixing length and evolutionary models converge again into the known tracks and seem to 'forget' their initial setup.

Burrows et al. (1997) state, that their evolutionary models are well constrained for ages ≥ 100 Myr, without further statements on limits and uncertainties at younger ages.

Also the models by D'Antona & Mazzitelli (1994, 1997) (not used in Neuhäuser et al., 2005) do not consider the initial phase of formation. Their models have different boundary conditions than assumed in BCAH98 or CBAH00, although their calculations start at much earlier ages than the ones of the BCAH98 or CBAH00. The concept of age is however also on dispute, since different descriptions exist when to attribute $t = 0$ to an object (see also the discussion in D'Antona & Mazzitelli, 1997, Sect. 4).

A different situation is found for the models of Wuchterl & Tscharnuter (2003). Evolutionary models for planets (formed in a circumstellar disk in either a core-accretion scenario or a disk instability scenario, following the nucleated instability hypothesis) and brown dwarfs (formed star-like by core-collapse of a marginally unstable Bonnor-Ebert sphere) are calculated *including* the very early phases of formation. As stated already in Wuchterl (2000) the inclusion of the formation process leads to an initial rise in the luminosity of all object formed by core-collapse models of about two order of magnitude at ages of 10^3 to 10^4 years and also results in an age shift between both scenarios. As a result, luminosities predicted from models of Wuchterl & Tscharnuter (2003) are much higher than the ones derived from the *hot start* models, and conversely, the masses derived from the models of Wuchterl & Tscharnuter (2003) are much lower than the ones from Baraffe et al. (1998); Chabrier et al. (2000) or Burrows et al. (1997). One should note, that the mass prediction of 1–2 M_{Jup} for the GQ Lup companion are based on the planetary models (covering 0.5 to 5 M_{Jup}) but not on the core-collapse models (covering only masses ≥ 13 M_{Jup}), as being shown in Neuhäuser et al. (2005, Fig. 4).

A first approach to test the new models is shown in Wuchterl (2005) for objects in Upper Scorpius (USco) and to GG Tau. Following the figures in Wuchterl (2005), most of the presented members in USco are either very low mass brown dwarfs or have even masses below 13 M_{Jup}. This is in contradiction with the mass determination for the very same objects in Mohanty et al. (2004b), using the effective temperature, surface gravity and luminosity, to calculate masses from first principles. Mohanty et al. (2004b) derive stellar masses for most of these objects and only few being in the brown dwarf regime or slightly below (see Mohanty et al., 2004b, Fig. 3) – revealing an apparent missmatch of the model predictions with the observations. Moreover, as Reiners (2005) has shown,

uncertainties in the band strength of the TiO ϵ-band, used for the determination of the effective temperature, and conversely (via luminosity and radius) also for their mass, lead to a shifts of all examined objects to even higher masses, being now predominantly in the stellar regime, the lowest mass members, formerly being well below 13 $M_{\rm Jup}$, now having masses of $\geq$ 30 $M_{\rm Jup}$. This demonstrates the need for more reliable anchor points to calibrate the models and possibly a revsision of the mass scale in Wuchterl & Tscharnuter (2003).

One additional anchor point, the young M4 spectroscopic binary UScoCTIO5 (Reiners et al., 2005) has a lower mass limit of $m \sin i = 0.32 \pm 0.02$ $M_{\odot}$ for the primary components and its mass is only slightly underestimated by the BCAH98 and BCAH00 models. The mass predictions from the Wuchterl & Tscharnuter (2003) models are however too low by a factor of about 5, judging from a plot in Gädke (2005).

At even lower masses and younger age there is only one anchor point, the young brown dwarf eclipsing binary 2M0535-05 (Stassun et al., 2006, see also Sect. 5.3 in this thesis for further discussion). The secondary has a mass of about $\sim$38 $M_{\rm Jup}$. Comparing the luminosity and effective temperature derived by Stassun et al. (2007) with the predictions of the Wuchterl & Tscharnuter (2003) models (using Neuhäuser et al., 2005, Fig. 4), one finds an almost perfect match with a brown dwarf track of 13 $M_{\rm Jup}$, an underestimation in mass by a factor of 3. This has also been noted by McElwain et al. (2007).

One should also note, that the mass prediction of 1 to 2 $M_{\rm Jup}$ for the GQ Lup companion are based on the planetary models (covering 0.5 to 5 $M_{\rm Jup}$) but not based on the core-collapse models (covering only masses $\geq$13 $M_{\rm Jup}$), as being shown in Neuhäuser et al. (2005, Fig. 4).

To summarise, this demonstrates that the available models are mostly uncalibrated in the regime of young, low-mass objects. Their validity is uncertain and a function of age and observational parameters for the GQ Lup companion, especially in the case of the *hot star* models. Thus, the need for a model-independent determination of the mass of the GQ Lup companion is evident.

2. *Why is there an apparent inconsistency in the determination of the mass from different parameters for the same model?*

The most striking problem with the evolutionary models by Burrows et al. (1997) and Baraffe et al. (2002) is the apparent inconsistency in the models when determining the mass of the GQ Lup companion from different observational parameters (luminosity and effective temperature) and age. For both models a mass determined from effective temperature and age is much lower than when being determined from luminosity and age. Hence, either the evolutionary models are in itself inconsistent, or one of the observables (luminosity or effective temperature) of the GQ Lup companion in Neuhäuser et al. (2005) is erroneous. The luminosity is calculated from photometry, distance and a bolometric correction. Non of these parameters, although partly quite uncertain, seem prone to be substantially off. Still, the discrepancy is significant beyond the already large error bars. Thus, one might suspect a problem with the effective temperature.. Its value is based on a low resolution, low signal-to-noise, long-slit K-band spectrum ($R \sim 700$) of the GQ Lup companion acquired with NACO. This spectrum was analysed in terms of spectral indices provided by various authors and by comparison with synthetic PHOENIX spectra in a GAIA-dusty configuration.

Guenther et al. (2005) present an extended analysis of this NACO spectrum and argue that the best fit is achieved with a synthetic spectrum of an effective temperature of 2000 K. As can be seen in Guenther et al. (2005, Fig. 5), spectra of this effective temperature and a surface gravity of $\log(g)$=2–4 fit the overall shape of the spectrum quite well, but the depth of CO bandheads at 2.3 μm is overestimated, for all surface gravities. The authors assign this mismatch to either veiling or a problem with the synthetic spectra. It is pointed out, that the depth of the CO bandheads is similar to the ones in the companion to AB Pic, a young ($\sim$30 Myr) low-mass object of spectral type L0 to L3. Both, spectral type and depth of the CO bandhead seem to match well. However, judging from Guenther et al. (2005, Fig. 2 and 3), the shape of the blue part of the respective K-band spectra of the GQ Lup companion and the AB Pic companion is not matching at all. In the spectrum of the AB Pic companion the continuum level at 2.0 μm barely drops below the depth of the first CO bandhead. In the spectrum of the GQ Lup companion the continuum level already drops below this level at 2.15 μm and is continously decreasing towards shorter wavelength. Moreover, the spectrum of the AB Pic companion peaks at 2.18 μm while the spectrum of the GQ Lup companion peaks 2.26 μm, revealing a different continuum shape. Hence, it is still possible that the determined effective temperature is off by several hundred Kelvin and may account for the inconsistency between luminosity and effective temperature when compared to the evolutionary models of Burrows et al. (1997) and Baraffe et al. (2002). It is also noteworthy that the best estimates given for the effective temperature (T_{eff}= 2050 $\pm$ 450 K) and for the radius of $R \simeq 2$ R_{Jup} Neuhäuser et al. (2005) are inconsistent with their derived luminosity of $\log(L/L_{\odot})$= -2.37 ± 0.41..

Hence, it seems desirable to acquire a new spectrum of much broader coverage, higher signal-to-noise and higher resolution for a more reliable determination of the effective temperature and surface gravity.

1.2   Objectives of this study

To improve our understanding of the GQ Lup companion it is necessary to collect more data, both in quantity and quality to address to questions raised before. This accounts foremost for a much improved spectral analysis, based on better data. Given the general uncertainties in the evolutionary models and the extreme scarcity of calibration points in the ultra low-mass and young age regime, it seems also worthwhile to obtain a mass estimate from observables alone, based on a more accurate and precise determination of the surface gravity.

Thus, I formulate the goals of this study as the following:

1. Obtaining a $1.2 - 2.5$ μm (JHK) spectrum of the GQ Lup companion with higher resolution and higher signal-to-noise than the previous NACO spectrum.

2. Detailed analysis of this spectrum in terms of possible contamination from the only $0\rlap{.}''7$ separated bright star GQ Lup A.

3. Comparison of this spectrum with an extended grid synthetic spectra, ideally from independent origin.

4. Comparison of this spectrum with empirical spectra of old and young low-mass objects.

5. Determination of the effective temperature and surface gravity of the GQ Lup companion.

6. Determination of the mass of the GQ Lup companion from these quantities alone.

7. Consistency check with the current evolutionary models.

1.3   Near infrared spectroscopy - state of the art

The choices in how to obtain a high quality spectrum of a faint ($K \simeq 13.1$ mag) object next ($d \simeq 0\overset{''}{.}7$) to a bright star ($\Delta K \simeq 6$ mag) are rather limited. The close separation and the high contrast ratio require a large telescope and an adaptive optics (AO) system to achieve the necessary spatial resolution and sensitivity. Eventhough the separation of the GQ Lup companion and its primary is rather forgiving, being more than one order of magnitude larger than the diffraction limit of an 8 m-class telescope in the NIR, a high strehl ratio is desired to suppress the flux contamination from the extended wings of the point spread function (PSF) of GQ Lup A at the position of the GQ Lup companion. Since AO systems deliver reasonable strehl ratios only in the near infrarad (NIR), one is limited in the choice of wavelength. Moreover, the peak of the spectral energy distribution (SED) of a rather cool object like the GQ Lup companion, is anyway in the NIR and sharply drops towards the optical, making NIR observations more efficient.

The default option would have been to use NACO again and obtain long-slit spectra of the GQ Lup companion in J,H and K-band with a maximal resolution of $R \sim 1400$. The classical design of long-slit spectrographs has a long-standing tradition in astronomical instrumentation. It suffers, however, from several shortcomings that can not easily be corrected by standard calibration techniques:

1. Achromatic slit losses due to a possible mismatch of the slit width and the (ususally seeing limited) FWHM of the PSF (if FWHM $\gg$ slit width).

2. Achromatic changes in the resolution due to a possible mismatch of the slit width and the (ususally seeing limited) FWHM of the PSF (if FWHM $\ll$ slit width).

3. Achromatic slit losses from pointing (centering) errors and/or a mismatch of nodding direction and slit angle.

4. Chromatic slit losses from differential chromatic refraction (DCR) in case the slit angle is not the parallactic angle.

In case of an AO-fed long-slit spectrograph – like NACO – the DCR effect is not any longer a dominating source of error, since the DCR is much smaller in the NIR than in the optical (see e.g. Roe, 2002). On the other hand, the achromatic slit losses and the effective resolution changes originating from the mismatch of slit width and FWHM of the PSF get chromatic, since the slit width is usually chosen to match the FWHM of the diffraction limited core of the PSF, and this quantity gets a linear function of wavelength (FWHM$\sim \lambda$) instead of a slow function in the seeing limited case (FWHM$\sim \lambda^{-1/5}$). This effect has been studied in detail by Goto et al. (2003, 2005).

It should be emphasised here that this effect could in principle be corrected using a telluric- or flux standard star. However, this imposes two difficulties. First, the stars used for wavefront sensing are different and in addition to natural seeing variations, the strehl ratio is usually not the same for the standard star and the target. Second, while

a long-slit spectrograph collects all flux in the slit, thus also the flux in the wings of the PSF, the differential effect may eventually be recovered. However, in the situation of very dim targets, the flux in the extended wings will likely fall below the sky background noise or the read noise of the detector. Hence, while for the bright standard star all flux inside the slit is recorded, for the target only the flux inside the diffraction limited core is preserved and differential effects in the strehl ratio can not be recovered. Such effects can account for a tilted continuum of up to 20% at both ends of the H-band as compared with the center flux in the same band (Goto et al., 2003). Also off-slit-pointing effects become more achromatic and can add another 10% flux variations on both ends of the H-band.

All these effects scale with the relative ratio of covered wavelength ($\Delta\lambda$) and central wavelength (λ_c) of each spectrum. Hence, the J and H-band are more prone to these effects than the K-band. As has been expressed in Neuhäuser et al. (2005) and Guenther et al. (2005), the first NACO spectrum of the GQ Lup companion has not suffered dramatically under these effects since a relatively wide slit (172 mas) in comparison to the diffraction limited FWHM in the K-band ($\sim$56 mas) has been used. As I will show in Section 3.2 other effects have nonetheless dramatically affected the throughput in the spectra of the GQ Lup companion, leading to a erroneous interpretation of the spectra.

It seems thus desireable to look for alternatives. A much better choice, since basically free of all the above mentioned effects, are integral field spectrographs (IFS). Due to the access limitations for for European astronomers, SINFONI at the Very Large Telescope (VLT) is the only instrument of choice. SINFONI[5] is a combination of two instruments: A MACAO[6] type curvature adaptive optics (AO) module with visual wavefront sensor and 60 actuators (see Bonnet et al., 2003, for further details on the AO module). Second, a mid-resolution near-infrared spectrograph with an integral field unit: SPIFFI[7] (see Eisenhauer et al., 2003; Bonnet et al., 2004, for further details).

Among the various instrumental concepts, SINFONI realises a design where an image slicer cuts the field-of-view (FOV) into 32 slitlets, each sampled by 64 spatial pixels and re-arranges these slitlets in a single long slit. The light is dispersed by a grating and the spectrum is imaged on a large format detector (2k×2k HAWAII 2RG). During data reduction the information on the chip is reformatted into a datacube, containing images of the source, reconstructed from the spectrum itself, for each wavelength bin. A simplified sketch of the concept is shown if Figure 1.1.

Thus, for each point of a given spatial resolution in the FOV a spectrum is recorded in the third dimension, a so called *spaxel*. The advantage of this design is that no slitlosses can occur and all effects of varying source position, regardless of being due to atmospheric or instrumental effects, are no issue due to the continuous spatial coverage. The effective

[5]SINFONI: Spectrograph for INfrared Field Observations
[6]MACAO: Multi-Application Curvature Adaptive Optics
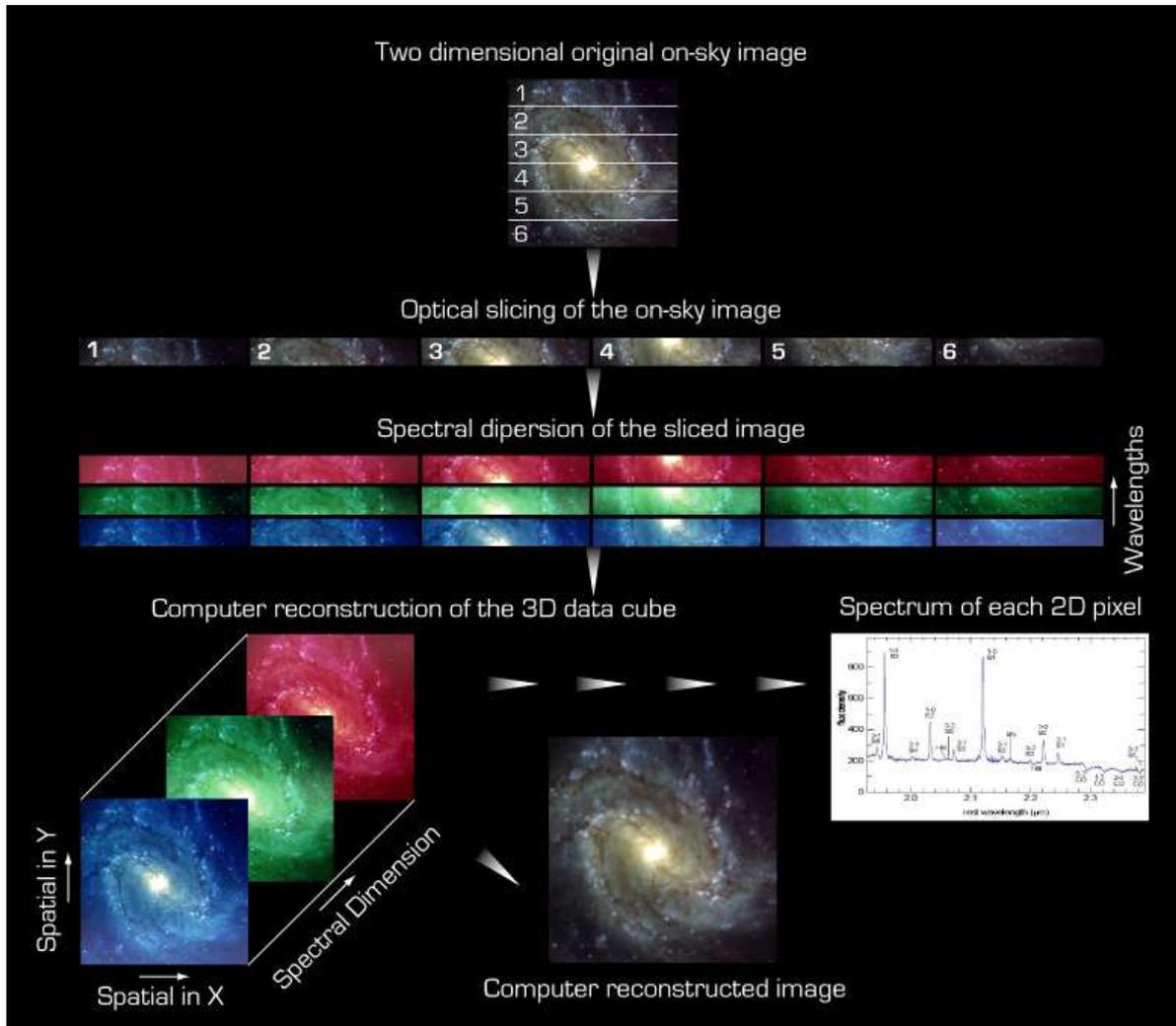[7]SPIFFI: SPectrograph for Infrared Faint Field Imaging

Figure 1.1: Simplified sketch demonstrating the working concept of a integral field spectrograph (ESO press release photo 24i/04).

spectral resolution[8] of SINFONI varies from $R \sim 2000$ in J-band to $R \sim 4000$ in K-band.

For spectroscopic studies of faint companions to bright stars integral field spectrographs offer the advantage of delivering a wealth of spectral and spatial information around the target which eases the subtraction of background light from nearby sources. Whereas long-slit spectrographs give only a 1D spatial information (a cut) and background subtraction relies on the symmetry of the PSF of the contaminating source (like the PSF of GQ Lup A for the spectrum of the GQ Lup companion), integral field spectrographs provide full 2D spatial information and the PSF of contaminating sources can be modeled and subtracted much more adequately.

Elaborate techniques to subtract the PSF of the primary in a datacube are presented in Sparks & Ford (2002), making use of the unique combination of 2D spatial and 1D spectral information. An extension of this work for the special application to SINFONI

---

[8]calculated for Nyquist sampling

is presented in Thatte et al. (2007). The authors demonstrate at the example of the low-mass companion AB Dor C, being only $0\rlap{.}''2$ separated from the bright star AB Dor A, that a contrast ratio of up to 9 mag is achievable at such separations with SINFONI, a domain usually assigned to coronographs.

In the case of the GQ Lup companion, where the contrast ratio is $\Delta K \sim 6$ mag at a distance of $0\rlap{.}''7$, a simple 2D modeling of the background from GQ Lup A can be expected to outperform a long-slit NACO spectrum in terms of spectral pureness, spectral resolution and signal-to-noise ratio. Hence, SINFONI was the instrument of choice for this study.

CHAPTER

SINFONI near-infrared integral field spectroscopy of the GQ Lup companion

2

2.1 Observations

The first SINFONI spectrum was proposed for as DDT[1] program. The proposal was accepted shortly after SINFONI, equipped with its final 2k×2k science grade detector, became available to the community. Observations have been carried out in K-band in the night of Sept 16, 2005 (Prog.-ID 275.C-5033(A), PI Ralph Neuhäuser). The observation strategy followed the standard scheme of sky nodding for background subtraction in a continuous $ABBA$ pattern, where position A denotes the on-target position and B denotes the sky position. Eight AB nodding cycles with an integration time of 300s per frame were obtained in service mode. The smallest pixel scale (12.5×25.0 mas) of the instrument was chosen, yielding a field of view of $0.8'' \times 0.8''$ to optimally sample the diffraction limited core of the target PSF. The bright primary, GQ Lup A, was used as the AO guide star and was placed outside the FOV. The companion was centred in the field.

The DIMM[2] seeing during the science observations was 0.8–1.1″. The strehl ratio, computed on a short integration of GQ Lup A was ~40% and more than 99% of the energy was encircled in a core of ~200 mas FWHM.

After the first successfull SINFONI observation of the GQ Lup companion in DDT, a regular proposal was written to obtain H and J-band observations in ESO period 77. The proposal was granted and data have been obtained in the nights of April 24 and September 18, 2006, respectively, again in service mode (Prog.-ID 077.C-0264(A), PI Ralph Neuhäuser). Ten (nine) target-sky nodding cycles of 300s exposure time have been taken in the H and J-band, respectively. Five frames in each band had a sufficiently high signal-to-noise and are used in the dataprocessing.

The DIMM seeing for the five useful H-band observations was 1.0–1.4″. The strehl ratio, measured similarly as for the K-band, was ~20% and more than 99% of the energy was encircled in a core of ~250 mas FWHM.

---

[1] Directors Discretionary Time
[2] Seeing value in the optical (λ ~500nm), measured at zenith.

No PSF calibration was possible for the *J*-band, since no observations of GQ Lup A were recorded. In situ strehl computations on the companion are not reliable because of the background contamination from GQ Lup A. I therefore judge from the seeing value during the *J*-band observations (0.8–1.1″), the airmass and the performance of MACAO on a strehl ratio of 5–10%. The core size of the 99% quartile of the encircled energy is estimated to be of the order of 350 mas FWHM.

2.2   Data reduction

The data format of SINFONI is highly complex. As explained on page 9, the FOV of the instrument is sliced into 32 slitlets and remapped onto a pseudo-slit and dispersed by a grating. The original FOV has to be reconstructed from this spectrum. The success of this process depends on the proper identification of the slitlet positions on the detector and involves the correction of nonlinear distortions. Quite a number of calibration frames are associated with each target observation to provide the necessary input for the reconstruction. These calibration files are suited to be processed by a dedicated pipeline. The first step of the data reduction process was thus performed by using the SINFONI data reduction pipeline version 1.3 offered by ESO (Jung et al., 2006; Modigliani et al., 2007). The reduction routines of this pipeline were developed by the SINFONI consortium (Abuter et al., 2006) and adopted to ESOs standard data reduction environment *ESOREX*.

These first steps of the data processing follow a sequence described in Abuter et al. (2006). The raw science frames are sky subtracted and flatfielded, cleaned from bad pixels, corrected for image distortions and wavelength calibrated. From this pre-calibrated image a cube is reconstructed and the spatial position is corrected for atmospheric dispersion. In Figure 2.1 a schematic overview of all involved reduction steps is shown. The output of this procedure is a 3D fits cube containing about 2000 images of the source in wavelength steps according to the chosen setting of the grating.

A sum along the wavelength axis of such a cube is an equivalent of a broad-band image in *J*, *H*, or *K* band, respectively. In Fig. 2.2 such images for the GQ Lup companion are shown for all three bands. The companion is well visible in the centre of each image. Depending on the different strehl ratio in each band, the target is still contaminated by light from the halo of GQ Lup A, whose PSF core is outside the FOV. This contamination is spectral variable since the Airy pattern of the PSF of the primary is wavelength dependent. This effect is strongest in the *K*-band, since here the strehl ratio is the highest, and can readily be seen in the datacubes as a movind wave pattern when browsing through the wavelength.

For a proper extraction of the target spectrum one has to eliminate this contamination as far as possible. I decided to use the *Starfinder* package of IDL (Diolaiti et al., 2000) for an empirical PSF fitting of the companion in each of the ∼2000 images of the three observed bands. For this purpose a template PSF is created from the observation of a
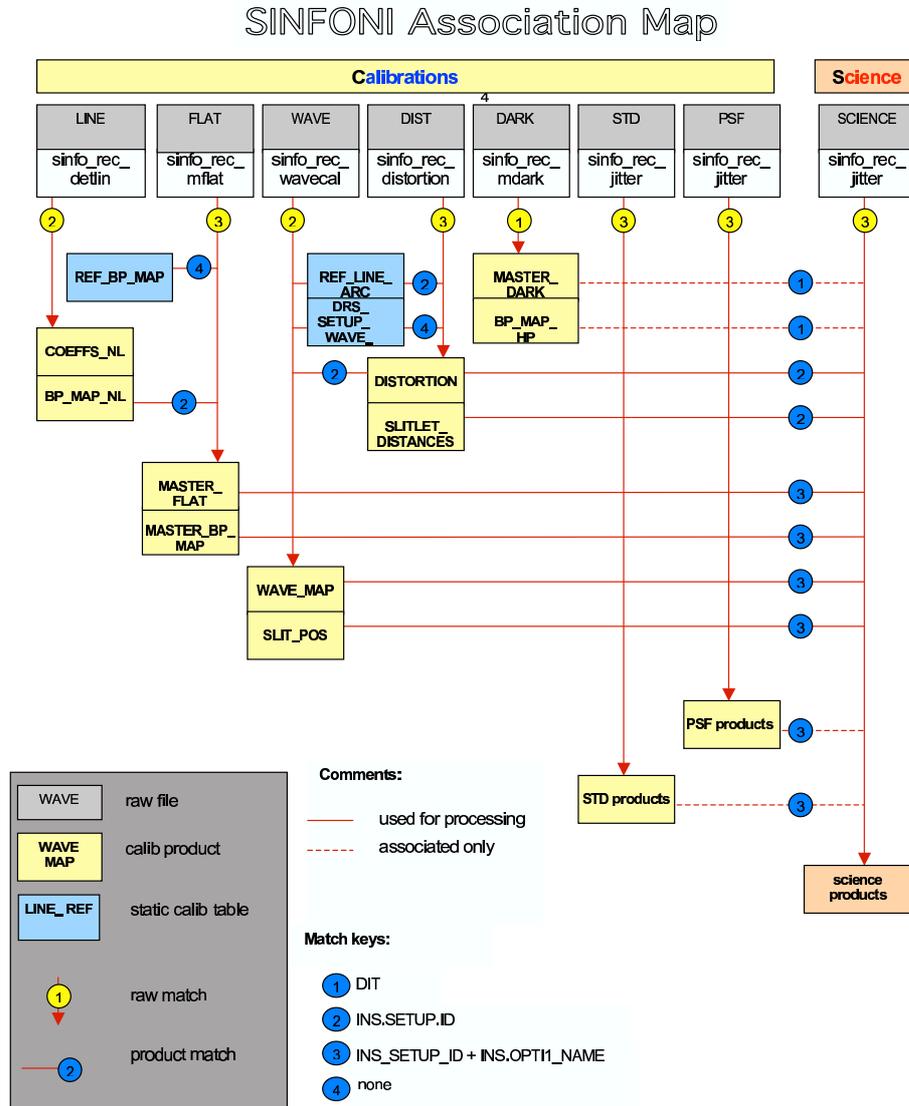
Figure 2.1: Data reduction sequence, showing raw calibration and science frames as input (top row), their associated pipeline recipes as well as the pipeline products and dependencies (Modigliani et al., 2007, Fig. 5)

standard star right before or after the target observation. The PSF of the standard star is thereby spatially supersampled from the $\sim$2000 individual images of the source. The *Starfinder* algorithm determines the flux of the companion in each wavelength bin by fitting the previously created template PSF to the target. I found that one PSF template for each band is sufficient to ensure high correlation values (usually $\gtrsim 0.9$) in the fitting process, despite the fact that the PSF shape is slightly variable over the covered bands. In an iterative process the background (mainly the PSF halo of GQ Lup A) is subtracted as well. The lower column in Fig. 2.2 shows the images of the companion after the subtraction.
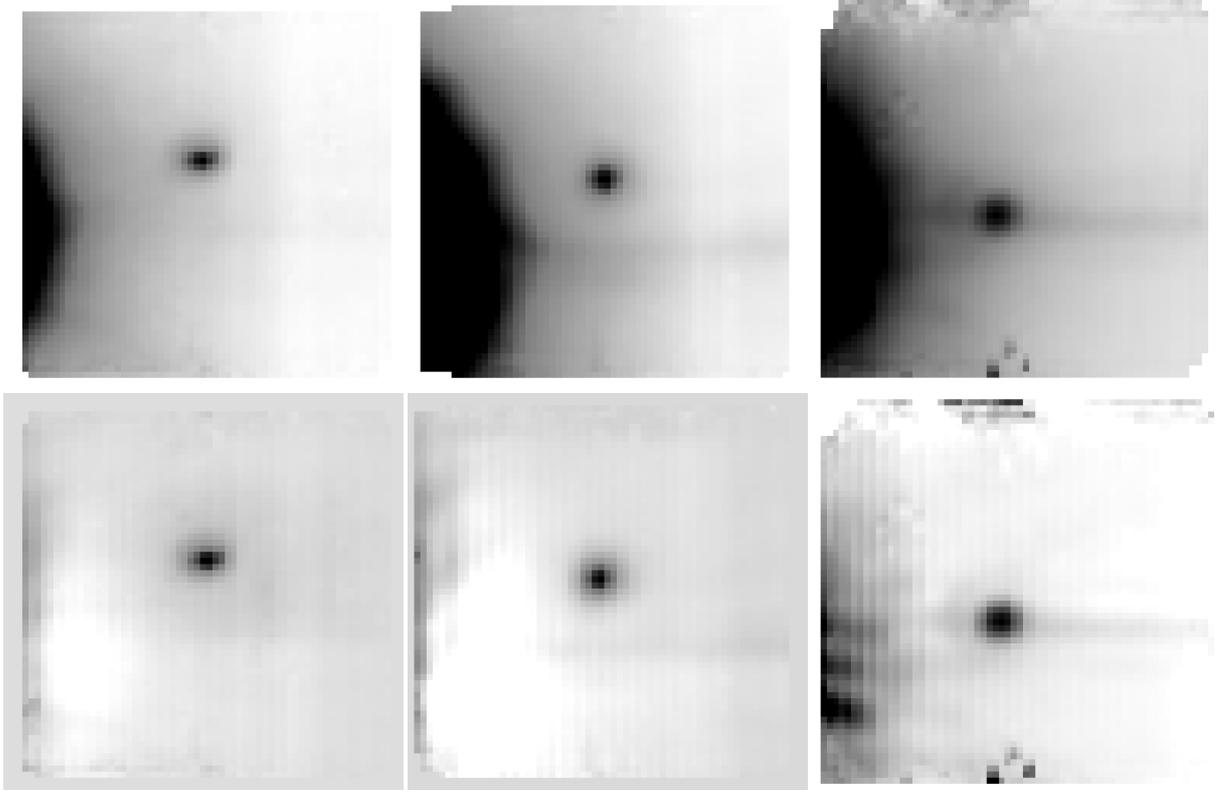
Figure 2.2: *From left to right:* SINFONI *J*, *H* and *K*-band cubes of the GQ Lup compan-
ion, integrated over the wavelength axis of each cube. *Top row*: Before the subtraction of
the halo of GQ Lup A, the background is high and not flat in the vicinity of the GQ Lup
companion.   *Bottom row:* After the subtraction process the background in the vicinity of
the GQ Lup companion is low and flat – background contamination is minimised. North
is up and east is left. The FOV is $0.8'' \times 0.8''$

I also applied an alternative method to verify these results: I masked the position
of the GQ Lup companionand subsequently fitted and subtracted a 2D polynomial in
each spatial plane of the datacubes. The degree of the polynomial is limited and high
frequencies are not fitted in order to avoid ovsershoot in the background close to the
position of the GQ Lup companion. The drawback of this precaution is that speckles in
the halo of GQ Lup A and a spike in the *K*-band can not be filtered by this process.
Also a slight overshoot at the edges of the FOV is noticeable, but uncritical since no
information is retrieved from this part of the datacube. The flux at the position of the
GQ Lup companion is then extracted using aperture photometry. The comparison showed
similar results for both extraction techniques but revealed an enhanced signal-to-noise and
robustness for the empirical PSF fitting by *Starfinder*. Moreover, empirical PSF fitting
is less prone to remaining contamination from super-speckles that are deviant from the
typical shape of the PSF. Thus, the background contamination in the spectrum of the
GQ Lup companionis certainly below the noise floor from readout and photon noise.

Finally, a spectrum of the GQ Lup companion was obtained from each single nodding

cycle in J, H and K-band, respectively. These spectra are corrected for telluric absorption by the division through the spectrum of an early type telluric standard star, extracted similarly as the spectrum of the GQ Lup companion. The following standard stars were chosen at the observatory to match the airmass of the science observations: HIP 087140 (B9V) and HIP 083861 (B2V) in the J-band, HIP 082652 (B3III) in the H-band, and HIP 93193 (B9V) in the K-band. All standard stars are early type hot dwarfs or giants and intrinsically featureless, apart from weak helium and strong hydrogen lines. I have manually fitted these lines by Lorentzian profiles and removed them by division. The corrected standard star spectra were then divided by a blackbody spectrum to correct for the continuum slope of each standard star. The effective temperature of the blackbody was retrieved from the literature (e.g. Moon & Dworetsky, 1985) to $T_{\mathrm{eff}} \simeq 18000$ K for the standard stars of spectral type B2V, $T_{\mathrm{eff}} \simeq 10500$ K for spectral type B9V and $T_{\mathrm{eff}} \simeq 16500$ K for the B3III type star, respectively. Note, that in the far end of the Rayleigh-Jeans regime of the standard stars SED the steepness of the continuum slope is not particularly sensitive to small errors in the effective temperature and the error induced into the continuum shape of the science spectra is estimated to be less than 5%.

When the respective airmass of the standard star observation and of the science observation did not match perfectly, as was the case in the J-band, I interpolated between standard stars taken at different airmass bracketing the airmass of the respective science frame.

After this procedure the resulting spectra of the companion are essentially free of telluric absorption lines and corrected for the throughput of the spectrograph.

The individual spectra from each nodding cycle are combined by a weighted mean. The weights are derived from the correlation factor of the PSF fitting. A high correlation factor indicates a high strehl ratio, since the PSF of a bright standard star is used for PSF fitting. This assumption is confirmed by a notable correlation of the total countrate in the individual spectra and the correlation factor of the PSF fitting. Thus, the technique assigned higher weights to data of higher signal-to-noise ratio, following the basic concept of the optimal extraction algorithm of Horne (1986). The three combined J, H and K-band spectra are displayed in Fig. 3.1, 3.3 and 3.4, respectively.

The Nyquist sampled spectral resolution is $R \sim 2500$ in the J-band and $R \sim 4000$ in H and K-band. The signal-to-noise ratio of the spectra is ~ 50 in the J-band. The signal-to-noise ratio in H and K-band is, however, only ~ 30 and thus much lower as being expected from the exposure time calculator. These S/N was computed from the standard deviation in each spectral bin of the five (J and H-band) and eight (K-band) individual spectra, which have been reduced separately. The rather low S/N values origin from spectral undersampling. In the chosen setup each resolution element is sampled by only 1.5 pixels. Sub-pixel wavelength shifts between the individual nodding cycles induce artificial noise by enhancing telluric remnants. Nonetheless, most of the small-scale features seen in the spectra are not noise but unresolved absorption lines, as I will demonstrate in the next chapter.

Data analysis I – Empirical classification

3.1 Identification of spectral features

The identification of spectral features in the SINFONI spectra of the GQ Lup companion is based on various linelists and identifications given in McLean et al. (2003, 2007); McGovern et al. (2004) and Cushing et al. (2003). Also the NIST[1] Atomic Spectra Database was used (Ralchenko, et al., 2007) to identify atomic features and assign them a correct rest wavelength in vacuum.

J-band

The overall continuum shape of the *J*-band is slowly dropping from the blue to the red part (see Fig. 3.1). A water vapour ('hot steam') band absorption longwards of 1.33 μm causes a strong flux depression. Absorption lines of Potassium (K I doublets at 1.169 & 1.178 μm and at 1.244 & 1.256 μm), as well as Aluminium (Al I doublet at 1.313 & 1.315 μm), Sodium (Na I doublet at 1.139 and 1.41 μm) and Iron (Fe I at 1.189 and 1.198 μm) are clearly detectable. FeH accounts for a number of features in the spectrum. In addition to three rather prominent bandheads, stronger lineblends are marked in Figure 3.1, based on a linelist of Cushing et al. (2003). A rather broad and V-shaped absorption feature centred at 1.20 μm is most likely due to VO (McGovern et al., 2004), while the presence of TiO ϕ-bands, proposed by the same authors and seen in M giants ($\log(g) \simeq 0$) can not be confirmed.

The most prominent feature is the Paschen β emission line at 1.282 μm, that can already be seen in the raw data cubes. This line shows an inverse P-Cygni profile in GQ Lup A. The profiles are shown in detail in Figure 3.2. The easiest explanation would be a higher background from GQ Lup A at this wavelength. However, after background subtraction the situation is even clearer – the emission peak in the spectrum of the GQ Lup companion stands out and is independent of the line in GQ Lup A.

---

[1] National Institute of Standards and Technology
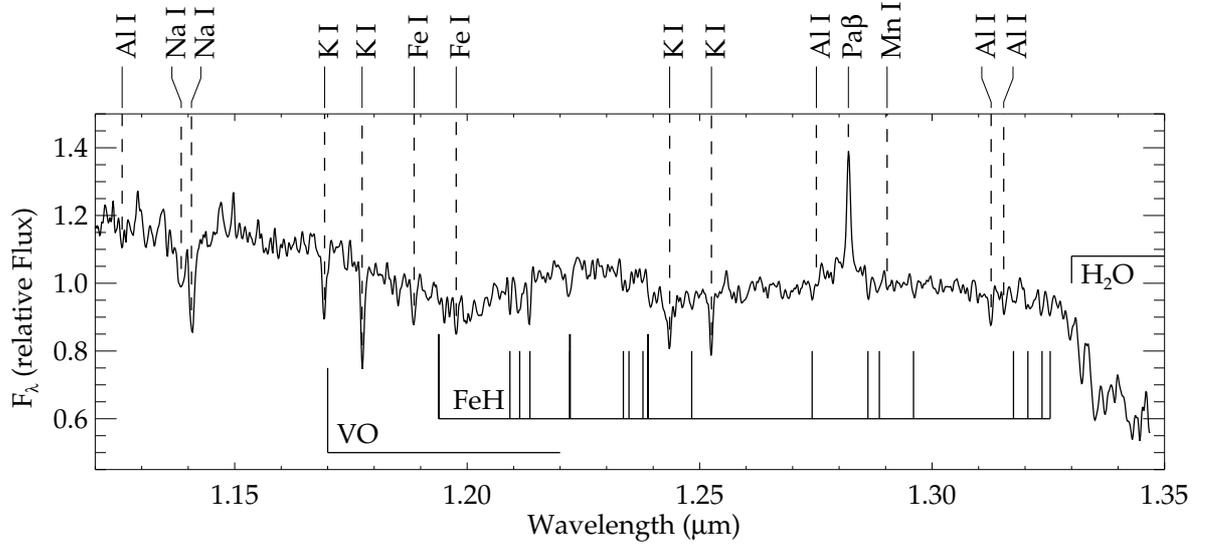
Figure 3.1: SINFONI *J*-band spectra of the GQ Lup companion. The Nyquist sampled spectral resolution is R~2500. Atomic lines and molecular bands are marked. Three FeH bandheads are denoted with longer tickmarks to distinguish them from other FeH lines. Note the strong Pa-β emission line. The signal-to-noise ratio is ~ 50, but degrades shortwards of 1.15 μm and longwards of 1.335 μm.

Moreover, if the emission feature in the GQ Lup companion would be an artifact from the background contamination of GQ Lup A, one would expect the same line profile (an inverse P-Cygni profile) in both objects, which is not the case. Hence, I conclude that the Paβ emission line in the GQ Lup companion is real.

This emission line is most likely due to accretion in both objects, especially since the effective temperature of the GQ Lup companion is not high enough to sustain a chromosphere that could produce such a strong emission feature. See Muzerolle et al. (2003) and Natta et al. (2004) for further discussion.
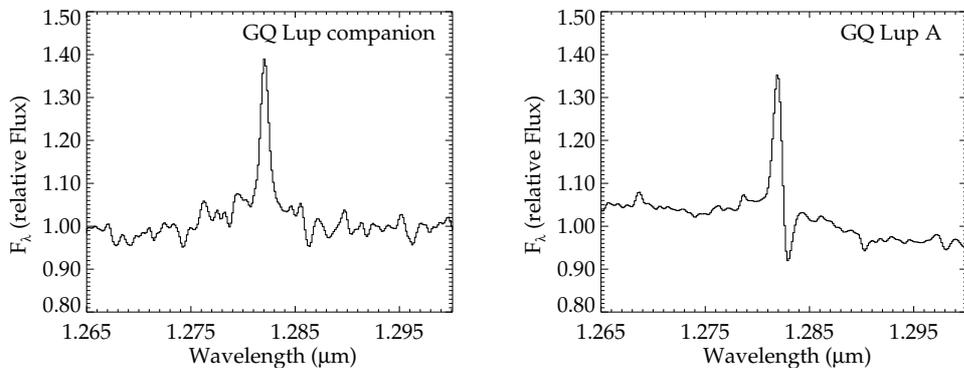
Figure 3.2: Paschen β line profiles in the GQ Lup companion and GQ Lup A, relative to the normalised continuum.

H band

The continuum slope of the H-band exhibits a strong triangular shape that is usually identified with low-gravity objects (see e.g. Gorlova et al., 2003; Allers et al., 2007). The nature of this feature is supposedly the H_2 collision induced absorption (CIA) as discussed by Kirkpatrick et al. (2006, see references therein). Also two H_2O hot steam bands, one ranging from the end of the J-band into the H-band, the other starting at 1.71 μm, add to the flux depression in the wings of the H-band. The whole region is essentially free of strong single absoption lines from metals and dominated by blended molecular features. The only remaining metal line, although extremely weak, is a K I absorption line at 1.517 μm. All other possible lines, mainly Al I and Mg I lines as well as the bandheads of the second overtone of ^{12}CO ($\nu = 3$), usually found in M giants (see e.g. Meyer et al., 1998) are completely absent.

The onset of FeH absorption can be seen (linelists from McLean et al., 2003; Cushing et al., 2003) but the features appear much weaker or are more blended than in the J-band, except for several stronger bandheads in the region of $\lambda\lambda$ 1.65 – 1.70 μm. Still, some stronger features seen in the SINFONI spectrum can also be seen in other spectra of low-mass young objects (see Section 3.3) but stay unidentified in the literature. Since they do not appear in the NIST database, they are presumably blends of molecular lines.
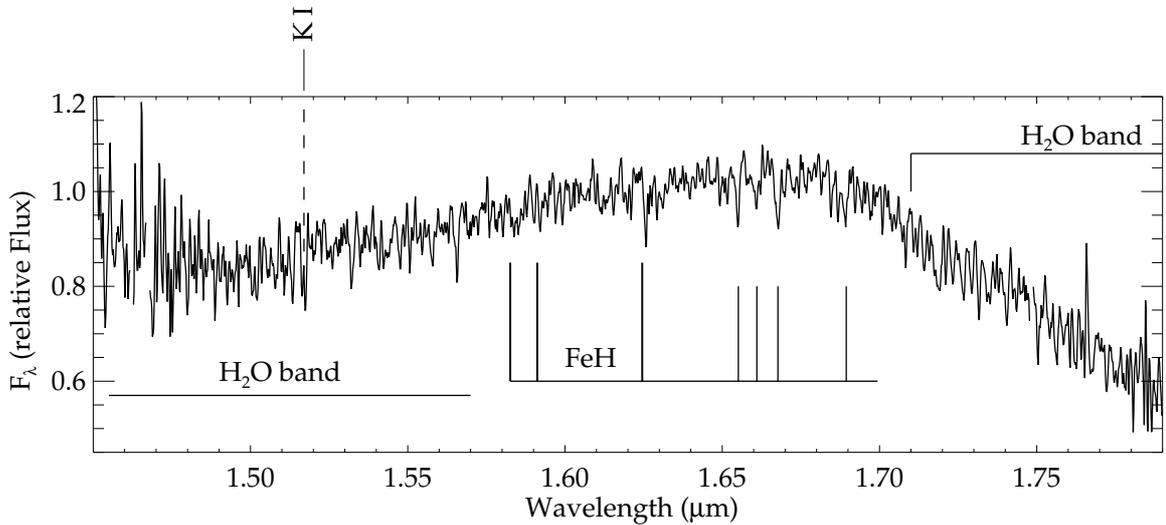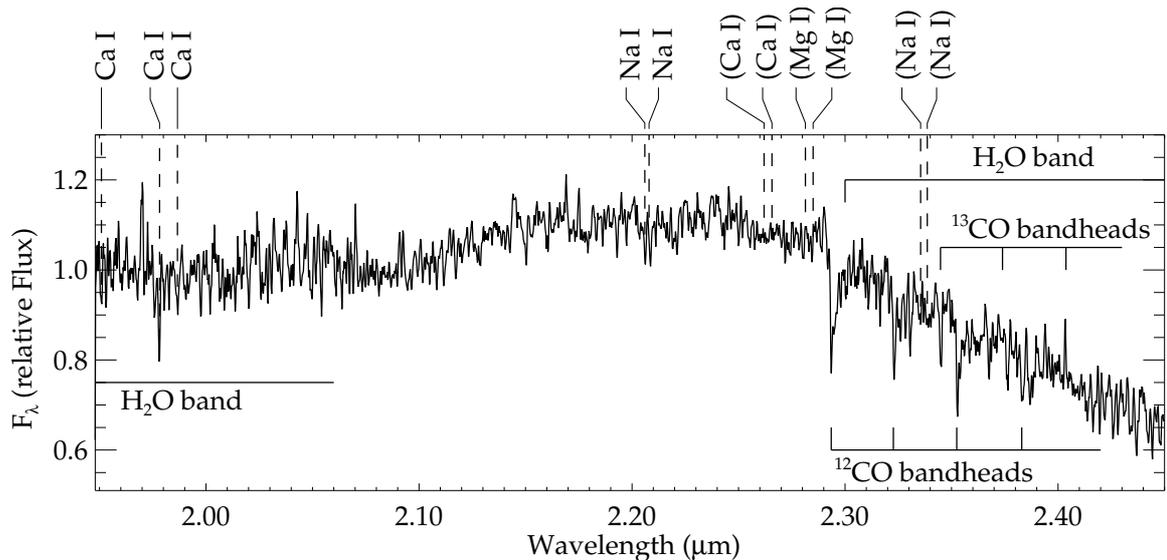

Figure 3.3: SINFONI H-band spectra of the GQ Lup companion. The Nyquist sampled spectral resolution is $R \sim 4000$. Three FeH bandheads and the strongest FeH lines are denoted with longer tickmarks to distinguish them from other FeH lines. The signal-to-noise ratio is ~ 30, and strongly degrades shortwards of 1.49 μm and longwards of 1.75 μm.

K band

The most prominent features in the K-band are the bandheads and linesystems of ^{12}CO and ^{13}CO ($\nu = 2$) longwards of 2.294 μm. Again, two H_2O hot steam bands at either side of the spectrum account for further flux depression. Unlike the H-band, the K-band is affected by CIA of H_2 as a whole (McLean et al., 2003). As noted for the H-band, from the wealth of metall lines that could in principle be present in cool objects (Kleinmann & Hall, 1986), only the Ca I lines at 1.951, 1.978, and 1.986 μm are detectable. All other Ca I lines in the region of 1.94 – 2.00 μm and the doublet at 2.263 μm can not be seen in the GQ Lup companion. The same is true for two Mg I lines at 2.281 and 2.285 μm. From the the Na I lines only the doublet at 2.206 and 2.209 μm is clearly detectable but still quite weak. The second doublet at 2.336 and 2.339 μm is blended with water and CO lines and is hard to identify. The Brγ line at 2.166 μm is not present, neither in absorption (which is not expected) nor in emission, unlike the Paβ line in the J-band. Since the Brγ line is instrinsically weaker than the Paβ line, Natta et al. (2004) find that from seven young low mass accretors in ρ Ophiuchus that show Paβ emission, only two are also showing Brγ emission, while all objects show 6.7 μm and 14.3 μm flux excess, indicating a circum-(sub-)stellar disk and ongoing accretion. It is thus not surprising to find no Brγ emission in the spectrum of the GQ Lup companion.

It is quite obvious that the K-band spectrum deviates in its continuum shape quite notably from the NACO spectrum presented in Neuhäuser et al. (2005) and Guenther et al. (2005), especially in the blue wing of the spectrum. This apparent discrepancy will be addressed in Section 3.2.

Figure 3.4: SINFONI K-band spectra of the GQ Lup companion. The Nyquist sampled spectral resolution is $R \sim 4000$. Identified atomic lines and the CO bandheads are marked. Non-detections that serve for further analysis are marked in parenthesis. The signal-to-noise ratio is ~ 30, and strongly degrades shortwards of 2.08 μm and longwards of 2.4 μm.

3.2   Re-evaluation of the NACO K-band spectrum

The SINFONI K-band spectrum shows an apparent mismatch to the original spectrum, obtained with NACO and published in Neuhäuser et al. (2005) and Guenther et al. (2005). While the NACO spectrum shows a strong flux depression in the blue part of the K-band, the SINFONI spectrum is rather flat between $1.95 - 2.1\ \mu\text{m}$. The question remains whether the object underwent a dramatic change in its apparent properties between the observations or whether shortcomings in the NACO spectrum itself are the reason for this discrepancy. I have therefore re-analyzed the original NACO data.

Dataset I: August 25, 2004

NACO spectra have been obtained in service mode during DDT under Program ID 273.C-5047(A). The first set of spectra was recorded in the night of August 25, 2004. 120 spectra with a detector integration time (DIT) of 15 s at 30 nodding positions (NDIT=4) have been taken in NACOs *S54_4_SK* setting through the 172 mas wide slit, warranting a nominal spectral resolution of $\sim$700 from 1.95–2.5 μm. The airmass of GQ Lup during the time of observation was 1.24–1.40. The DIMM seeing was rather constant around $0.9''$. A standard star (HIP 099265, B5V) was taken directly after the observation of GQ Lup at an airmass of 1.3, matching the airmass of the science observation.

The data reduction can now be directed in two ways. Either one co-adds the 30 nodded frames and extracts the flux from the 2D co-added frame (the standard procedure of the
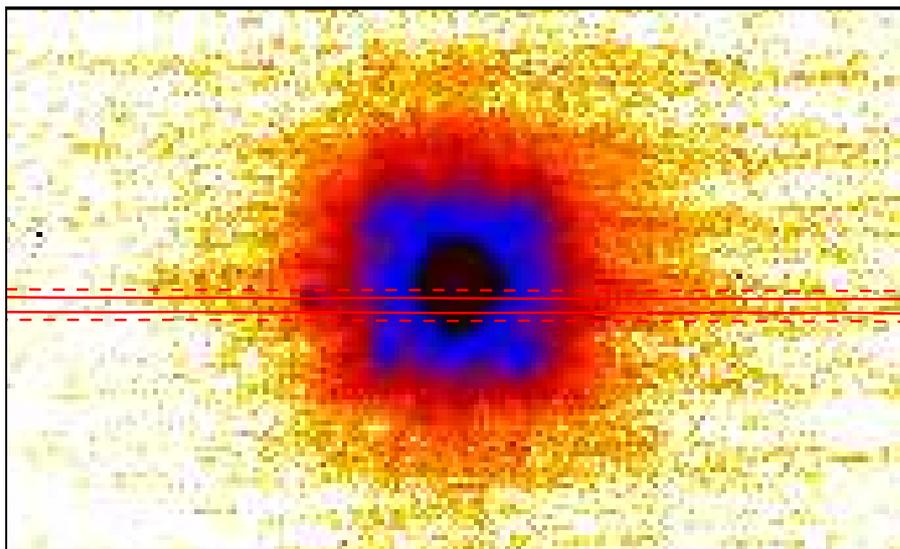
Figure 3.5: NACO acquisition image of GQ Lup, August 25, 2004. The GQ Lup companion can bee seen left (west) of GQ Lup A. The instrument rotation was set to 180° hence north is down and east is right. Overplotted are the contours of the slitimage. Solid lines show the maximum slit throughput, dashed lines the 50 percentile.

instrument pipeline) or one treats each nodding position separately and extracts the flux from each of the 30 spectra and co-adds the spectra in 1D rather than in 2D. I have chosen both ways to explore the possible differences and shortcoming of either of the methods, especially in the light of apparent slit alignment problems of NACO.

As can be seen in Fig. 3.5, neither GQ Lup A nor the GQ Lup companion were well centered in the slit. The GQ Lup companion is set on the edge of the slit, the PSF center of GQ Lup A is even outside the slit. In addition to this misplacement, the slit is slightly rotated in respect to the nominal instrument rotation angle. Hence, the nodding
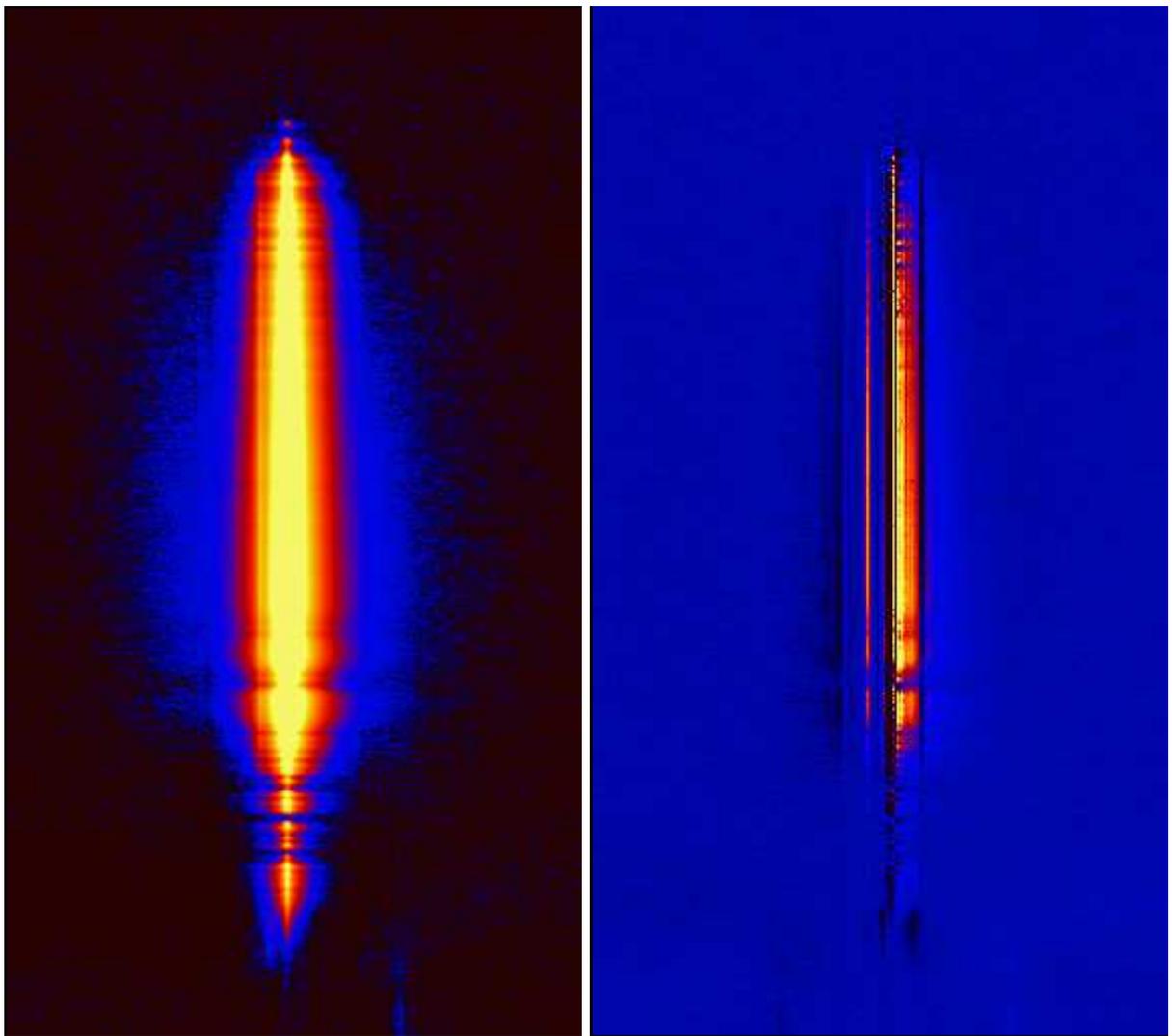
Figure 3.6: NACO spectrum of GQ Lup, August 25, 2004. *Left*: Co-addition of 30 nodded frames. The spectrum of the GQ Lup companion is visible as the thin signature left (west) of the spectrum of GQ Lup A (logarithmic scaling, [0,2000] ADU).
Right: Same frame after PSF subtraction and background fit around the spectrum of the GQ Lup companion (linear scaling[−10,100] ADU).

direction is not perfectly aligned with the slit. This is partly (but not fully) compensated by small additional telescope offsets during the nodding. However, the larger the nod-throw, the larger the potential mismatch between nominal and real slitposition. Slitlosses are unavoidable.

It is thus interesting to see how this effects the individual nodding positions. The data reduction follows these steps: First a wavelength solution for the spectral setting was derived from ThAr arc frames in comparison to the ThAr arc atlas from the NACO instrument website[2].

Second, a master flatfield was build from the flatfield calibration data. The (normalised) master flatfield and the raw frames from the science exposures are then piped to *eclipse/jitter* to shift and add the flatfielded frames at subpixel precision. The resultant 2D spectrum is shown in the left panel of Fig. 3.6. A copy of the frame was then flipped around the center of GQ Lup A and subtracted from the original frame in order to subtract the PSF wing of GQ Lup A at the position of the spectrum of the GQ Lup companion. Since the PSF of GQ Lup A is not fully symmetric (aberations, flux from super speckles etc.), the flux subtraction does not work perfectly, leaving remnants at the position of GQ Lup A. Thus, the background around the spectrum of the GQ Lup companion is not zero. To correct for this, I masked the position of the spectrum of the GQ Lup companion and fitted a second order polynomial to the remaining background for each row in dispersion direction and subtracted the spline at this position. This procedure results in a flat and clean background around the spectrum of the GQ Lup companion, see the image in the right panel of Fig. 3.6.

---

[2]http://www.eso.org/instruments/naco/inst/atlas/S54_4_SK_wc.pdf
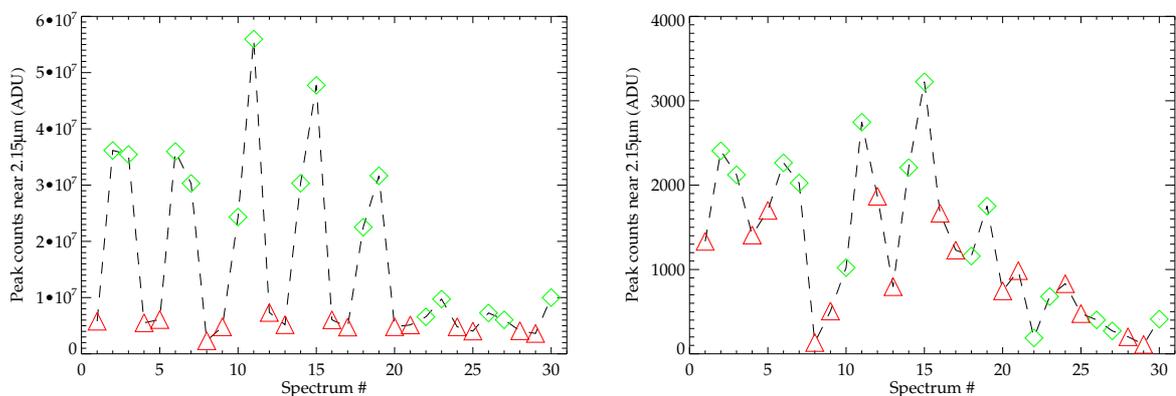
Figure 3.7: NACO spectra obtained August 25, 2004: Total flux in the spectra of GQ Lup A (*left*) and the GQ Lup companion (*right*) for all 30 nodding positions (*red triangles*: nodpos A, *green diamonds*: nodpos B). Note the higher throughput in all nodding positions B and the decreasing throughput towards the end of the sequence.

The flux of GQ Lup A and of the GQ Lup companion can now be extracted in the respective spectra (before and after PSF subtraction). This procedure was repeated for each of the individual nodding frames as well, in a slightly altered reduction recipe: After flatfield correction, the frames of adjacent nodding position were subtracted from each other (to subtract the sky background). The frames were then slightly rotated to align the spectrum with the rows of the frame. The flux of GQ Lup A was subtracted according to the procedure outlined above. 1D spectra of GQ Lup A and of the GQ Lup companion were extracted from each of the frames. The total flux in each of the spectra is strongly varying from one frame to the other. As can be seen in Fig. 3.7, the spectra from nodding positions B contain much more flux, speaking for a better centering of the target in the slit.

As a result only the 9 best spectra were combined to a final spectrum of the GQ Lup companion by building a mean over the 9 flux values in each spectral bin along the dispersion direction. A sigma clipping algorithm was applied to discard outliers. The standard deviation of the mean gives a good approximation of the statistical noise in each spectral bin. The advantage of this method over the extraction of the flux from a 2D co-added frame is the ability to discard spectra of mediocre quality and the ability to derive an estimate for the noise of the final spectrum.

Both spectra (from the 2D co-added frame and from the co-addition of the individual spectra) are in fact a convolution of the target spectrum and the atmospheric and instrumental throughput (see the discussion on the SINFONI spectra about this topic). The atmospheric and instrumental throughput can be estimated from the observation of a (telluric) standard star. The flux of the standard star was extracted after flatfielding and background subtraction (via A-B nodding correction). The ratio of the two standard star spectra (from nodding position A and B) should ideally be one. The actual ratio over the wavelength is shown in Fig. 3.8.
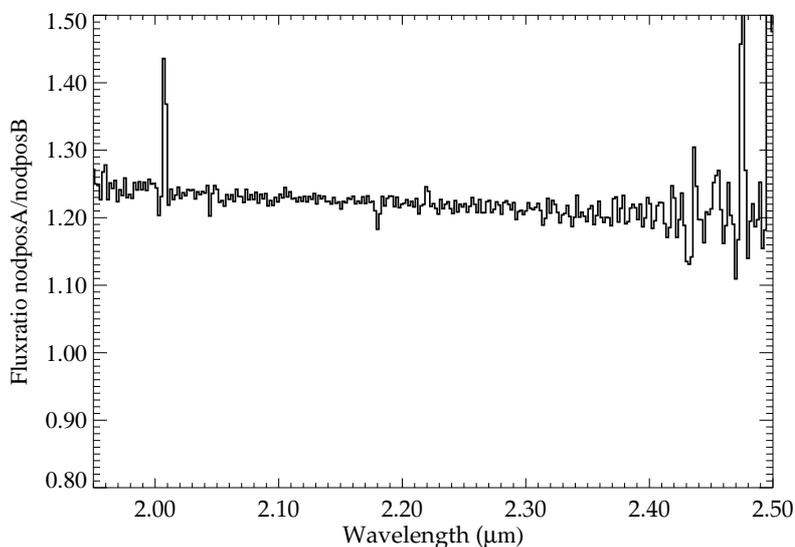
Figure 3.8: Ratio of the NACO standard star spectrum from nodding positions A and B, obtained August 25, 2004.

Any deviation, especially a slope, would indicate an imperfect slit centering of the standard star and would render the standard star spectrum useless. Eventhoug the observed ratio is not one (speaking for a different efficiency at one of the two nodding positions), it is rather flat and exhibits only a minor slope of ∼4% over the useful wavelength range of the spectrum. Hence, the uncertainty in the slope of the science spectrum induced by the standard star is less than 2% and I regard the standard star spectrum as useful. Devidind the standard star spectrum by a blackbody of $T_{\rm eff}$ =14000 K and correcting for the Br-γ absorption line in the standard star spectrum, results in the combined throughput of the instrument and the Earths atmosphere. This throughput function was used to correct the flux of GQ Lup A and of the GQ Lup companion.

As a consistency check, the spectrum of GQ Lup A was modeled by using a blackbody of $T_{\rm eff}$ =4060 K (appropriate for a spectral type of K7V) and multiplied with the throughput function. The result gives a good match with the observed NACO spectrum of GQ Lup A (see Fig. 3.9). Only in the regions of the CO bandheads GQ Lup A shows a deviation from the blackbody, as expected for a K7V star. However, the spectral lines in GQ Lup A are not as deep as the ones found in a normal main sequence late K type star
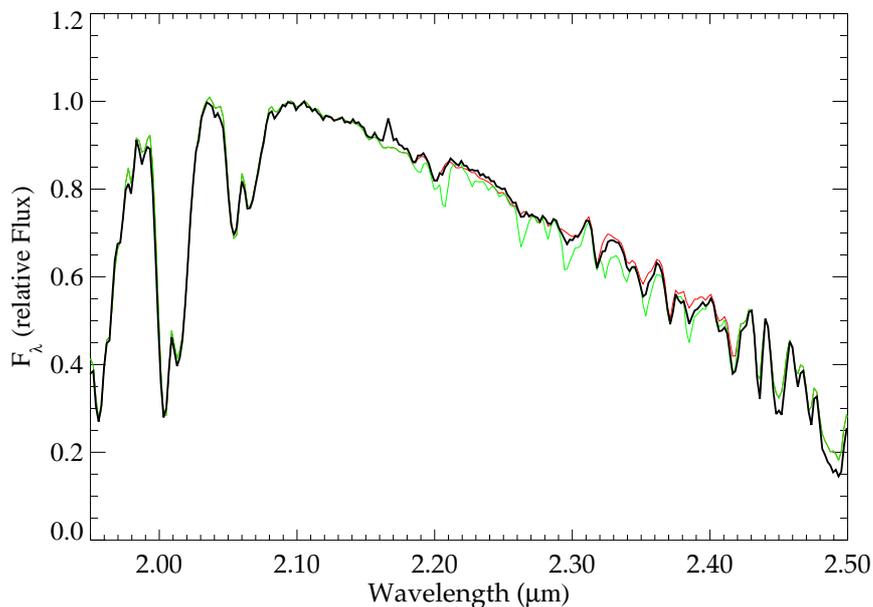
Figure 3.9: *Black*: NACO spectrum of GQ Lup A (raw spectrum), obtained August 25, 2004. *Red:* A blackbody of $T_{\rm eff}$ =4060 K multiplied with an atmospheric model spectrum (FASCODE and HITRAN) and the instrumental response curve combined to the throughput function (see text for details). *Green:* The same model but including the expected absorption features for a K8V main sequence star (from the GNIRS library). This plot demonstrates the validity (and limits) of the instrumental throughput function used for the spectrum of the GQ Lup companion.

(HD 113538, K8V, taken from the GNIRS spectral library[3]), as can be seen in Fig. 3.9. It should be noted that in most of the frames the peak flux of GQ Lup A was well above the linearity limit of the NACO detector, compromising the quality of the spectrum.

The resultant spectrum of the GQ Lup companion (both from the co-added frames and the final spectrum from the individual frames) is shown in Fig. 3.10. There is a good agreement between the two extraction methods. The spectrum resembles quite well the SINFONI K-band spectrum but deviated strongly from the previously published NACO spectrum.

---

[3]http://www.gemini.edu/sciops/instruments/nir/spectemp/speclib10.html
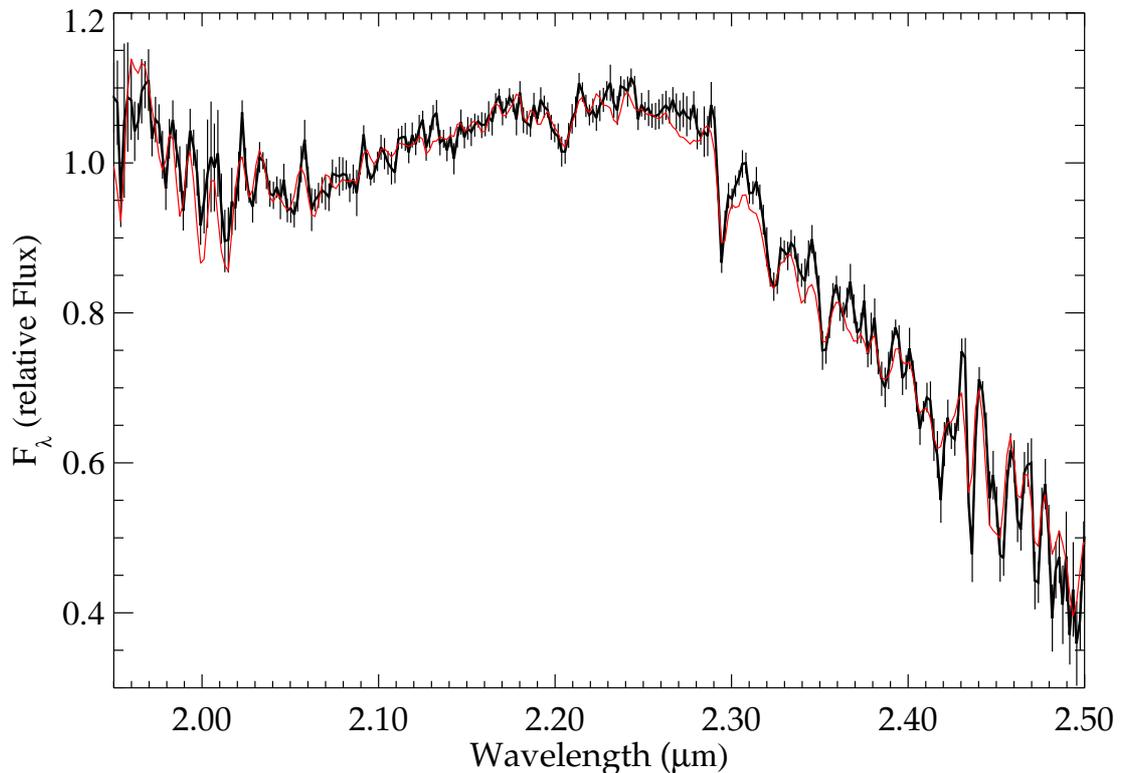
Figure 3.10: NACO spectrum of the GQ Lup companion, obtained August 25, 2004, from the average of the 15 best individual spectra (including error bars). Overplotted in red is the spectrum extracted from the 2D co-addition of all frames. Note the increase in noise near the atmospheric cut-offs on either side of the spectrum.

Dataset II: September 13, 2004

Guenther et al. (2005) give a S/N of 25 for the spectrum obtained in August 2004 and report that the observation was repeated on September 13, 2004 to replace the spectrum by a new one of higher quality, which was then used in the respective publications.

In this second observing campaign on September 13, 2004 the observing strategy was altered such that shorter detector integration times (DIT) were chosen (5 s instead of 15 s) and 12 instead of four exposures were co-added at each of the 30 nodding positions. The acquisition image (Fig. 3.11) of the second observing run reveals a further complication. Not only is the target again offset in respect to the slitcenter, also a diffraction spike sits on top of the GQ Lup companion. Eventhough the DIMM seeing in the second observing run is only 0.5–0.7″ and the strehl ratio measured in the PSF reference image at the beginning of each run is slightly higher in September than in August, the PSF of GQ Lup A is still much better defined and more symmetric in August. The average flux of the diffraction spike in the acquisition image is about 30% to 50% of the peak flux of the GQ Lup companion. Hence, the contamination from scattered light of GQ Lup A is very pronounced.

The data reduction followed the procedure outlined above for the data obtained in August 2004 until the step of the flux extraction. The co-added frames before and after PSF subtraction are shown in Fig. 3.12. The result of the PSF subtraction is less convincing than in the data from August. The spatial profile of the spectrum of the GQ
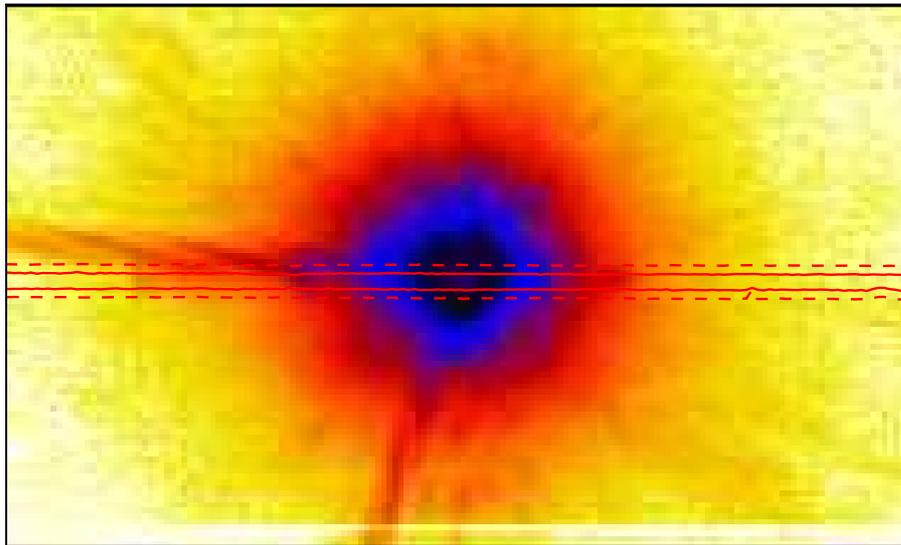
Figure 3.11: NACO acquisition image of GQ Lup, September 13, 2004. The GQ Lup companion can bee seen left (west) of GQ Lup A. Note the prominent diffraction spike atop of the GQ Lup companion. The instrument rotation was set to 180° hence north is down and east is right. Overplotted are the contours of the slitimage. Solid lines show the maximum slit throughput, dashed lines the 50 percentile.

Lup companion is less well defined and shows clear signs of an overlap with a spatially extended source (the diffraction spike?).

When comparing the flux at the different nodding positions (see Fig. 3.13), the nodding position B seems to warrant again a much higher throughput. The total number of useful nodding position is 15.

Unfortunately, the standard star taken during the second run has a rather unsuitable airmass (1.18) as compared to the science frames (spanning 1.29 to 1.48). Also the ratio
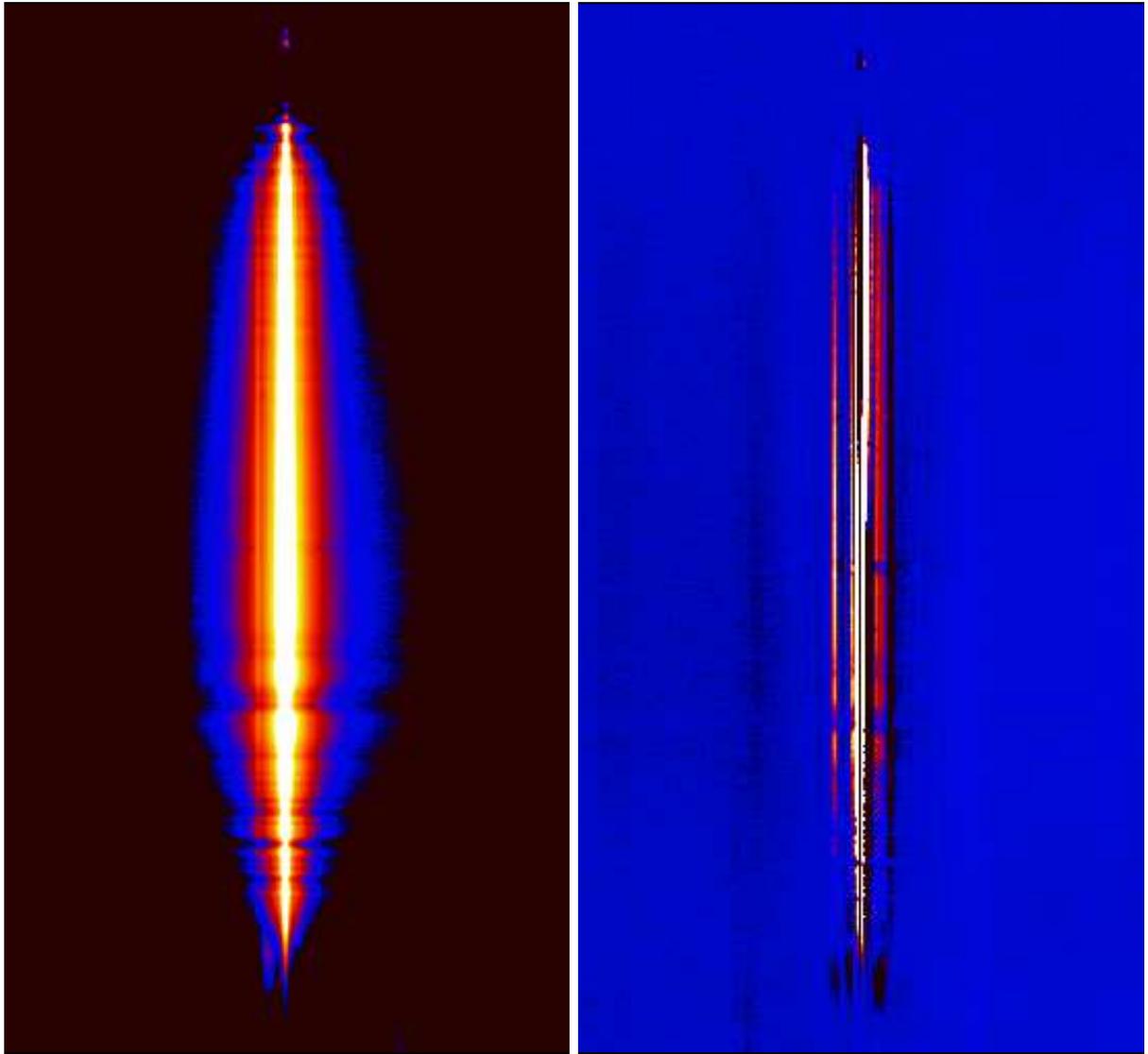
Figure 3.12: NACO spectrum of GQ Lup, September 13, 2004. *Left*: Co-addition of 30 nodded frames. The spectrum of the GQ Lup companion is visible as the thin signature left (east) of the spectrum of GQ Lup A (logarithmic scaling: [0,1000] ADU).
Right: Same frame after PSF subtraction and background fit around the spectrum of the GQ Lup companion (linear scaling: [−5,30] ADU).

between the two nodding positions of the standard star shows a strong slope, see Fig. 3.14. The flux at the red end of the spectrum is nearly 30% different from the blue end, making the standard star observation useless since it renders the slope of the continuum by 15% when taking the mean flux from both nodding positions.

I have therefore used the spectrum of GQ Lup A to correct for the instrumental throughput by dividing the spectrum of the GQ Lup companion by the spectrum of GQ Lup A and multiplying by the blackbody of T_{eff} =4060 K that was found a good fit already for the data obtained in August. However, this proceedure has the shortcoming that the spectral features of GQ Lup A, neither been fully adequatly fit by a blackbody, nor by a template spectrum of similar spectral type (see Fig. 3.9), can not be removed. Hence, the depth of the features in the spectrum of the GQ Lup companion (mainly the CO bandheads) will be underestimated (or overestimated when the template is used to correct for the featues in GQ Lup A), preserving only the continuum slope of the spectrum.

The resultant spectrum is shown in Fig. 3.15. In the second NACO run, the data shows a strong difference between the flux extraction methods (either only from the 15 best spectra or the flux extracted from the 2D co-added frame as delivered by the instrument pipeline). A close examination reveals, that the spatial profile of the spectrum of the GQ Lup companion at the nodding positions A shows a clear overlap with an extended source (diffraction spike?) while the spectra at nodding position B are nearly symmetric and the FWHM is comparable to what was observed in August. Hence, I suspect that at nodding positions A the spectra are contaminated from scattered light of GQ Lup A, due to a misplacement of the GQ Lup companion towards the lower edge of the slit, letting more light from the diffraction spike pass through the slit at the position of the target. The spectrum of GQ Lup A is close to a blackbody, hence is rising towards shorter wavelength. The contaminated spectrum, extracted from the 2D co-added frame, is showing exactly
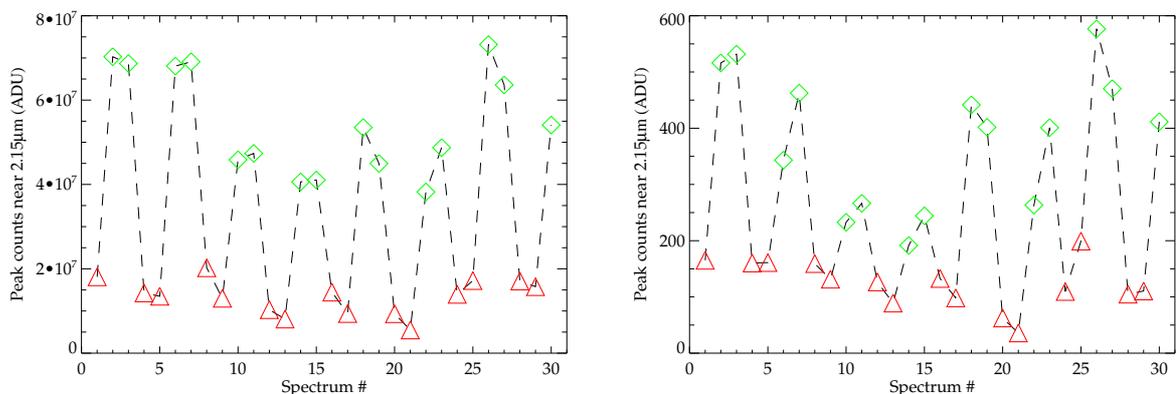
Figure 3.13: NACO spectra obtained September 13, 2004: Total flux in the spectra of GQ Lup A (*left*) and the GQ Lup companion (*right*) for all 30 nodding positions (*red triangles*: nodpos A, *green diamonds*: nodpos B). Note the higher throughput in all nodding positions B.
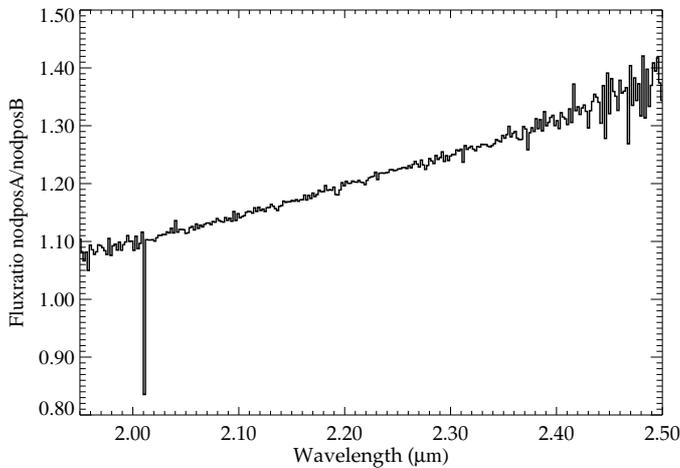
Figure 3.14: Ratio of the NACO standard star spectrum from nodding positions A and B, obtained September 13, 2004.

this effect - a flux excess in the blue. The continuum of the purer spectra extracted at nodding positions B only, are however in good agreement with the data obtained in August, but lacking the clear CO features due to the use of GQ Lup A as a standard star and shows a degraded S/N.
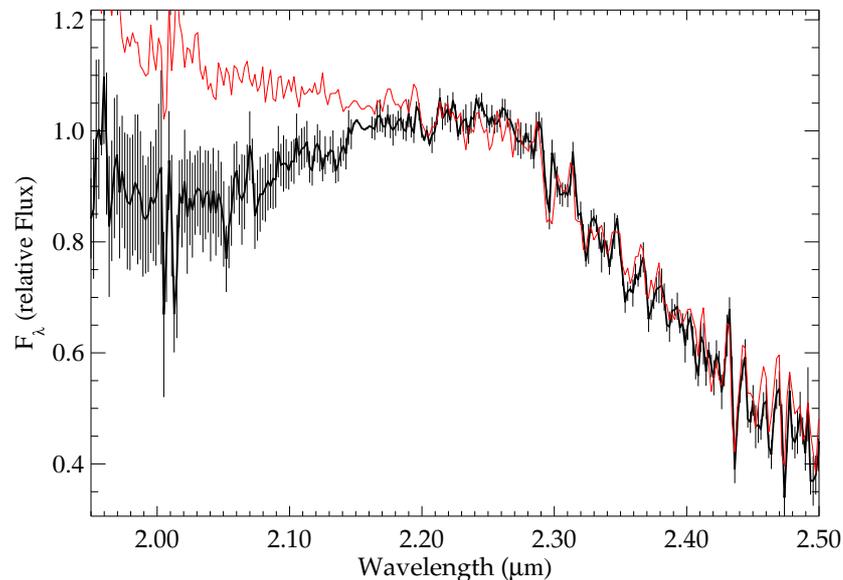
Figure 3.15: NACO spectrum of the GQ Lup companion, obtained September 13, 2004, from the average of the 15 best individual spectra (including error bars). Overplotted in red is the spectrum from the 2D co-addition of all frames. Note the increase in noise near the atmospheric cut-offs on either side of the spectrum and the flux excess in the blue part of the spectrum extracted from the 2D co-addition of all frames.

Summary

The spectrum obtained during the NACO run in September 2004 suffers much more shortcomings than the one from August 2004, eventhough the number of useful nodding positions is smaller in August than in September 2004. Most notably, in the September run the spectrum of the GQ Lup companion is severely contaminated by scattered light from GQ Lup A. Moreover, the poor quality of the standard star observation in September, both in terms of airmass and slit centering, severely affects the quality of the spectrum. Hence, I regard the NACO spectrum from August 2004 as the purer spectrum of the two and as a fair representation of the true flux of the GQ Lup companion.

However, I can not reproduce the NACO spectrum of the GQ Lup companion published in Neuhäuser et al. (2005) and Guenther et al. (2005) from any of the two datasets. In Fig. 3.16 I compare the NACO spectrum of the GQ Lup companion from August 25, 2004 with the SINFONI K-band spectrum smoothed to a spectral resolution of 700 and with the published NACO spectrum (taken from Guenther et al., 2005, Fig. 4). As can be seen from this figure, the NACO and SINFONI spectra are clearly consistent and the flux depression in the blue wing of the K-band is not real. This feature was used as an indicator for the very low effective temperature obtained in Neuhäuser et al. (2005) and is likely due to an error in the previous data analysis of the NACO spectrum in Neuhäuser et al. (2005) and Guenther et al. (2005).
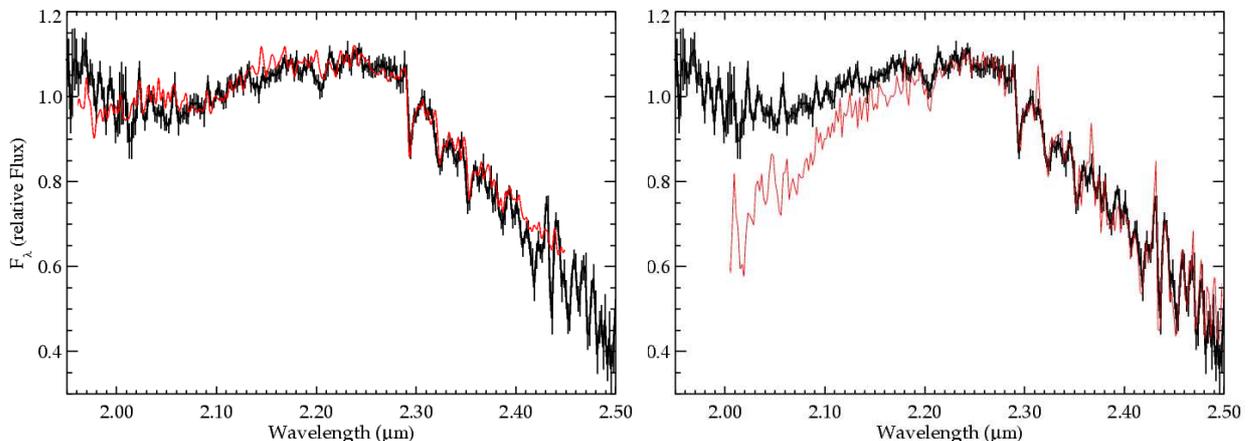
Figure 3.16: NACO spectrum of the GQ Lup companion, obtained August 25, 2004. *Left*: NACO spectrum (*black*) overplotted with the smoothed ($R \sim 700$) SINFONI spectrum (*red*). *Right*: NACO spectrum (*black*) overplotted with the published NACO spectrum (*red*) from Guenther et al. (2005, Fig. 4).

3.3 Empirical classification

After the first step of identifying the most prominent features in the SINFONI spectra of the GQ Lup companion, the next logical step would be an empirical classification of the GQ Lup companion by comparing its spectrum with other spectra of known old and young M and L dwarfs. Deriving a reliable spectral type (and thus effective temperature) from the comparison with a spectral sequence is however inhibited by the limited availability of JHK spectra of young, low mass objects at a resolution comparable to the one of the SINFONI spectra. Studies that concentrate on young, low mass objects are usually based on spectra with a resolution of much less than 1000, see e.g. Gorlova et al. (2003) or (Allers et al., 2007).

Classical spectral sequences in the domain of M and L dwarfs are one-dimensional. An equivalent of the luminosity class to account for the differences in the radius (and thus in the surface gravity distinguishing young and old objects) is not existing yet. This deficiency was already addressed by Kirkpatrick et al. (2006); Kirkpatrick (2007). Thus, caution has to be taken when deriving a spectral type from spectral indices and converting the spectral type into an effective temperature, a method applied also in Neuhäuser et al. (2005). Spectral indices are likely to be off by an unknown amount for young objects due to their lower gravity, which affects the strength of metal lines and the appearance of whole molecular bands as I will demonstrate in this section.

In the following section I use primarily the spectra of young objects from McGovern et al. (2004) and the JHK-band spectrum of a presumably young and cool field dwarf, 2MASS J01415823-4633574 (Kirkpatrick et al., 2006), provided in electronic form by Davy Kirkpatrick. For old field objects I make use of the NIRSPEC Brown Dwarf Spectroscopic Survey (BDSS; McLean et al., 2003)[4] and the SPEX/IRTF Spectral Library (Cushing et al., 2005)[5] to build a spectral sequence between M6 and L4, the most likely spectral type of the GQ Lup companion and the range given by Neuhäuser et al. (2005).

---

[4]Available online: `http://www.astro.ucla.edu/~mclean/BDSSarchive/`
[5]Available online: `http://irtfweb.ifa.hawaii.edu/~spex/WebLibrary/index.html`

J band

McGovern et al. (2004) presents J-band spectra taken with NIRSPEC[6] (R$\sim$2000) of two young (KPNO-Tau 4 and σ Ori 51) and one intermediate age (G196-3 B) brown dwarf together with the spectrum of a M giant (IO Vir) and two old field brown dwarfs (2MASS 0345+25 and σ Ori 47), the latter being previously erroneously identified as a member of the young σ Ori cluster. The author makes the case that the depth of the alkali lines in the J-band together with VO, TiO and FeH absorption allows one to distinguish old (high surface gravity) from young (low surface gravity) objects. As it becomes apparent from Figures 3.17 and 3.18 the depth of the K I lines is a good indicator of the surface gravity as is the shape of the FeH and VO depression at 1.20 μm. At lower surface gravity the K I lines are shallower and VO dominates with a broad V-shaped profile the blue part of the J-band. At higher surface gravity the alkali lines get stronger, VO vanishes and strong FeH lines blend to a narrow U-shaped feature at 1.20 μm.

In Figure 3.17 the GQ Lup companion resembles in remarkable detail the features in these young objects but is clearly deviating from the spectrum of KPNO-Tau 4, both in terms of the continuum shape and the depth of the K I lines at 1.17 μm. The similarity with G196-3 B is even less pronounced, mainly because the continuum of this object is even redder (cooler). The spectral type of G196-3B is given in the literature as L2 and the object has an assigned temperature of T_{eff}= 1800 $\pm$ 200 K (Rebolo et al., 1998) and T_{eff}= 1950 $\pm$ 150 K (Kirkpatrick et al., 2001). Also, reddening by local or interstellar material can not be the reason for the red spectrum of G196-3B, given its proximity to the sun and the rather evolved age (60-300 Myr). Hence, the GQ Lup companion appears clearly bluer, thus hotter, than G196-3B. For KPNO-Tau 4, Guieu et al. (2007) give an A_v of 2.45. The spectra in McGovern et al. (2004) are however not de-reddened, hence the continuum slope of KPNO-Tau 4 in Figure 3.17 is too red. De-reddening would bring the spectrum closer in its appearance to the one of the GQ Lup companion. I note that the depth of the K I lines of the GQ Lup companion appear to be intermediate between those of KPNO-Tau 4 and G196-3B.

In Figure 3.18 the GQ Lup companion is compared with σ Ori 51 which, despite the lower signal-to-noise ratio in the NIRSPEC spectrum, makes a reasonable match. Still, the continuum in the GQ Lup companion is slightly bluer (hotter) than that of this young M9 dwarf, suggesting a slightly higher effective temperature for the GQ Lup companion, since the extinction for σ Ori is too low ($A_v \sim$0.15 Zapatero Osorio et al., 2000) to explain the remaining deviation.

It seems that the SINFONI spectrum of the GQ Lup companion shows a bluer continuum than the young objects presented in McGovern et al. (2004), at least judging from the J-band. Hence, the GQ Lup companion must have an earlier spectral type than M9 in this scale.

In Figure 3.19 I compare the SINFONI spectrum with a spectral sequence of *old* field M and L dwarfs. The comparison reveals that the continuum slope of the GQ Lup

---

[6]NIRSPEC: Near-Infrared Echelle Spectrograph, at the Keck II Telescope, Mauna Kea, Hawaii

companion is comparable with an old M8 dwarf but the shape of the H_2O hot steam band is slightly better fitted by a later spectral type (M9) while the K I lines are better fitted by spectral type earlier than M6. This is a typical situation when determining effective temperature and surface gravity – the ambiguity of these two parameters for a single spectral feature. Lower surface gravity can easily be mimicked by lower effective
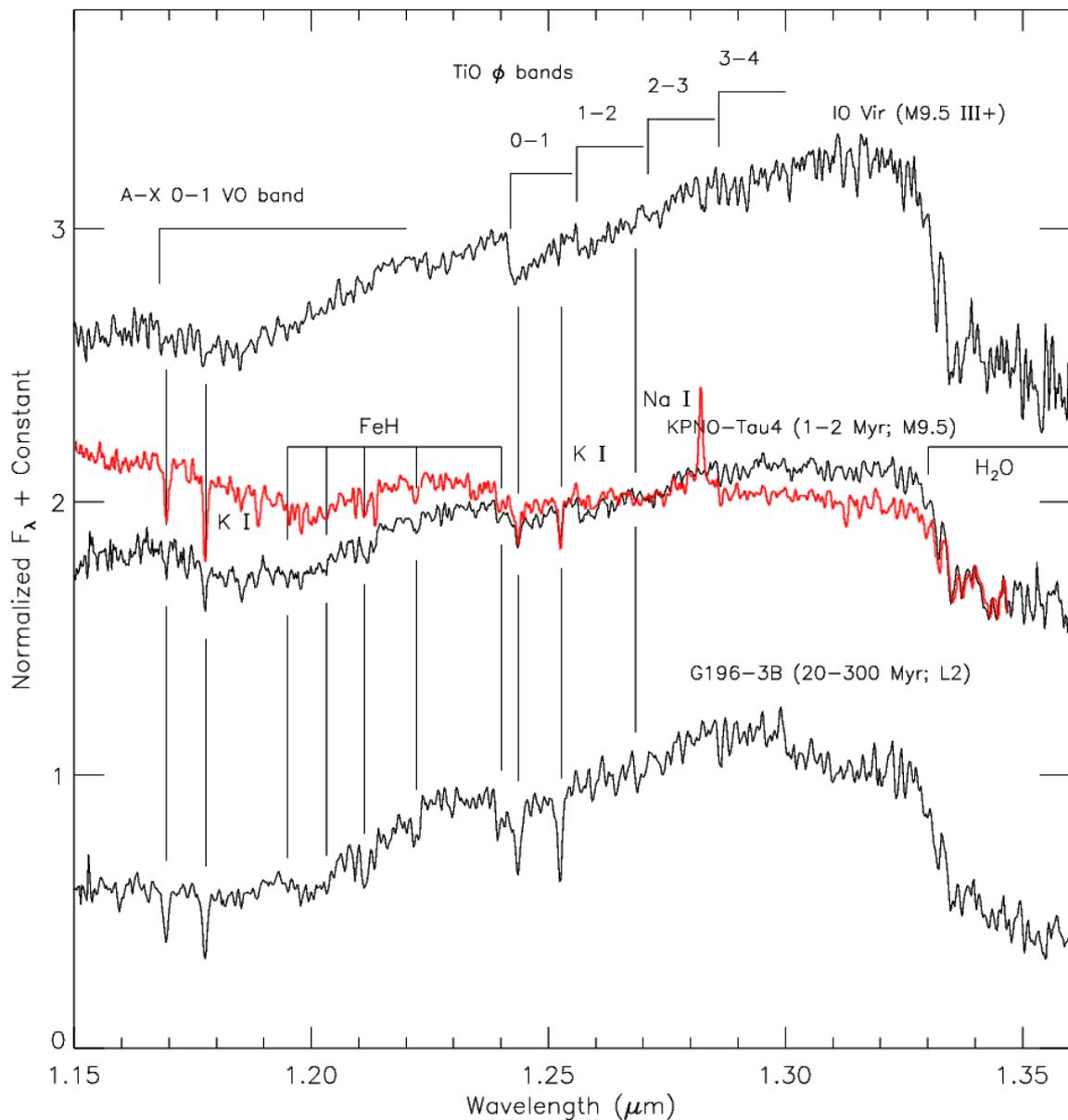

Figure 3.17: NIRSPEC J-band spectra of young, low-mass brown dwarfs and the late M giant IO Vir, reprint of McGovern et al. (2004, Fig. 1). The scaled spectrum of the GQ Lup companion is overplotted in red.

temperature (later spectral type) in most features. Hence, caution has to be taken when assigned a spectral type based on a one-dimensional spectral sequence. The mismatch in the depth of the K I lines and the Na I line at 1.14 μm for the whole spectral series emphasise again the lower surface gravity in the GQ Lup companion, since it can not at all be matched by any of the spectral templates. Note also the increasing depth of all features with later spectral type. Again, earlier templates than M9 give the better match.
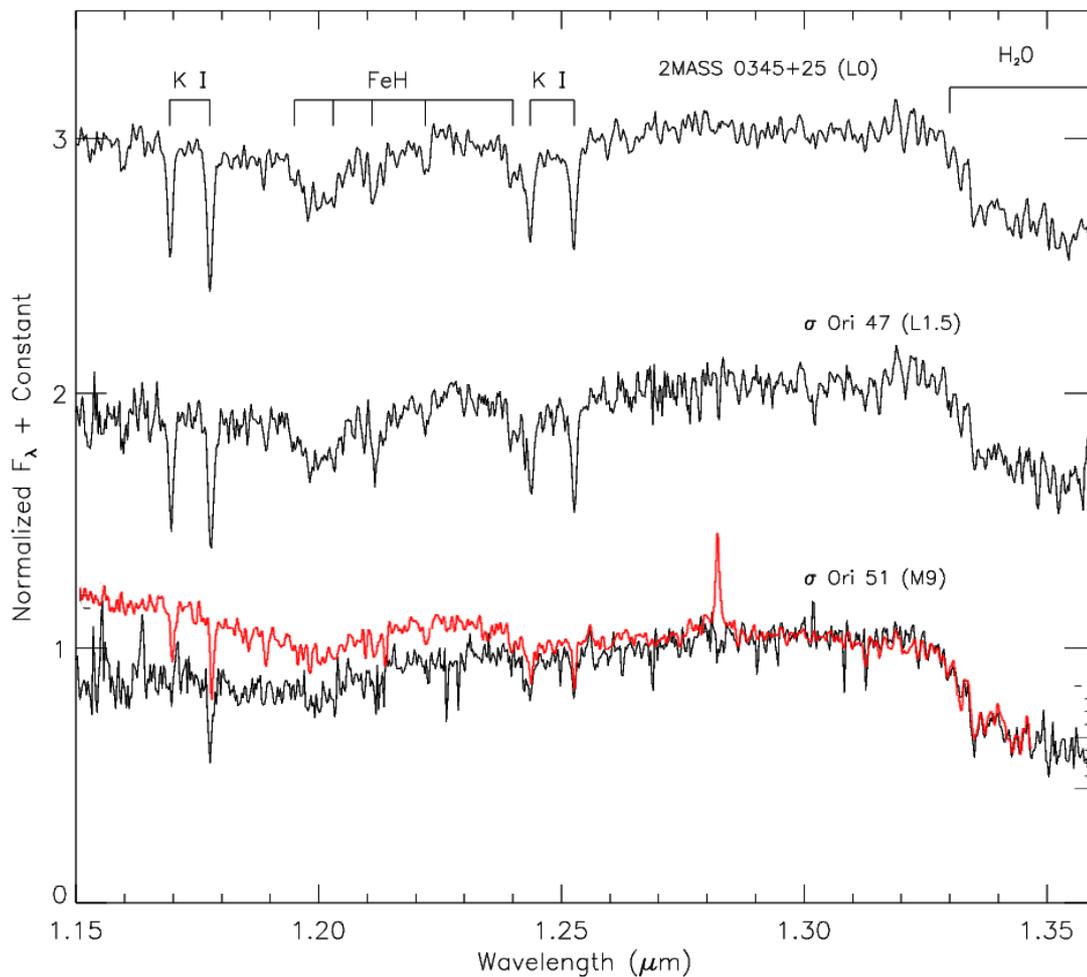
Figure 3.18: NIRSPEC J-band spectra of 2MASS 0345+25 (an old field L0 dwarf), σ Ori 47 (an old foreground L1.5 dwarf, previously erroneously identified as a member of the young σ Ori cluster) and σ Ori 51 (a young, low-mass M9 dwarf, a bona fide member of the young σ Ori cluster). The figure is a reprint of McGovern et al. (2004, Fig. 3). The scaled spectrum of the GQ Lup companion is overplotted in red. Note the missmatch in the depth of the K I lines and the shape of the FeH feature at 1.20 μm between the GQ Lup companion and the old dwarfs at the top and centre.
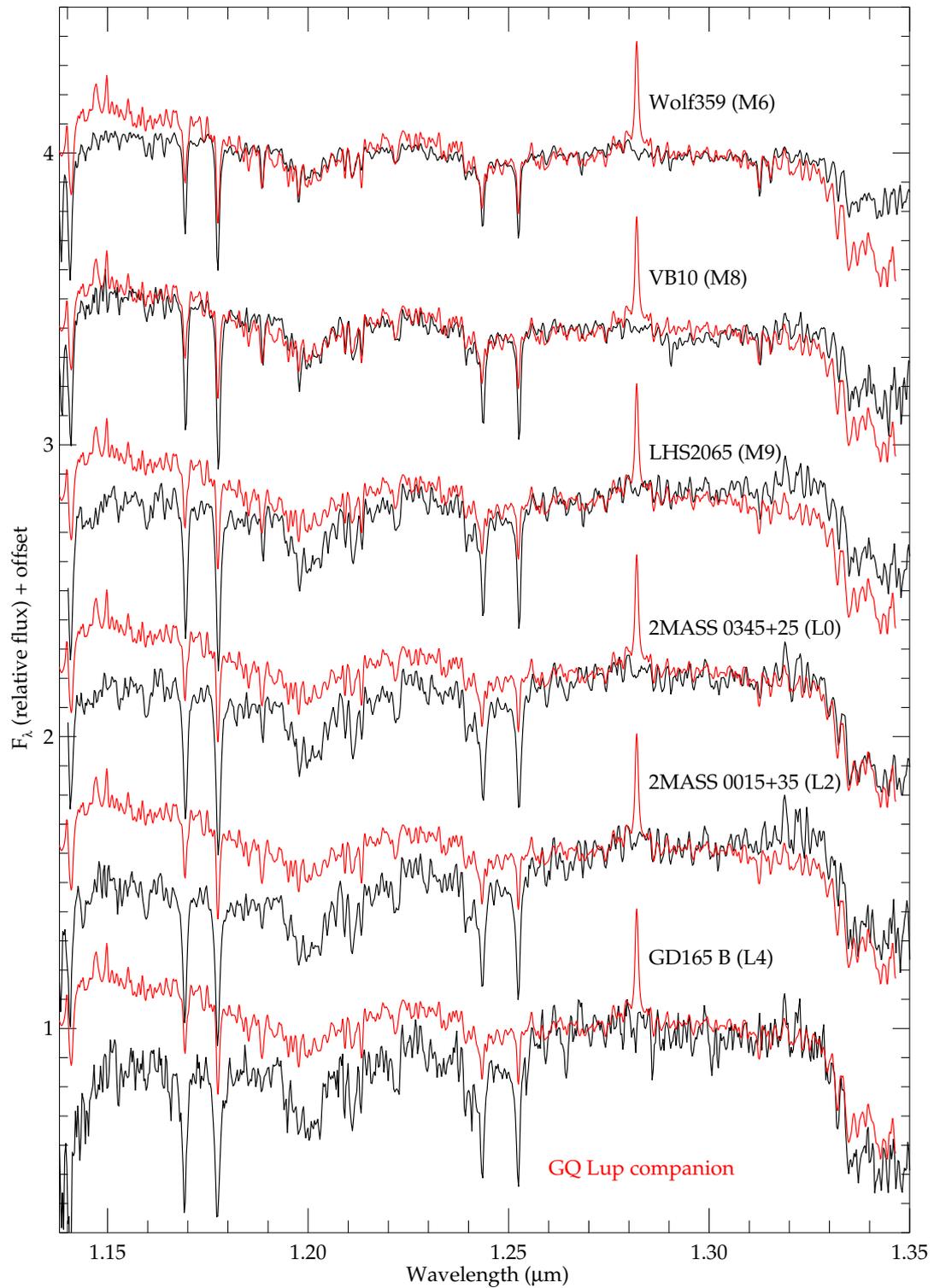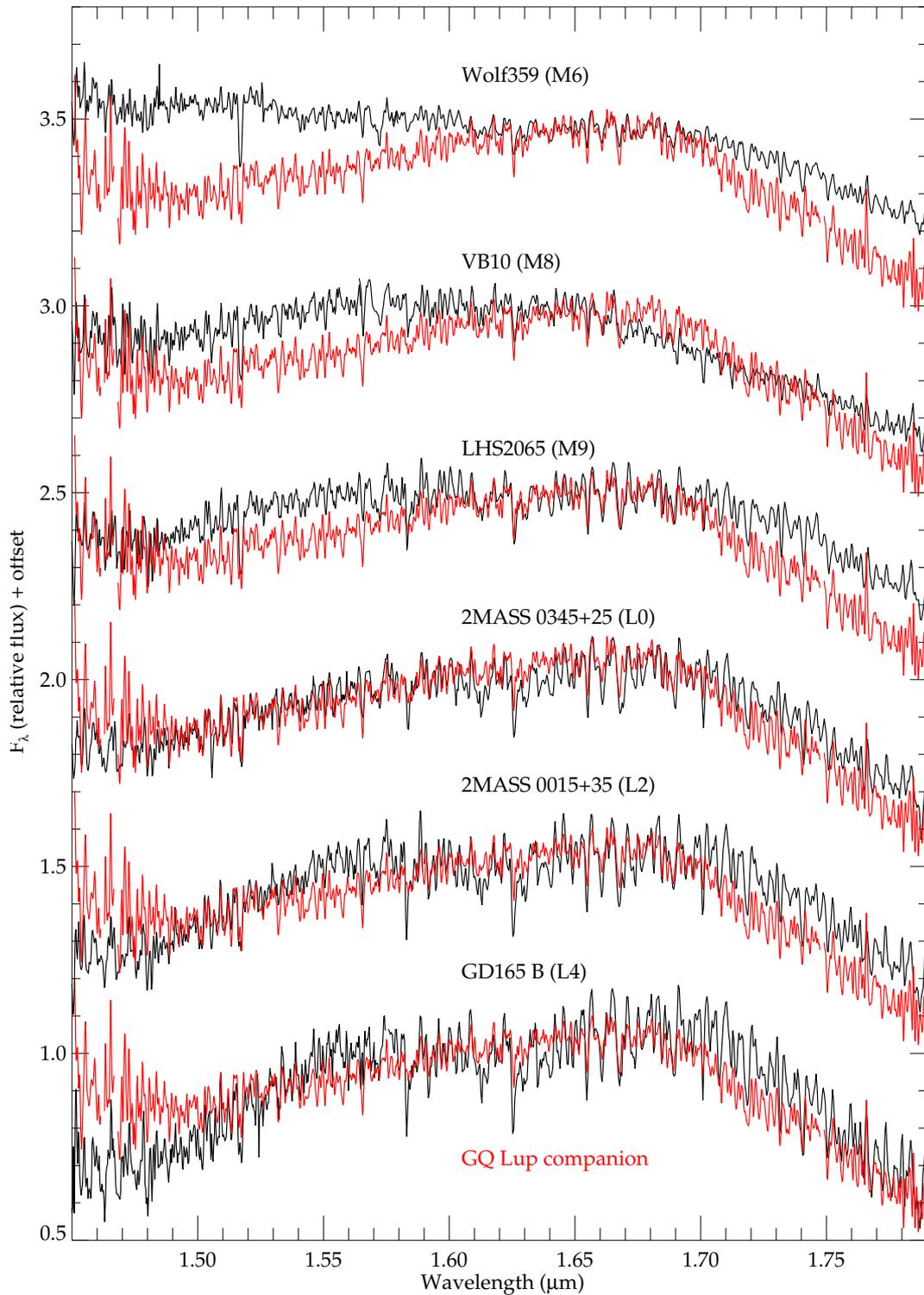
Figure 3.19: NIRSPEC *J*-band spectral sequence of old (high surface gravity) stars and brown dwarfs from the BDSS. The scaled spectrum of the GQ Lup companion is over-plotted in red. The common resolution is $R \sim 2000$. See annotations in Figure 3.3 for line identifications.

H band

In the H-band, the same spectral sequence of old M and L dwarfs reveals an even more complex picture. With increasing spectral type – decreasing effective temperature – the peak of the SED shifts toward longer wavelength. Consequently, flux is partly shifted from the blue into the red wing of the H-band. At the same time collision induced absorption (CIA) by H_2 molecules gets stronger, shaping the continuum as the absorption profile is a function of wavelength (Borysow et al., 1997). Similarly, the contribution from H_2O absorption gets stronger with decreasing effective temperature and remodels the continuum shape. These three contributions lead to a more and more peaky, 'triangular' shaped continuum and a redwards shifted maximum with decreasing temperature.

But also absorption by FeH gets stronger with decreasing effective temperature, 'eating away' the peak flux in the H-band. The net effect is that the shape of the H-band gets rounder with decreasing effective temperature.

All contributors mentioned so far are also sensitive to the surface gravity. FeH and CIA weakens with decreasing surface gravity while the hot steam bands get even stronger. As a result, the H-band continuum of an old M or L dwarf does not look alike the one of a young, low surface gravity object and it becomes hard to match the spectrum of the GQ Lup companion with any of the templates shown in Figure 3.20. The peakedness of the H-band is thus a general indicator for the youth (low surface gravity) of a substellar object in the literature (see e.g. Allers et al., 2007).

Consequently, the steepness of the blue wing of the spectrum of the GQ Lup companion seems best reproduced by a L0 dwarf, but the red wing does not fit until L2. The central regions are always too low among the templates, due to the FeH absorption that is much less pronounced in the GQ Lup companion. Again an argument for its youth. Note also the changing depth in all spectral feature with spectral type. Here M8 to M9 seems to fit best.

The H-band seems to offer the worst fit, since the spectral features and broad-band opacities being largely counter-acting on effective temperature and surface gravity. The only available H-band spectrum of a young low-mass object, presented in Figure 3.23, reveals a much better fit, eventhough the effective temperature of this object is likely lower than that of the GQ Lup companion, judging from its J-band spectrum. Hence, I discard the H-band spectrum for the determination of spectral type in comparison to old field objects.
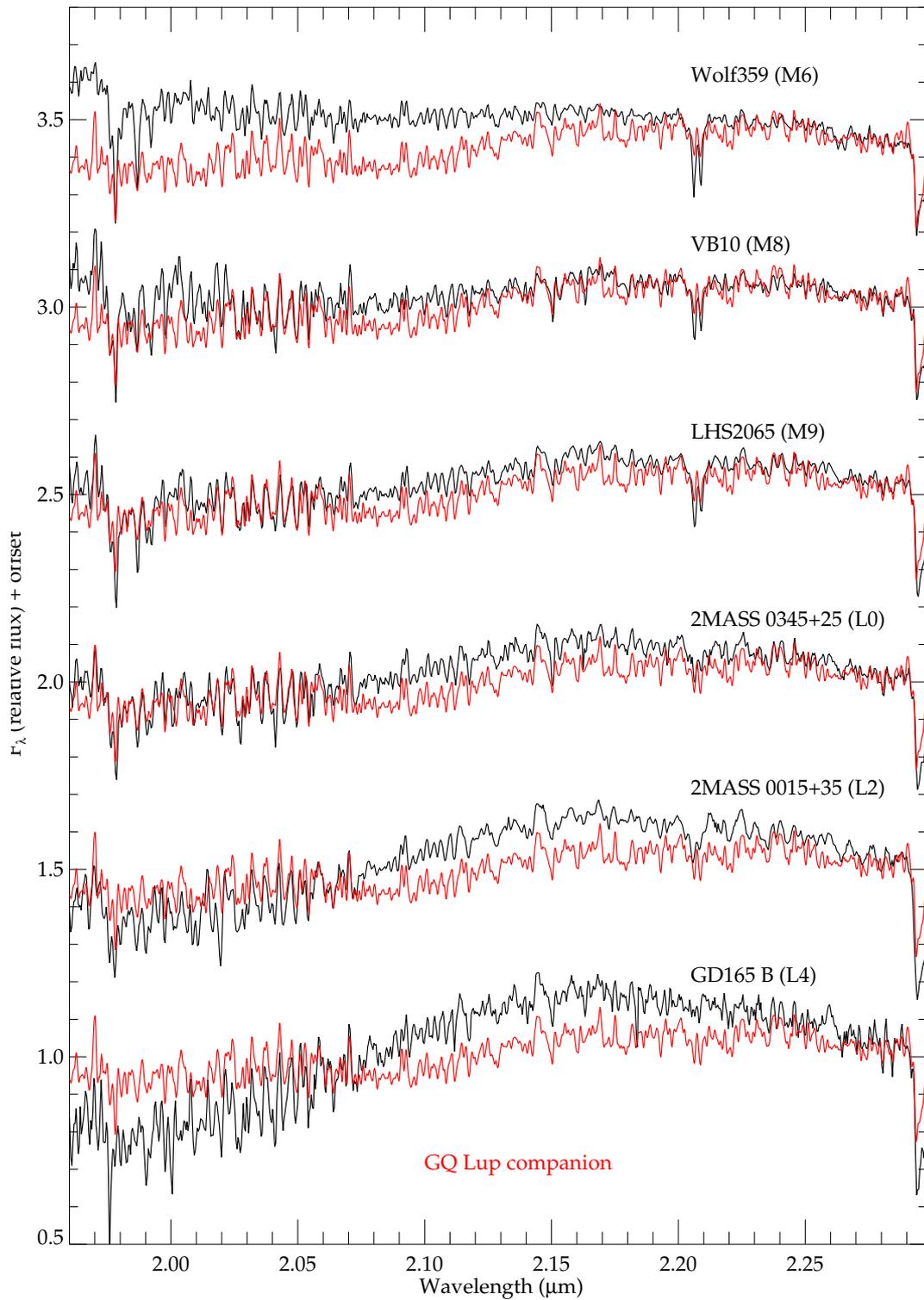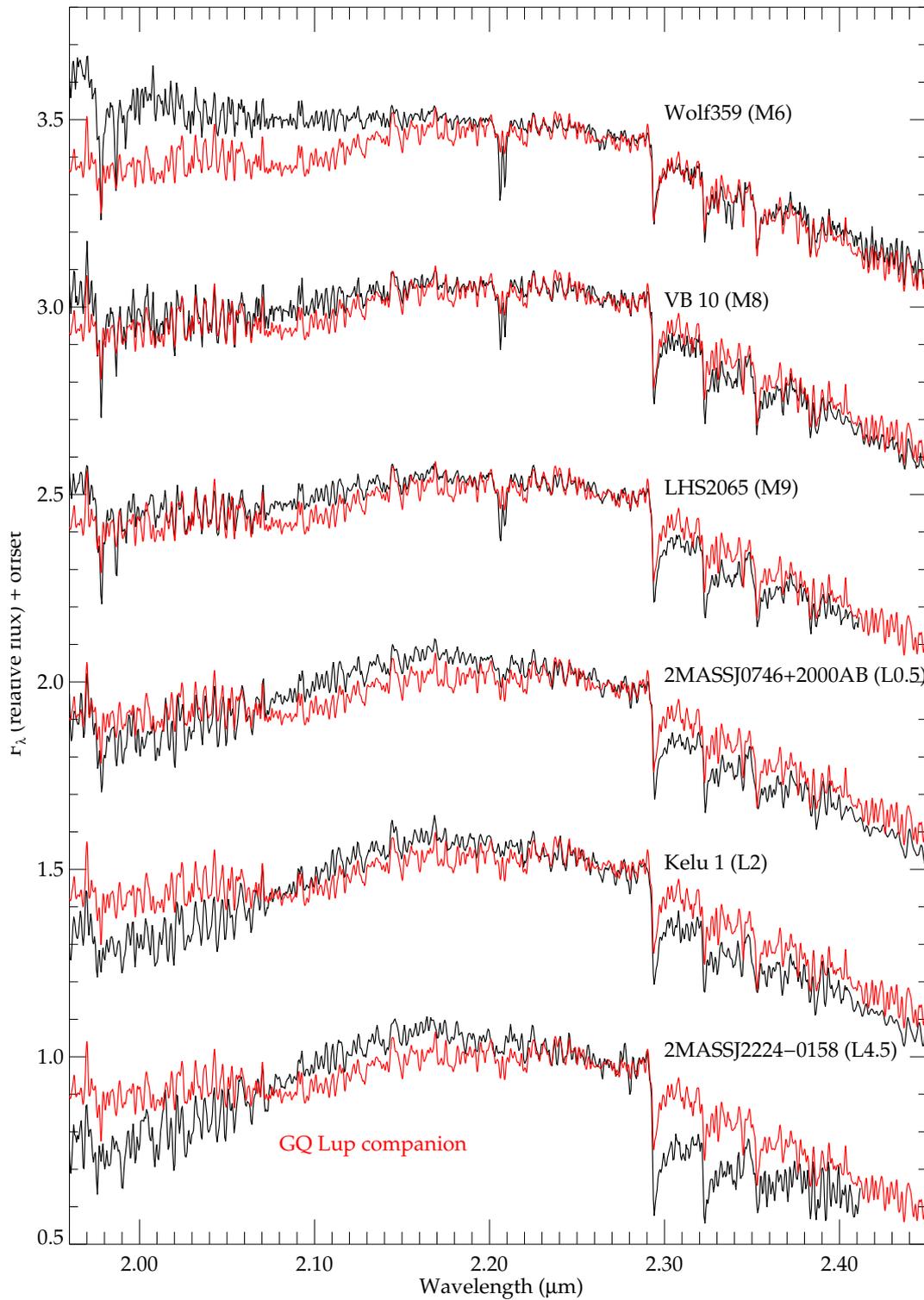
Figure 3.20: NIRSPEC H-band spectral sequence of old (high surface gravity) stars and brown dwarfs from the BDSS. The scaled spectrum of gqlupb is overplotted in red. The common resolution is $R \sim 3000$. See annotations in Figure 3.3 for line identifications. The flux of the GQ Lup companion is normalised to the template spectra at $1.66\ \mu$m.

K band

The NIRSPEC spectra do not cover the interesting spectral region longwards of 1.30 μm with its CO bandheads. Only the first ^{12}CO bandhead at 1.292 μm is partly visible. Thus, I have added a similar spectral sequence from the IRTF/SPEX[7] library that offers a slightly lower resolution ($R \sim 2000$) than the NIRSPEC library but offers a higher spectral coverage out to 2.45 μm. See Figures 3.21 and 3.22 for comparison.

The blue wing of the K-band offers a number of spectral features, such as the hot steam band shortwards of 2.06 μm, the Ca I lines at 1.95–2.00 μm and the Na I doublet at about 2.21 μm. The red part is dominated by the CO bandheads and another hot steam band.

The overall level of complexity in the K-band seems somewhat relaxed when compared to the H-band. Still, the flux maximum shifts slightly to longer wavelength with decreasing effective temperatures but since we are moving farther into the Rayleigh-Jeans tail of the SED at the covered effective temperatures, this effect gets less and less pronounced and the K-band continuum becomes less sensitive to changes in the effective temperature.

On the other hand the opacity of CIA by H_2 is strongest in the K-band, but its wavelength dependence is less steep and thus more monochromatic than in the H-band (see Borysow et al., 1997, Fig. 7, upper right panel). Hence, the shape variations of the pseudo-continuum with decreasing effective temperature are smaller than in the J and H-band.

The ^{12}CO bandheads get deeper with decreasing effective temperature (as is apparent from Figure 3.22) but also with decreasing surface gravity, since they are seen the strongest in M giants (Kleinmann & Hall, 1986). The hot steam band at the blue end of the K-band spectrum reacts similarly, lower effective temperature and lower surface gravity will strengthen the absorption. The sodium doublet at 2.21 μm shows opposite behaviour: the line gets shallower with decreasing effective temperature (McLean et al., 2003, Fig. 7,19) and with decreasing surface gravity (Lyubchik et al., 2004; Gorlova et al., 2003). The same applies for the stronger Ca I lines at 1.946, 1.951, 1.978, and 1.987 μm, where only the last three can be identified in the GQ Lup companion. Note also the non-detection of the Ca I doublet at 2.264 μm and the extremely weak Na I doublet at 2.336 μm. These lines disappear at spectral types later than M8 at this resolution. Hence all features in the K-band have the same cross-talk between surface gravity and effective temperature. The only exception seems to be the Mg I doublet at 2.28 μm, just before the onset of the first ^{12}CO bandhead. The feature gets stronger with later spectral type and is not seen earlier than L0. Unfortunately nothing is known about its surface gravity dependence (the line is e.g. not mentioned in Lyubchik et al., 2004), but it most likely shows a pressure broadening effect similarly to all other alkali metals and gets weaker with decreasing surface gravity. The non-detection of this line in the GQ Lup companion sets therefore

---

[7]SPEX: 0.8-5.5 Micron Medium-Resolution Spectrograph and Imager at the IRTF: the NASA Infrared Telescope Facility

only a weak constraint on the spectral type but adds to the impression that a spectral type later than L2 is most unlikely.

The best fit for the CO bandhead is formally achieved with the M6 dwarf, while the hot steam band is best matched by an M9 to L0 template. Note that a L0.5 already notably underestimates the flux in this region when the continuum level stays fixed at 2.29 μm. The metal lines, because of their sensitivity to surface gravity are weaker, thus (with the exception of the Mg I lines) mimicking a later spectral type than one would derive from the effective temperature alone.

Summary

In this section I have shown that the spectrum of the GQ Lup companion is in the very details reproducible by typical M and L dwarf spectra, giving further evidence that the observed wealth of spectral features in all bands in not noise but real. On the other hand a comparison with old field M and L dwarfs shows that a single template alone can not fit all the features seen in the GQ Lup companion and some features, like the depth of the K I lines in the J-band and the peculiar peak of H-band can not be reproduced at all by old M or L dwarfs but are clearly signs of low surface gravity, hence youth. As outlined before, neither is the determination of a spectral type unambiguous and ranges between M6 and L0, nor does it make much sense when one does not take the mismatch in surface gravity into account. In the cases where a later spectral types is preferred, it is thus mostly because of a lower effective temperature will mimic the effects of lower surface gravity. Hence, temperature-wise the spectral type best fitting the effective temperature of the GQ Lup companion is probably M6–M8.

Figure 3.21: NIRSPEC K-band spectral sequence of old (high surface gravity) stars and brown dwarfs from the BDSS. The scaled spectrum of the GQ Lup companion is overplotted in red. The flux is normalised to a point at 1.28 μm, just before the onset of the ^{12}CO bandhead. The common resolution is $\sim$2600. See annotations in Figure 3.4 for line identifications.

Figure 3.22: SPEX K-band spectral sequence of old (high surface gravity) stars and brown dwarfs from the SPEX/IRTF library. The scaled spectrum of the GQ Lup companion is overplotted in red. The flux is normalised to a point at 1.28 μm, just before the onset of the ^{12}CO bandhead. The common resolution is $R \sim 2000$. See annotations in Figure 3.4 for line identifications.

The special case of 2MASS J01415823-4633574

2MASS J01415823-4633574 was found to be a nearby object ($\sim$35 pc) and shows a very peculiar spectrum (Kirkpatrick et al., 2006). Low- and mid-resolution SPEX and NIR-SPEC spectra presented by Kirkpatrick et al. (2006) show typical features of low surface gravity, hence of a young object, such as shallow alkali lines, a fully intact H-band peak and a pronounced VO feature in J-band. Hence, this object could well serve as a prototype of a young low-mass object. However, it could not yet be assigned to a specific association and its age is thus unknown. Moreover, the spectrum does not look alike any other known M or L dwarf and fitting a synthetic model spectrum to 2MASS J01415823-4633574 shows that no model atmosphere, regardless of chosen effective temperature and surface gravity can reproduce the whole spectrum. Only after adding a blackbody with roughly the same effective temperature than the underlying model ($\sim$2000K) gives a reasonable, if not good, fit to the observed spectrum of 2MASS J01415823-4633574. This can be either interpreted as an indicator of an unusual thick cloud deck (or finer particle size distribution) in 2MASS J01415823-4633574 or as a sign of badly incorporated H_2 CIA opacities in the model. The details of this work are beyond the scope of this study and will be presented elsewhere (Schmidt at al., 2007). Either way, 2MASS J01415823-4633574 is likely too cool and too peculiar to serve as good comparison object to the GQ Lup companion in the sense to learn about its intrinsic parameters.

However, a simple comparison as shown in Figure 3.23 reveals the different sensitivities of the J, H and K-band to the effective temperature, since the surface gravity of 2MASS J01415823-4633574 and the GQ Lup companion is are most likely comparable. The match in the K-band is reasonable and judged from this band alone one could conclude that both objects are not too different. The H-band shows for the first time the intact triangular shape seen in the GQ Lup companion – hence no strong FeH absorption features – but the slope is already noticeably different. The J-band finally reveals the gross difference between 2MASS J01415823-4633574 and the GQ Lup companion.

This is an impressive demonstration that K-band spectroscopy alone has a severely reduced sensitivity to effective temperature and that the J-band will yield the highest constraint level, both on the effective temperature (from its slope) and to the surface gravity (from the depth of the alkali lines), followed in sensitivity by the shape of the H-band, by far outperforming the K-band at the given spectral resolution.
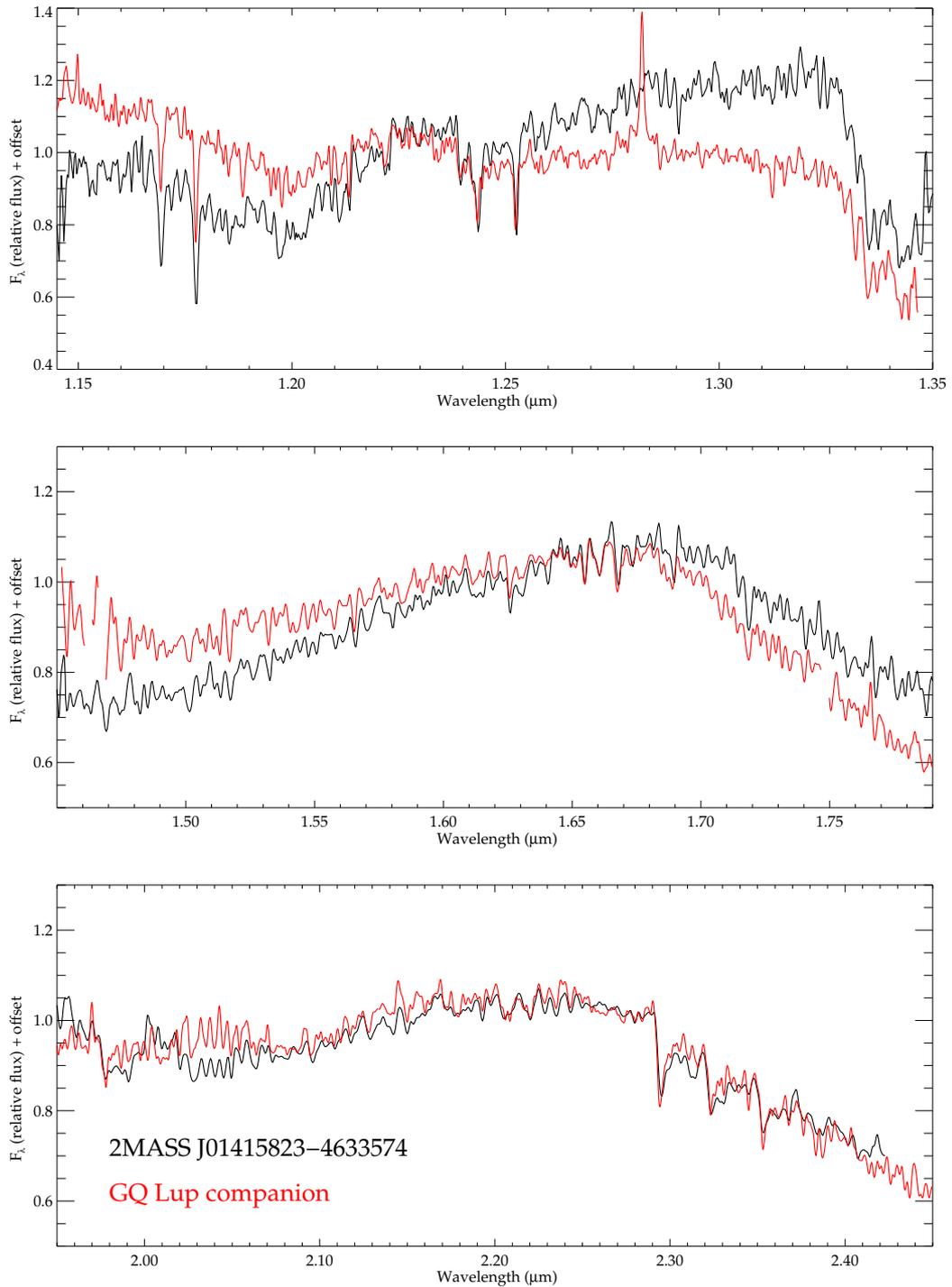
Figure 3.23: NIRSPEC J and SPEC HK-band spectra of 2MASS J01415823-4633574, a presumably young ($\log g \sim 3.5$–4.5) and cool ($T_{\text{eff}} \simeq 2000$ K) field dwarf (Kirkpatrick et al., 2006). The spectrum in electronic form was kindly provided by Davy Kirkpatrick. The scaled spectrum of the GQ Lup companion is overplotted in red. The common resolution is $R \sim 2500$ in J-band and ~ 1200 in H and K-band, respectively. See text for details.

Data analysis II – Comparison to synthetic model spectra

4

Given the difficulties in determining a spectral type, hence, an effective temperature from the current base of published mid-resolution M and L dwarf spectra, the next step is to fit the spectrum of the GQ Lup companion by synthetic atmospheric models to derive effective temperature and surface gravities by determining the best fit over a grid of spectral models, spanning the anticipated range of parameters.

Currently there are several groups producing synthetic spectra for low-mass stars, substellar objects and giant extrasolar planets:

1. Peter Hauschildt and France Allard, University of Hamburg and Observatoire de Lyon. The models (aka *Lyon* models) are based on the PHOENIX code (Hauschildt et al., 1999), a general purpose radiative transfer code with implemented linelists and opacity sources suited to represent the complex physics and chemistry in the atmospheres of cool objects (Allard et al., 2000). The PHOENIX code is also used by other groups who currently implement a complex dust treatment from self consistent dust models by Woitke & Helling (2003, 2004), improving the spectral synthesis in the region of cooler ($T_{\mathrm{eff}} \ll 2400$ K) substellar objects where dust settling becomes important.

2. Takashi Tsuji, University of Tokyo. The models are stand-alone LTE calculations including similar linelists and opacity tables as in the case of the PHOENIX models (see e.g. Tsuji & Ohnaka, 1995; Tsuji, 2002), also incorporating an empirical dust treatment.

3. Adam Burrows, University of Arizona. Burrows developed atmospheric models (aka *Arizona* models) for his own evolutionary models. His work is lately focused more on (irradiated) giant extrasolar planets (EGPs) (see e.g. Burrows et al., 1997, 2006).

4. Mark Marley & Andrew Ackerman, NASA Ames Research Center. Their work concentrated rather early on the chemistry and rainout of refractory elements in

the atmospheres of cool objects and their spectral models are rarely used for hotter objects, like low mass stars or heavy substellar objects (see e.g. Ackerman & Marley, 2001; Marley et al., 2002)

Only the first two groups made models over a wide grid of parameters available to me. These models allowed a spectral fitting of the spectrum of the GQ Lup companion at a level of detail and reliability that make the determination of physical parameters from spectral fitting a reasonable approach.

Methodology

To allow a quantitative analysis of physical parameters from the fitting of various spectral models, I use a χ^2 approach following Bevington & Robinson (2003). After normalising the respective continua of the measured spectrum and the synthetic model spectrum (that is to be fitted), a figure of merit for the fit in a certain wavelength window ranging from λ_1 to λ_2 is computed from

$$\chi_i^2 = \sum_{\lambda 1}^{\lambda 2} \frac{(F_\lambda^{obs} - F_\lambda^{model})^2}{\sigma_\lambda^2} \tag{4.1}$$

where σ denotes the noise in the measured spectrum. Afterwards, the χ^2 values are normalised to the number of pixels involved in the computation of each value. Hence, with this method I determine a reduced χ^2 that gives a measure to quantify the deviation of the respective model fit in relation to the noise in the measured spectrum.

The minimum of χ^2, calculated over the whole grid of effective temperatures and surface gravities for certain spectral feature or spectral sub-regions is searched for to determine the best fitting model, and thus, the most likely values of T_{eff} and $\log(g)$. Regions of $min(\chi^2) + 1, +4, +9$ indicate where the physical parameters deviate 1, 2, or 3 σ from their most likely value (see *Theorem D* in Press et al., 1992, Chapter 15.6).

Caution has to be taken with this approach since the strict analytical proof of this method assumes that the involved elements (here pixels) contain statistically independent information, which is not true since the pixel merely sample information that is linked via the instrumental (spectral) response function. Also, the face value of the minimal χ^2 looses its meaning since the quality of the fit does not primarily depend on the signal-to-noise level of the measurement (as it is assumed for a statistical approach towards χ^2) but is mainly limited by the spectral models themselves. Nonetheless, equation 4.1 represents a valid least-squares approach that will surely identify the point of the model grid where the synthetic spectra fits best to the measured spectrum in the chosen wavelength bin. The interpretation of the goodness-of-fit and the respective *deviations* from this optimum, hence, the quantification of the uncertainties of the sought-for parameters T_{eff} and $\log(g)$ have to be carefully reviewed on a case-by-case basis.

4.1   Fitting GAIA-cond models

A main source of synthetic spectra have been the models by Peter Hauschildt and France Allard. These spectra are used in the framework of evolutionary models by the group in Lyon (formost G. Chabrier, I. Baraffe, F. Allard and others), resulting in the BCAH98 and CBAH00 evolutionary tracks (Baraffe et al., 1998; Chabrier et al., 2000)), as already mentioned in Section 1.1 (see e.g. Homeier et al., 2005, for a short review). The incorporation of the spectral models allowed a major improvement in the evolutionary tracks over previous models, based on grey atmospheres. This advance led to the differentiation into distinct classes of models, mainly based on the different treatment of dust opacities in the atmospheres of cold, low-mass objects.

Following the nomenclature of these authors, the spectral models come in three different 'flavors'. DUSTY represents the case where dust forms in the atmosphere of cold objects at all places permitted in chemical equilibrium phase. The dust fully remains at its place of formation. Dust near an optical depth of one ($\tau = 1$) adds significantly to the total opacity and dominates the SED of the respective objects, causing very red NIR colours. COND represents the case where dust formes as in the DUSTY case but rains out completely from the photosphere into deeper layers and, hence, does not contribute at all to the total opacity. The region where $\tau = 1$ is free of dust and the NIR colours are much bluer than in the DUSTY models. Both cases represent two extremes in the evolution of brown dwarfs and planetary mass objects. DUSTY atmospheres seem appropriate to describe objects with effective temperatures between $\sim$2400 K and $\sim$1800 K, a temperature range where dust formes and most likely remains in higher atmospheric layers. COND atmospheres are representing objects with effective temperatures well below $\sim$1300 K, where most of the dust has rained out into deeper layers of the atmosphere (Allard et al., 2001). For effective temperatures above $\sim$2400 K, a domain where no (or only little) dust has formed, both models give the same result, since their treatment of dust formation and replenishment of refractive elements is the same. Since dust is yet not abundant enough it does not significantly contribute to the opacity in either model.

The process of dust settling, hence the domain of objects with temperatures of $\sim$1300 – 1800 K, is described by the *SETTL* models which try to bridge the gap between the two extreme cases of DUSTY and COND. Early versions of such models are released, yet too much fine tuning is needed in order to use a grid of SETTL spectra as a useful base for determining T_{eff} and $\log(g)$.

In late 2006, when I started the modeling, I retrieved a complete grid of GAIA-cond v2.0 spectra from Peter Hauschildt. The grid spans a range of $T_{\mathrm{eff}}{=}1800$–$3500\,\mathrm{K}$ in steps of 100 K and $\log(g){=}0.0$–6.0 in steps of 0.5 dex. The GAIA-cond grid (Brott & Hauschildt, 2005) is based on the COND models described above, with the major improvement of an enhanced water vapour line list (Barber et al., 2006). A comparison of such models and high resolution optical spectra of brown dwarfs (Reiners et al., 2007) showed a decent agreement between observations and theory but indicated also stronger deviations in some molecular bands and for atomic Na and K features.

Fitting of these models to the J, H and K-band SINFONI spectra of the GQ Lup companion is presented over the next couple of pages.

J band

The GAIA models for J-band lack the vanadium oxide (VO) band around 1.2 μm completely and have also shortcomings to reproduce the continuum up to the Paschen beta line, regardless of the chosen effective temperature and surface gravity. I thus decided to split the analysis in two parts:

(1) The water vapour feature longwards of 1.32 μm is fitted by normalising the continuum to the region from $\lambda\lambda$ 1.29–1.31 μm and deriving a χ^2 according to equation 4.1 from the full feature longwards of 1.32 μm including the relative continuum shape.

(2) The fit of the remaining part of the J-band shortwards of 1.32 μm follows a similar approach but is performed on the high-pass filtered spectra and model in order to balance the missing VO broad band opacity in the models by excluding broad features and fitting only narrow and unresolved lines. After the high-pass filter the continuum is rectified and normalised. Following equation 4.1, χ^2 values for the whole J-band between 1.135 and 1.32 μm as well as for distinct wavelength windows around sensitive features were computed. In Figure 4.1 I show the respective 1, 2 and 3σ contours in the T_{eff} –$\log(g)$ space for the H_2O feature, the K I doublets and the Na I line as well as for the whole spectral window of 1.135–1.32 μm . As is apparent from this plot, the best fit for the water vapour depression is only in marginal agreement with the metal features and both features react differently on the physical parameters. While the water vapour gives some
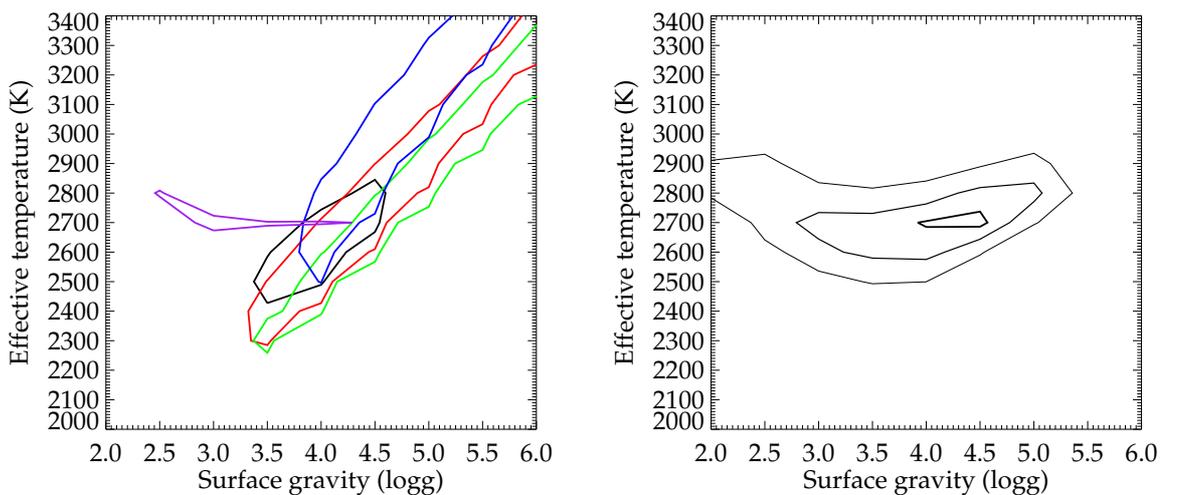
Figure 4.1: χ^2 values for the GAIA model fit in the J-band. *Left panel:* Contours for individual fits of the Na I line at 1.14 μm (blue), the K I doublet at 1.17 μm (red) and at 1.25 μm (green) as well as for the whole J-band (black) and the H_2O feature (purple). *Right panel:* Combined χ^2 values for the GAIA model fit in the entire J-band.

tight limits for the effective temperature ($\sim$2700 K) it is much less sensitive to the surface gravity, allowing basically $\log{(g)}$=2.5–4.2. In contrast, all metal features show equal sensitivity to both parameters with a high degree of correlation. The optimum set of parameters for the metal features is however somewhat shifted in respect to the the optimum for the water vapour, favouring higher surface gravities at $T_{\mathrm{eff}}\simeq$ 2700 K or too low temperatures at $\log{(g)}\leq$ 3.5. Combining the different χ^2 values to a final best fit of the whole J-band leads to the contours shown in the right panel of Figure 4.1, where I have relaxed the constraints on the overlapping χ^2 values.

The best fitting grid point and its deviations (observed - computed : O-C) values are shown in Figure 4.3. More figures of the same kind, exploring the possible parameter space are shown in the Appendix, page ii ff. For this fit (T_{eff}=2700 K, $\log{(g)}$=4.0) the water vapour band shows some overshoot, while the K I lines are too shallow. The latter can be improved with a slightly higher surface gravity, while the fit in the water vapour band can be improved by a slightly lower effective temperature. Hence, the best fit is probably achieved with T_{eff}=2650 K, $\log{(g)}$=4.2. Even better overall fits would require combinations of both parameters that are mutually exclusive. Note that this does not narrow the solution in a sense of reducing the 1σ uncertainties on the parameters but points to problems with the existing model grid at this wavelength regime.

Finally, in Figure 4.2 the fit is shown for the whole J-band with the preserved continuum to demonstrate the overall fit quality in the J-band.
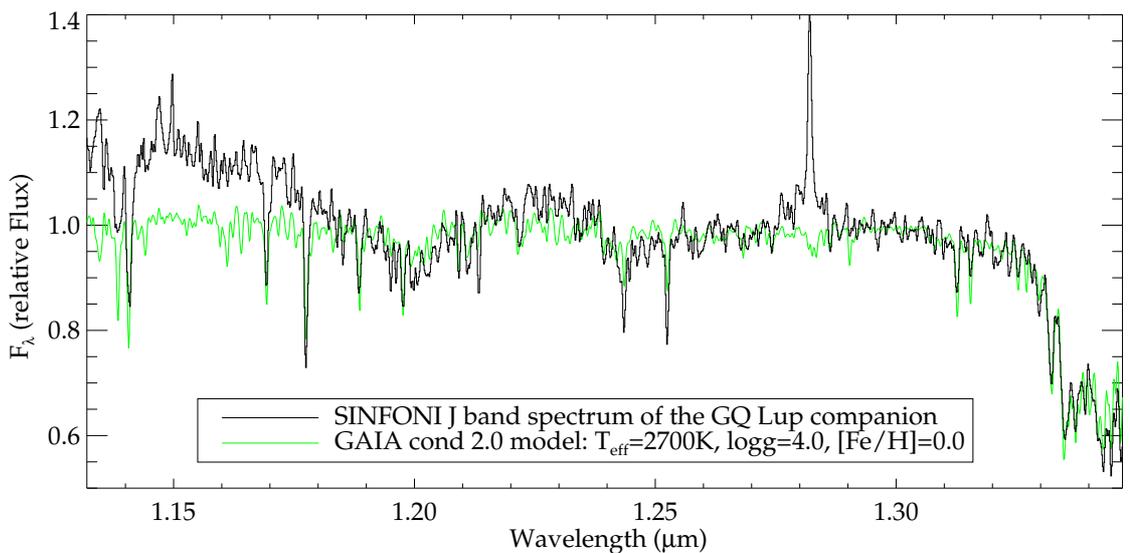
Figure 4.2: GAIA model fit (T_{eff}=2700 K, $\log{(g)}$=4.0) to the SINFONI J band spectrum of the GQ Lup companion. Same fit as in Figure 4.3 but showing both spectra with the original continuum.
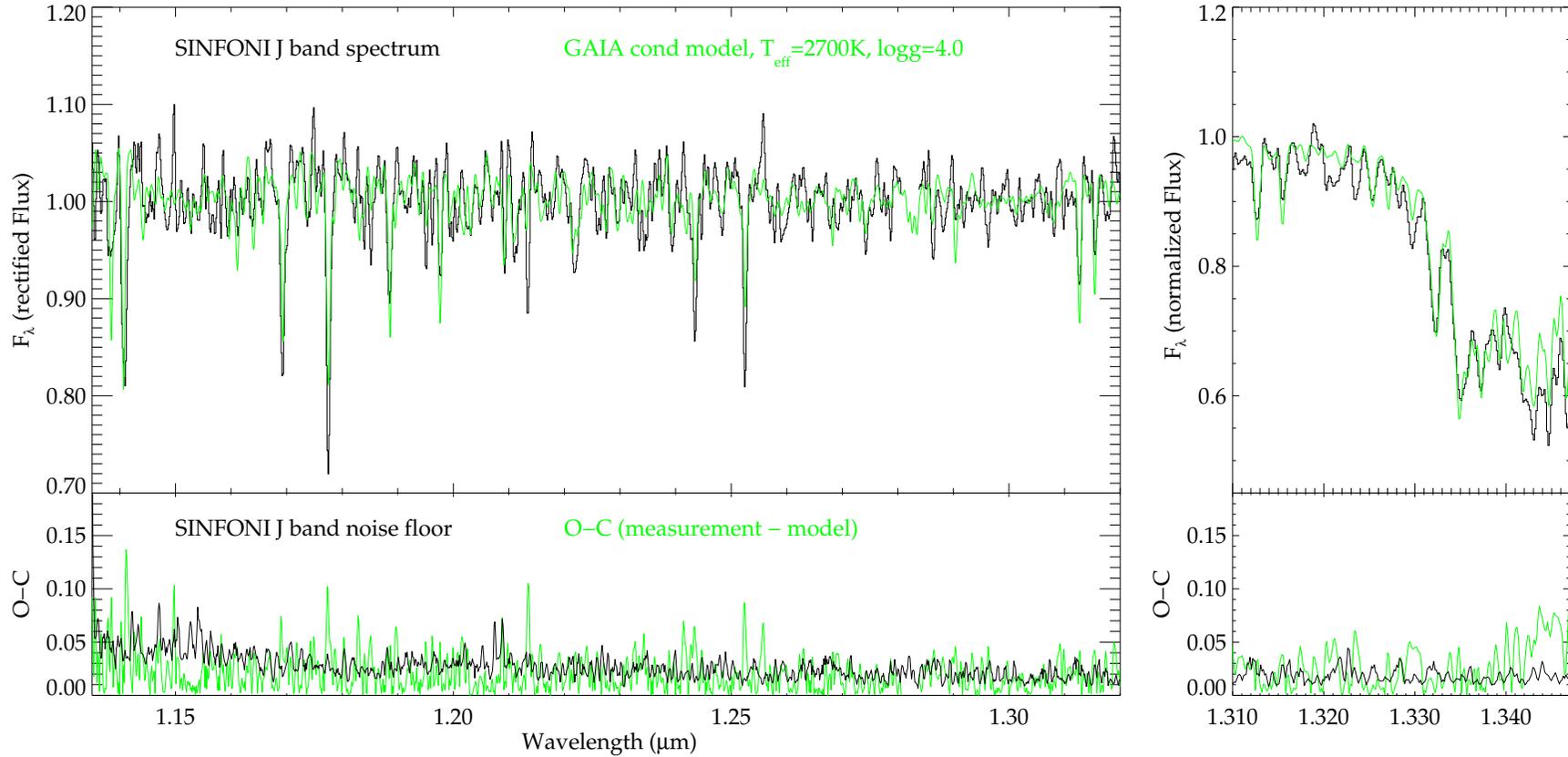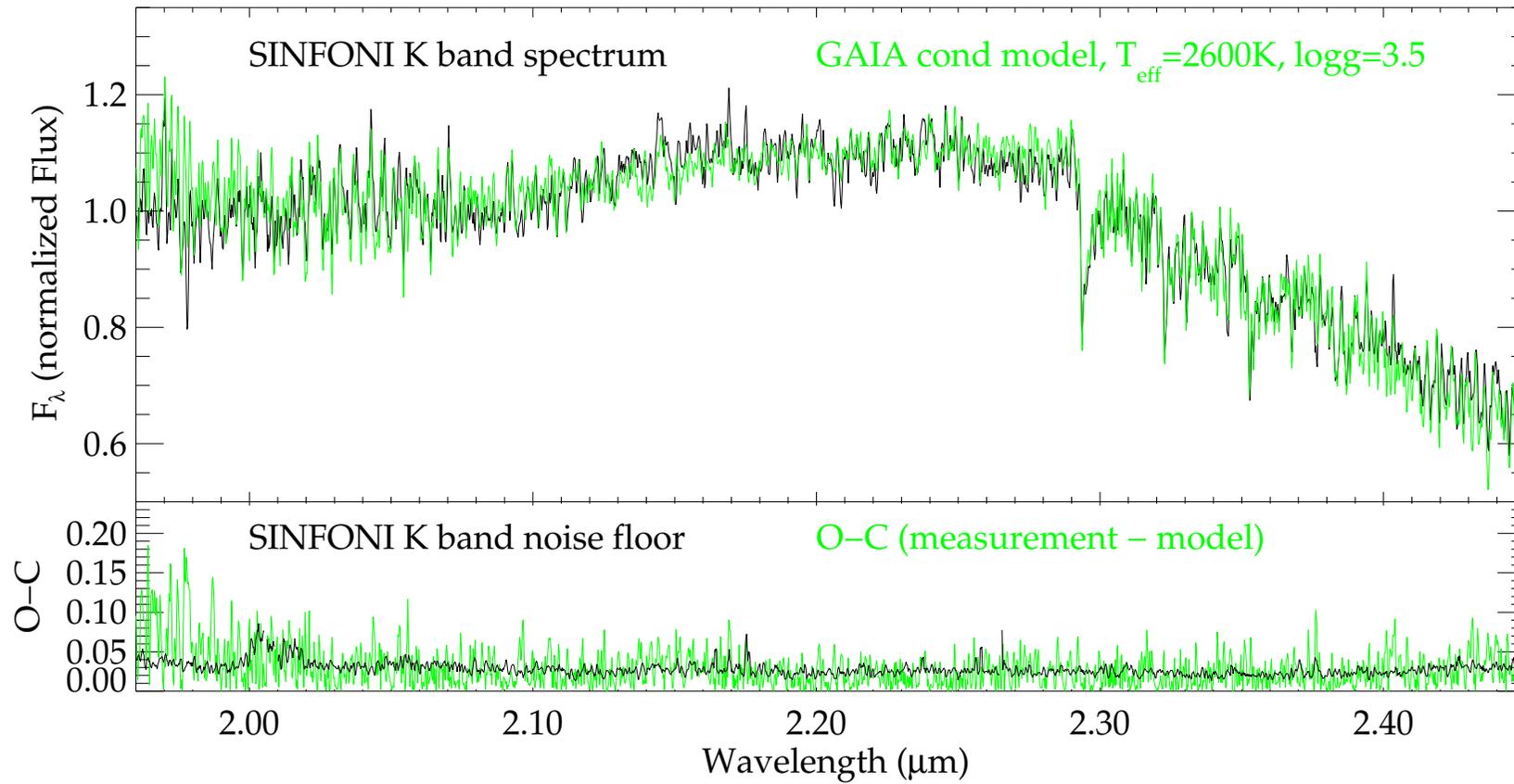
Figure 4.3: GAIA model fit (T_{eff}=2700 K, $\log(g)$=4.0) to the SINFONI J band spectrum of the GQ Lup companion. In the left uppermost panel the measured spectrum (black) is overplotted by the model (green) after rectification of the continuum. The upper right panel shows the same for the water vapour feature at the red end of the J-band, including the continuum shape. For both panels, the bottom panel shows the noise floor of the SINFONI spectrum (black) and the O-C values (observed - synthetic spectrum; green). Note especially the fit in the K I lines (see Figure 3.1 for line annotations) in the left panel and the water vapour band in the right panel.

H band

The GAIA models for H-band give a good representation of the continuum shape, so both collision induced absorption (CIA) by H_2 and the water vapour bands on either end of the H-band seems well incorporated in the models. However, the models seriously underestimate the strength of the FeH absorption for higher gravities (see the discussion on page 37). Thus, the surface gravities that the model fit suggest are generally unbound towards the high end and maybe shifted in whole by +0.5 dex. This is also witnessed by the missing lines in the centre of the H-band, the region where FeH has its most prominent features. In contrast, the water vapour bands are quite well fitted, with only slight overshoot when going to higher gravities.

The χ^2 contours, in this case calculated for the entire H-band as a whole, are shown in Figure 4.4. The best fitting grid point (T_{eff}=2700 K, $\log(g)$=4.0) and its deviations (observed - computed : O-C) values are shown in Figure 4.5. Only little improvement is possible by lowering T_{eff} or $\log(g)$ by 50 K and 0.5 dex, respectively. More figures of the same kind, exploring the possible parameter space are shown in the Appendix, page v ff. Note how the continuum in the blue wing of the H-band lies below the measured spectrum for $T_{\text{eff}} \leq 2500$ K and is generally too steep, while it is too low and generally to flat at $T_{\text{eff}} \geq 2800$ K.
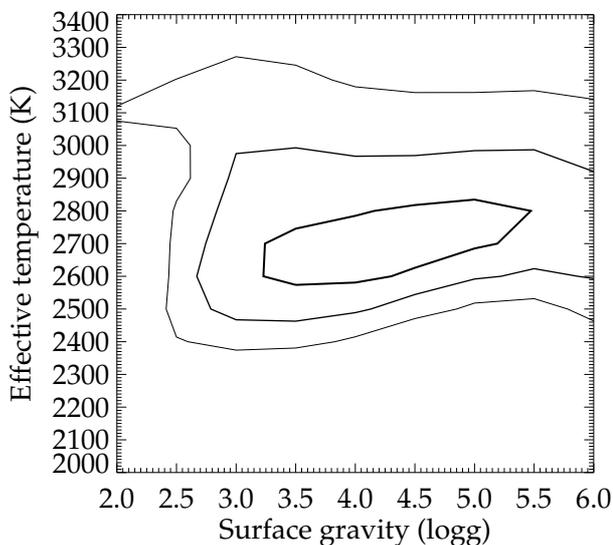
Figure 4.4: χ^2 values for the GAIA model fit in the H-band. Note that the models tend to overestimate the surface gravities slightly and seem unbound at the high end of the surface gravity.
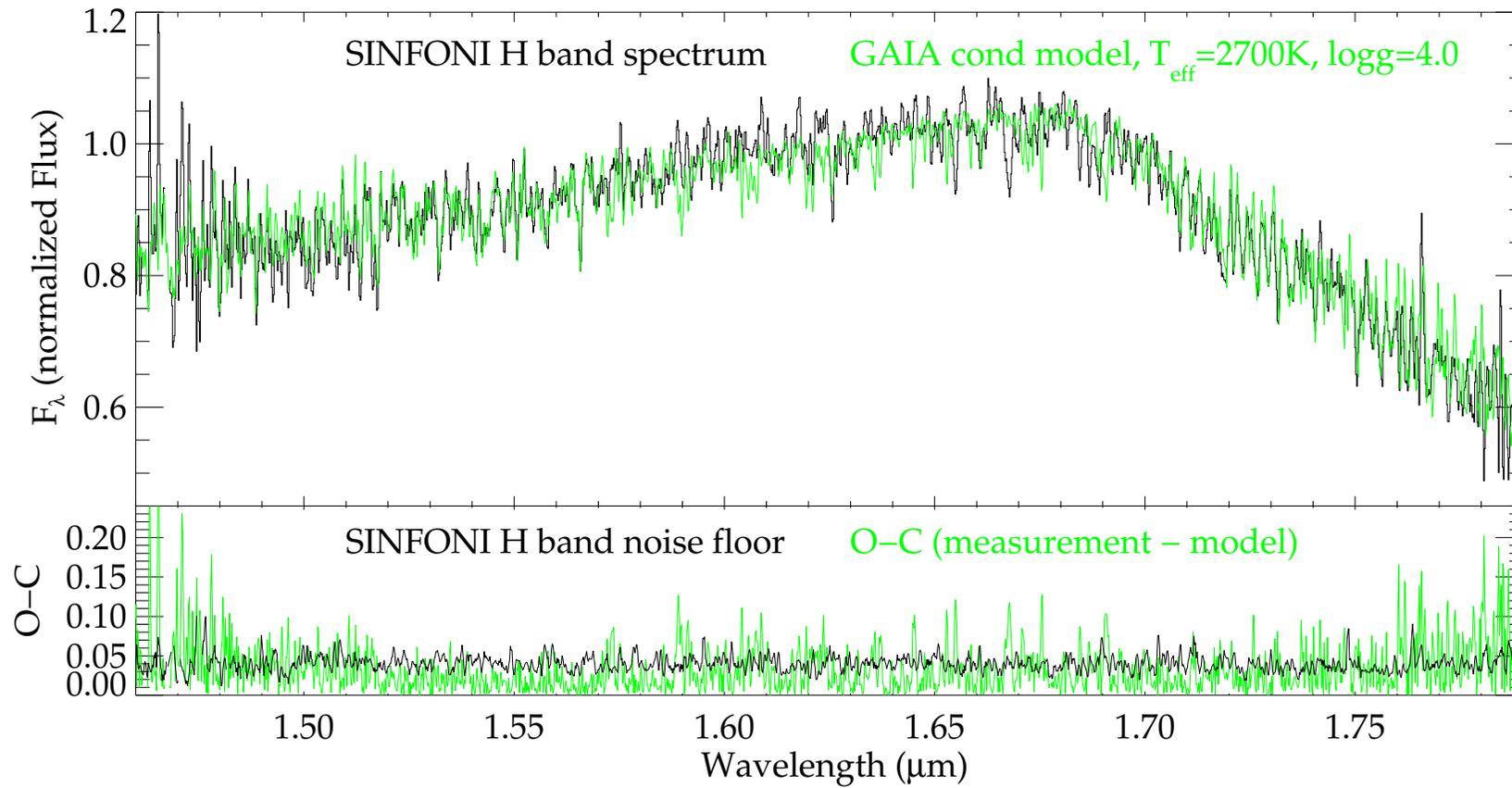
Figure 4.5: GAIA model fit $T_{\rm eff}$=2700 K, $\log{(g)}$=4.0) to the SINFONI H band spectrum of the GQ Lup companion. In the left uppermost panel the measured spectrum (black) is overplotted by the model (green). The lower panel shows the noise floor of the SINFONI spectrum (black) and the O-C values (observed - synthetic spectrum; green). See Figure 3.3 for line annotations.

K band

The GAIA models for K-band fit well to the continuum shape and the CO bandheads. A slight overshoot is noticeable though in the water vapour bands at both ends of the K-band. This overshoot is stronger than in H and K-band and the reasons can be manyfold. Either the oscillator strength of the lines in K-band is erroneous, or some physical reason, like a broad band excess emission induces a veiling that causes the lines in the measured spectrum to appear too shallow. One should also consider that the instrumental resolution in the K-band is somewhat degraded. An artificial smoothing of the model spectra does indeed improve the overall fit quality. The exact reason for the degraded fit stays dubious, since most of the lines are not resolved and highly blended. In addition the instrumental profile of SINFONI is hard to determine.

Still, the model fit gives tight constraints on the effective temperature, being in excellent agreement to the J and H-band. The surface gravity, however, is lower by about 0.5 dex than in the J-band. Note, that the fit of the sodium doublet at 2.20 μm would require a higher surface gravity than the best fit value of $\log{(g)} \simeq 3.5$, being again more in agreement with a value of $\log{(g)} \simeq 4.0$ or even slightly higher as derived from the J-band fit. This is especially noteworthy since the depth of individual lines in the K-band is generally rather overestimated in the K-band. Hence, this points to the same inconsistency involving the metal lines as in the J-band.

The χ^2 contours, in this case again calculated for the entire K-band as a whole, are shown in Figure 4.6. The best fitting grid point (T_{eff}=2600 K, $\log{(g)}$=3.5) and its deviations (observed - computed: O-C) values are shown in Figure 4.7. Some improvement is possible by incrising T_{eff} or $\log{(g)}$ by max. 50 K and 0.5 dex, respectively. More figures of the same kind, exploring the possible parameter space are shown in the Appendix, page viii ff. Note the overshoot in at both ends of the spectrum, while the continuum shape is well fitted.
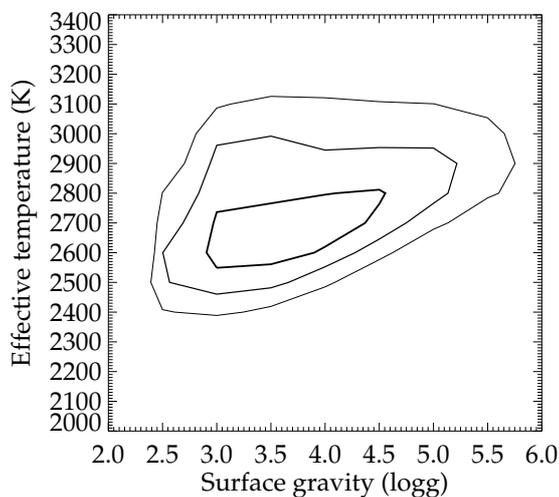
Figure 4.6: χ^2 values for the GAIA model fit in the K-band.

Figure 4.7: GAIA model fit (T_{eff}=2600 K, $\log{(g)}$=3.5) to the SINFONI K band spectrum of the GQ Lup companion. In the left uppermost panel the measured spectrum (black) is overplotted by the model (green). The lower panel shows the noise floor of the SINFONI spectrum (black) and the O-C values (observed - synthetic spectrum; green). See Figure 3.4 for line annotations.

Final χ^2 from GAIA-cond

The left panel of Figure 4.8 shows the χ^2 contours for the GAIA model fit of each of the three JHK bands, respectively. The overlap defines the final χ^2 and thus, the final best fit and uncertainties of T_{eff} and $\log{(g)}$ obtained from the GAIA models. As is apparent from Figure 4.8, all three bands give the same, rather tight constraints towards the effective temperature, with its best value of $T_{\mathrm{eff}}= 2650 \pm 100$ K.

The surface gravity is less constrained and the J-band points to a noticeably higher $\log{(g)}$ than the K-band. The overlap of all χ^2 contours would pinpoint the surface gravity to $\log{(g)}= 4.0 \pm 0.25$. Such tight constraints would however underestimate the uncertainties in the assumed metallicity (fixed at [M/H]=0.0) and would neglect the intrinsic inconsistencies observed in the fit of the metal lines, pointing to either a general shortcoming in the model grid or simply a slightly higher metallicity in the GQ Lup companion than solar.

Thus, I adopt $\log{(g)}= 3.7 \pm 0.5$ as the best guess for the surface gravity.
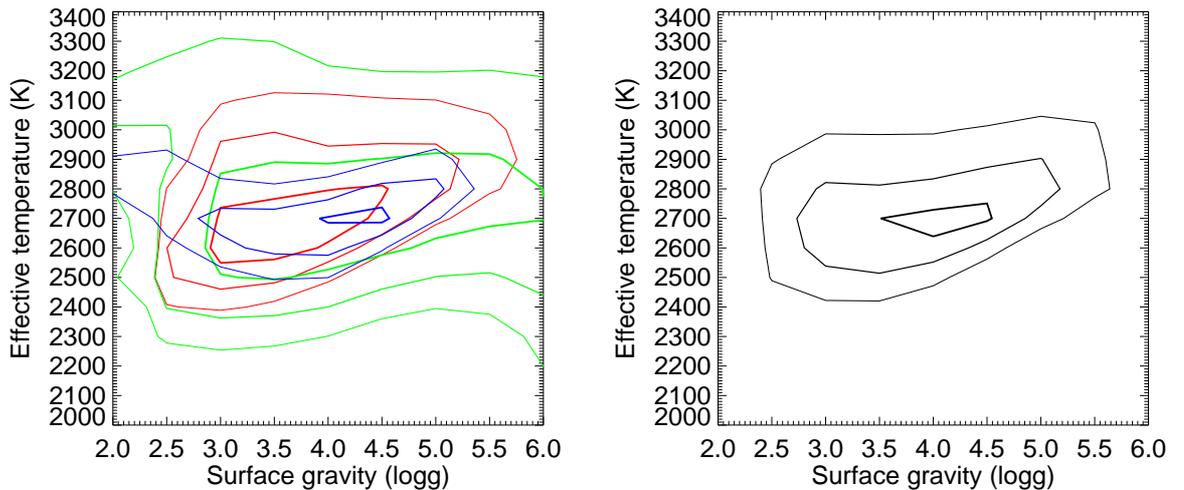
Figure 4.8: *Left panel:* χ^2 values for the GAIA model fit in the J-band (blue), H-band (green) and K-band (red). 1, 2, and 3 σ contours are coded by decreasing line thickness.*Right panel:* Final χ^2 values for the GAIA model fit, with slightly relaxed constraints on the surface gravity.

4.2   Fitting models by T. Tsuji

Takashi Tsuji (University of Tokyo, Japan) developed similar models than the ones origi-
nating from the PHOENIX code. Again, two cases were considered, representing the two
extremes in the treatment of dust in the atmosphere of ultracool dwarfs: A dusty model
in which dust grains are sustained throughout the photosphere (called *case B*, similar to
the DUSTY model class of the PHOENIX spectra) and a dust-segregated model in which
all the dust grains have precipitated below the observable photosphere (called *case C*,
similar to the COND model class of the PHOENIX spectra) (Tsuji, 2000). Other than
the group around Peter Hauschildt, Takashi Tsuji developed rather soon a common class
of models incorporating these two extremes and describing the transition between them
with a simple empirical rainout mechanism. The resulting unified photospheric model
of ultracool dwarfs is known as the Unified Cloudy Model (UCM) (Tsuji, 2000, 2001).
The transition between the extreme cases B and C (DUSTY and COND) would be the
equivalent of the SETTL models, however with a much simpler approach and a limited
list of dust species (three to be precise: Iron, corundum, and enstatite). The transition is
mainly governed by a critical temperature (T_{cr}) at which dust grains grow large enough
to segregate from the gas and precipitate below the photosphere. Thus, T_{cr} marks the
lower end of the cloud level in the atmosphere, while T_{cond} marks the upper level at which
temperatures are low enough for the formation of dust grains. Depending on the actual
value of the critical temperature (effectively regulating the thickness of the cloud deck) a
smooth transition from case B (T_{cr} well below the photosphere, hence $T_{cr} \ll T_{eff}$) to case
C ($T_{cr} \geq T_{eff}$) is reached.

   Takashi Tsuji was kind enough to make an expanded grid of UCM spectra at R∼50000
available to me. The grid extends now also to low surface gravities. I used the UCM in case
C, since it offered the widest parameter space (T_{eff}=1800–3000 K and log (g)=3.0–5.5) and
allowed a better comparison with the COND model used in the previous chapter. In an
overlapping region (T_{eff}=1800–2600 K) with a UCM of T_{cr}=1800 K, both models resulted
essentially in identical fits. As outlined above, at the expected effective temperature of
∼2700 K for the GQ Lup companion, no effect is expected from different dust treatment,
given that the effective temperature is higher than the condensation temperature for most
species (see also Tsuji et al., 1996, Fig. 2).

   The following model fitting used the same methodology as for the GAIA-cond model
grid. I shortly review the results achieved with the UCM grid for the three SINFONI
spectra:

J band

As is the case for the GAIA models, the UCM models lack the vanadium oxide (VO) band around 1.2 μm completely and have similar shortcomings to reproduce the continuum up to the Paschen beta line. This, is again independent of the chosen effective temperature and surface gravity. Thus the analysis had to follow the same approach as for the GAIA-cond grid, that is to rectify the continuum before fitting for wavelength shortwards of 1.31 μm.

In Figure 4.9 I show the respective 1σ contours in the T_{eff} –$\log(g)$ space for the H_2O feature and the K I doublets as well as for the whole spectral window of 1.135 − 1.32 μm. Other than for the GAIA model fit, the UCM fit shows a consistent result for the water vapour band (which is mainly sensitive to the effective temperature) and for the K I lines (being also quite sensitive for the surface gravity). The final best fit of the whole J-band was derived from the χ^2 contours shown in the right panel of Figure 4.1 (1–3σ contours) and yields T_{eff}=2700 K and $\log(g)$=4.0, very similar to the result obtained from fitting the GAIA grid.

The best fitting grid point and its deviations (observed - computed : O-C) values are shown in Figure 4.11. More figures of the same kind, exploring the possible parameter space are again shown in the Appendix, page xi ff. I note that the prominent Na I line at 1.14 μm and the weaker Aluminium doublet at 1.31 μm is missing in the UCM models. Also the model seems poorer in the overall content of spectral lines and performs also worse in reproducing the water vapour depression when compared to the GAIA model with the same basic parameters (T_{eff}=2700 K, $\log(g)$=4.0). However, the K I lines seem to fit better and would rather indicate a slightly lower surface gravity by max. -0.5 dex.
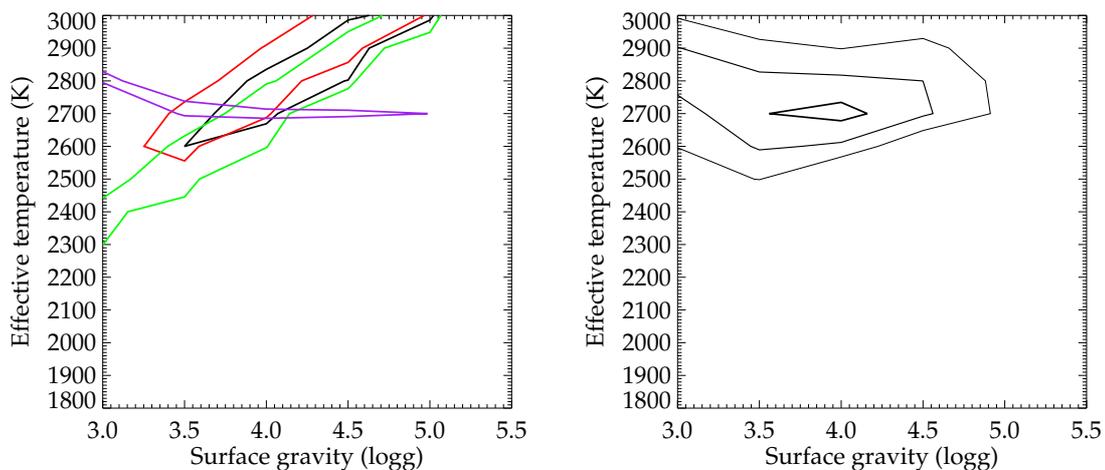
Figure 4.9: χ^2 values for the UCM fit in the J-band. *Left panel:* Contours for individual fits of the the K I doublet at 1.17 μm (red) and at 1.25 μm (green) as well as for the whole J-band (black) and the H_2O feature (purple). *Right panel:* Combined χ^2 values for the UCM model fit in the entire J-band.

However, the K I lines seem to fit better and would rather indicate a slightly lower surface gravity by max. -0.5 dex. Finally, in Figure 4.10 the fit is shown for the whole J-band with the preserved continuum to demonstrate the overall fit quality in the J-band.
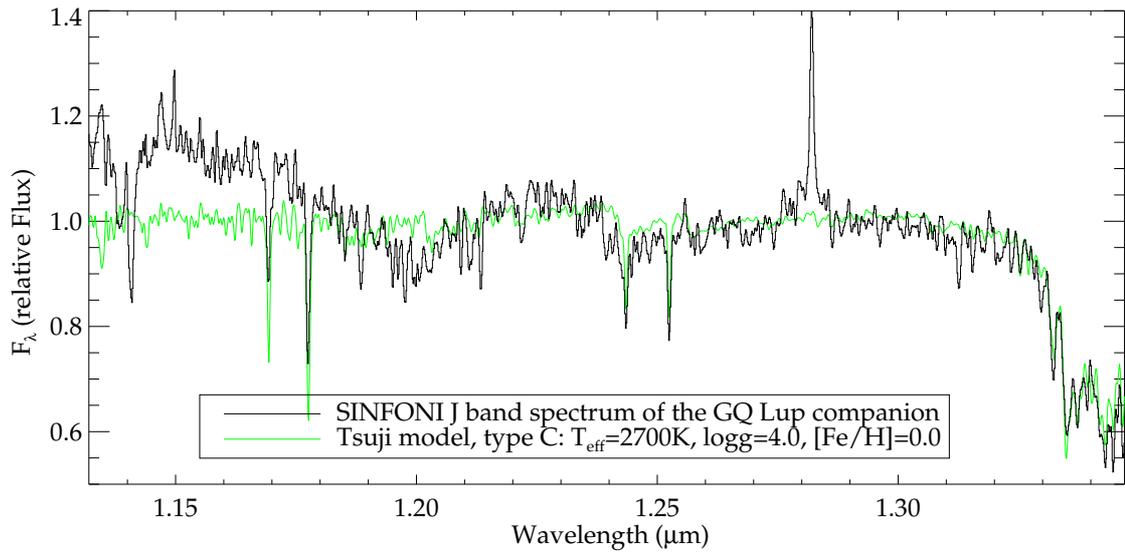
Figure 4.10: UCM model fit to the SINFONI J band spectrum of the GQ Lup companion. Same fit as in Figure 4.11 but showing both spectra with the original continuum.
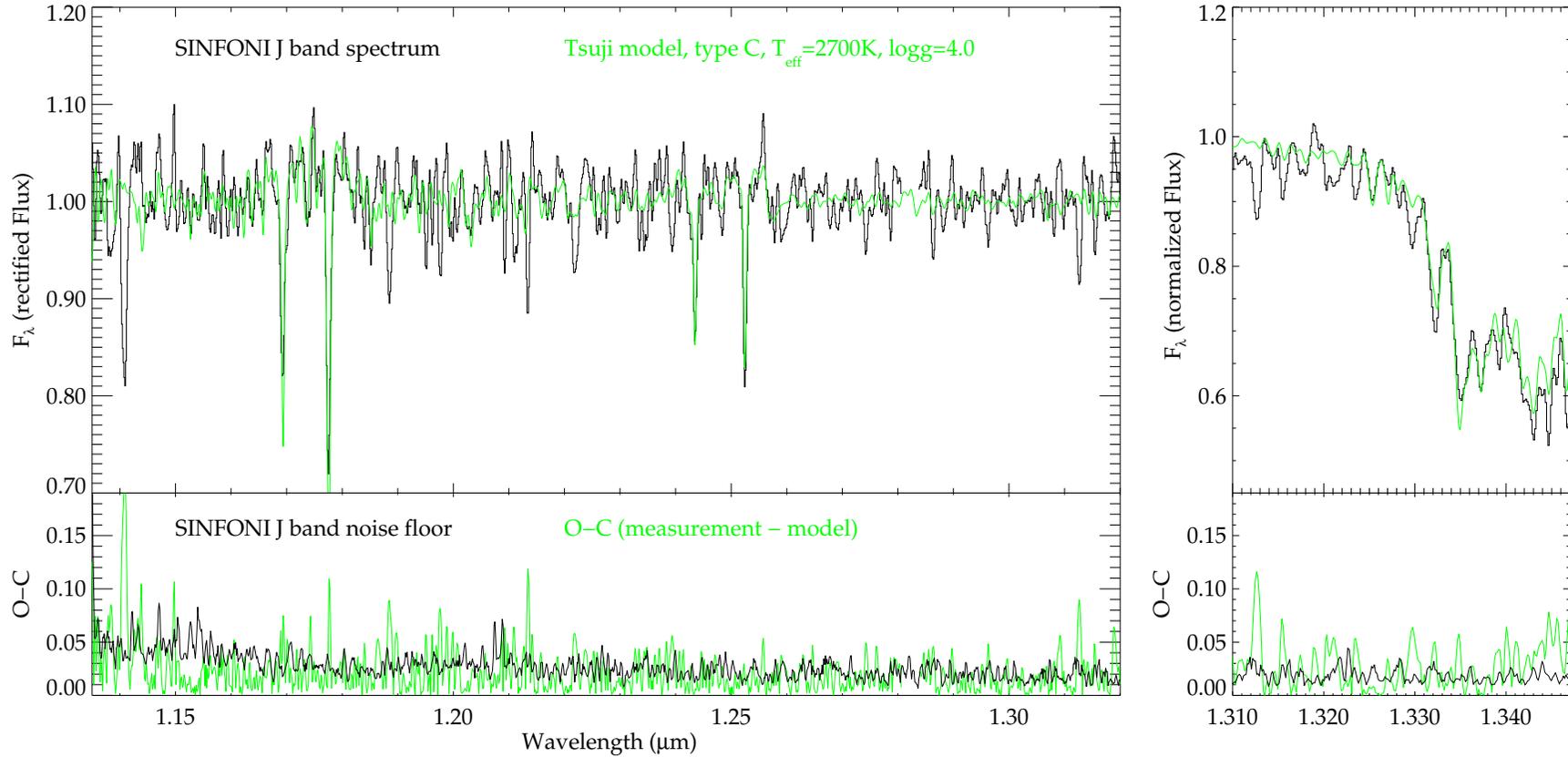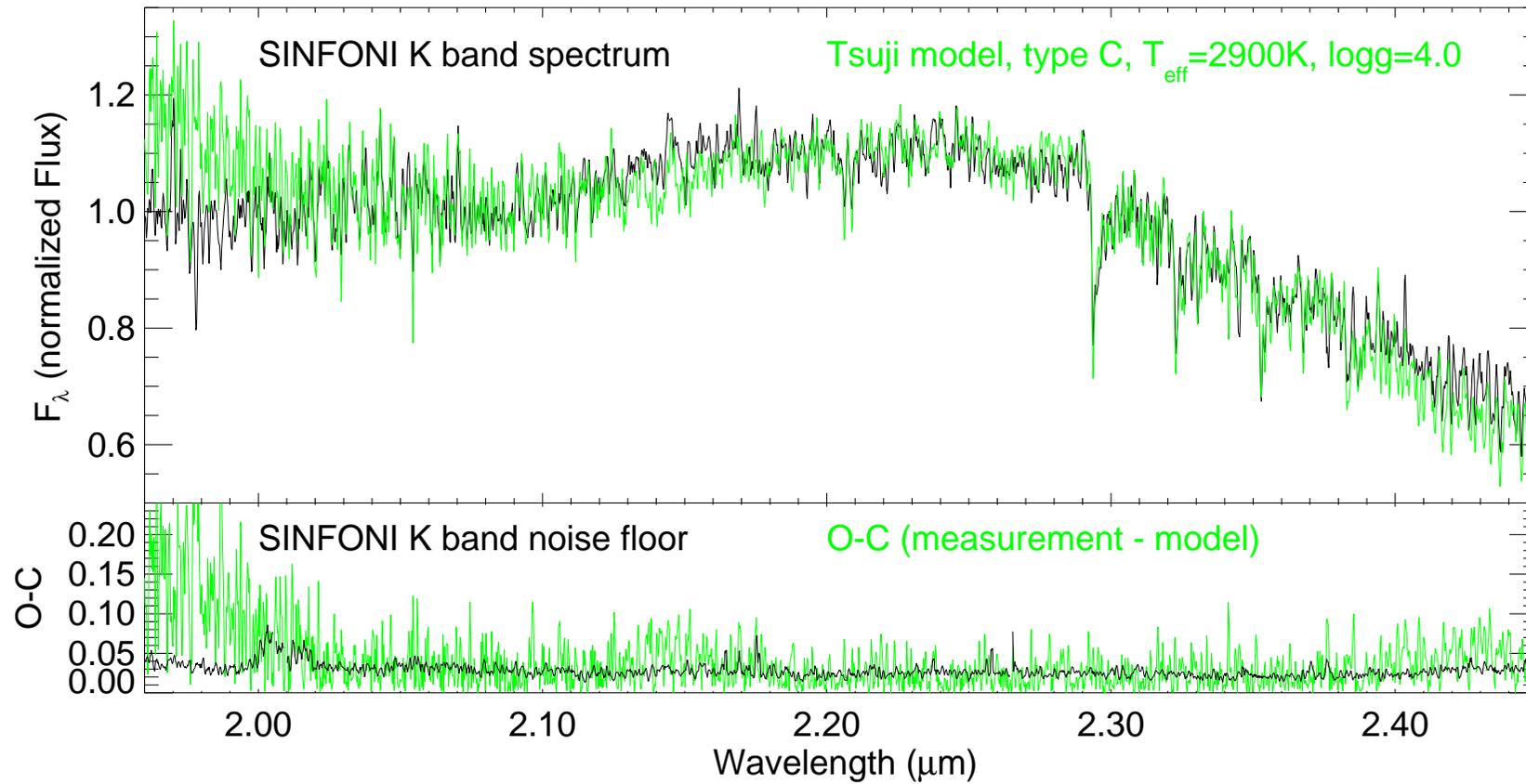
Figure 4.11: UCM fit (T_{eff}=2700 K, $\log{(g)}$=4.0) to the SINFONI J band spectrum of the GQ Lup companion. In the left uppermost panel the measured spectrum (black) is overplotted by the model (green) after rectification of the continuum. The upper right panel shows the same for the water vapour feature at the red end of the J-band, including the continuum shape. For both panels, the bottom panel shows the noise floor of the SINFONI spectrum (black) and the O-C values (observed - synthetic spectrum; green). Note especially the fit in the K I lines (see Figure 3.1 for line annotations) in the left panel and the water vapour band in the right panel.

H band

The UCM for H-band give a near-perfect representation of the continuum shape. However, as in the case of the GAIA grid, the models seriously underestimate the strength of the FeH absorption for higher gravities (see the discussion on page 37) and the overall line density is again lower as in the case of the GAIA models. Thus, the surface gravities that the model fit suggest are also generally unbound towards the high end and maybe shifted in whole by more than +0.5 dex. Again, quite a number of rather strong lines in the centre of the H-band are missing, a region where FeH has its most prominent features.

The χ^2 contours, in this case calculated for the entire H-band as a whole, are shown in Figure 4.12. The best fitting grid point and its deviations (observed - computed : O-C) values are shown in Figure 4.13. The best fit parameters are T_{eff}=2800 K, log (g)=5.0. Any deviation from this value degrades the fitting. More figures of the same kind, exploring the possible parameter space are shown in the Appendix, page xiv ff. Note how the continuum in the blue wing of the H-band gets too steep for T_{eff}< 2800 K and too flat for T_{eff}> 2800 K.
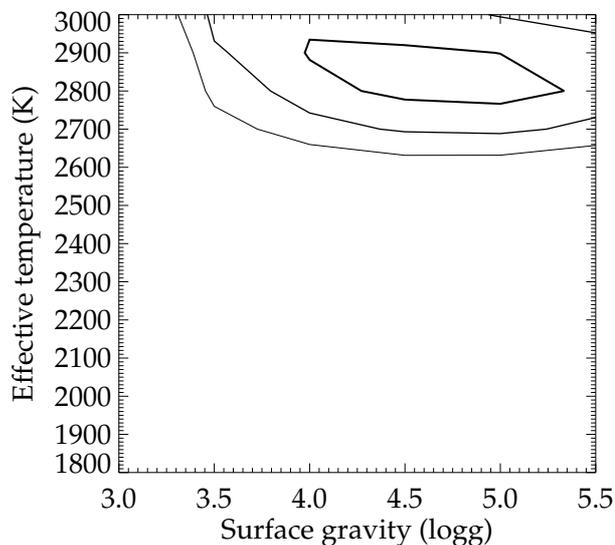
Figure 4.12: χ^2 values for the UCM fit in the H-band. Note that similar to the GAIA models, the UCM spectra tend to overestimate the surface gravities and seem unbound at the high end of the surface gravity.
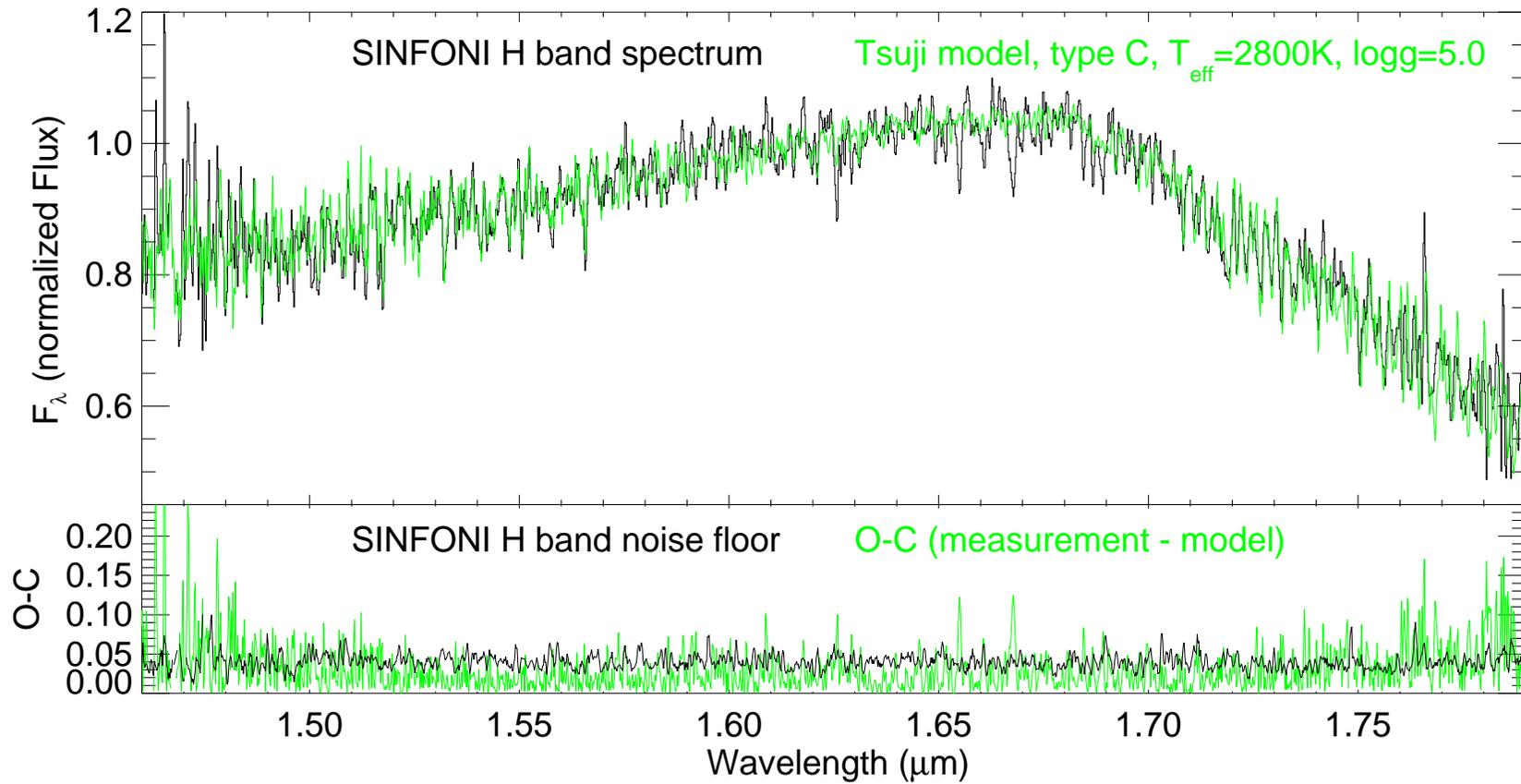
Figure 4.13: UCM fit (T_{eff}=2800 K, $\log{(g)}$=5.0) to the SINFONI H band spectrum of the GQ Lup companion. In the left uppermost panel the measured spectrum (black) is overplotted by the model (green). The lower panel shows the noise floor of the SINFONI spectrum (black) and the O-C values (observed - synthetic spectrum; blue). See Figure 3.3 for line annotations.

K band

The UCM for K-band show a degraded fit when compared to the GAIA models. A decent fit is only achieved at a rather high effective temperature ($T_{\text{eff}} \geq$ 2900 K) but the depth of the CO bandheads and the water vapour bands at either and of the K-band spectrum do not fit. The overshoot in the red end of the observed spectrum can be again attributed to excess emission from a disk which would also induce veiling that causes the lines in the measured spectrum to appear too shallow. In addition the same limitations to the reliability of the K-band spectrum apply as previously mentioned for GAIA grid fitting. Still, the UCM grid performs worse than the GAIA model grid and the effective temperature is inconsistent with the value obtained in the J-band. The χ^2 contours, in this case again calculated for the entire K-band as a whole, are shown in Figure 4.6. The best fitting grid point and its deviations (observed - computed : O-C) values are shown in Figure 4.15. The fit yields T_{eff}=2900 K, $\log(g)$=4.0. Note, that the fit of the sodium doublet at 2.20 μm would require a slightly higher surface gravity by $\sim$ 0.25 dex than the best fit value of $\log(g) \simeq$ 4.0. As can be seen from the figures in the Appendix, page xvii ff., a value of $\log(g)$=4.5 produces already an overshoot.

Only little improvement is possible by decreasing T_{eff} and increasing $\log(g)$ by max. 100 K and 0.5 dex, respectively. While a decrease in the effective temperature improves the fit in the blue part of the spectrum, the fit of the CO bandheads degrade. This can be partly compensated by increasing the surface gravity, but on the cost of a mismatch of the sodium doublet, see the figure for T_{eff}=2800 K, $\log(g)$=4.5 in the Appendix, page xvii ff.
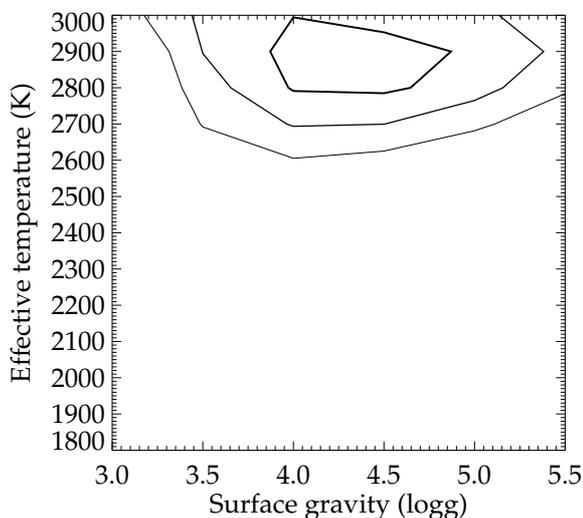
Figure 4.14: χ^2 values for the UCM fit in the K-band.

Figure 4.15: UCM fit (T_{eff}=2900 K, $\log{(g)}$=4.0) to the SINFONI K band spectrum of the GQ Lup companion. In the left uppermost panel the measured spectrum (black) is overplotted by the model (green). The lower panel shows the noise floor of the SINFONI spectrum (black) and the O-C values (observed - synthetic spectrum; green). See Figure 3.4 for line annotations.

Final χ^2 from UCM

The left panel of Figure 4.16 shows the χ^2 contours for the UCM fit of each of the three JHK bands, respectively. As in the case of the GAIA models, the overlap defines the final χ^2 and thus, the final best fit and uncertainties of T_{eff} and $\log(g)$ obtained from the GAIA models. In contrary to the GAIA model fit (see figure 4.8 for comparison), the H- and K-band yield a higher effective temperature (by nearly 200 K) than the J-band. Also the surface gravity is only marginally consistent. Hence the formally tight constraints for the physical parameters resulting from satisfying the best possible combined fit of all three bands are not representing these uncertainties and do not include the uncertainties in the assumed metallicity (fixed at [M/H]=0.0). Thus I have to adopt $T_{\text{eff}}= 2800 \pm 100$ K and $\log(g)= 4.0 \pm 0.5$ as the best guess for the sought for physical parameters from the UCM grid.
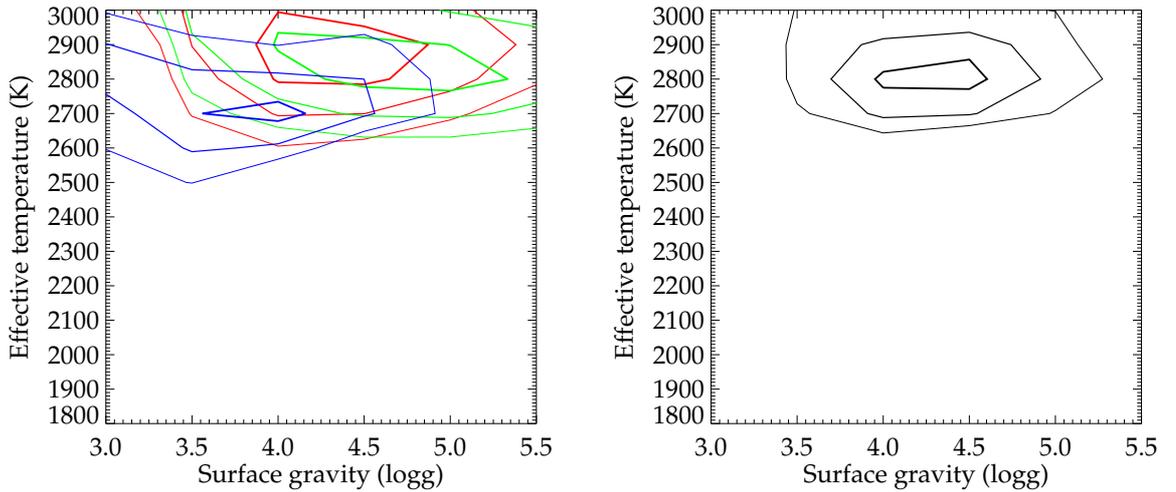
Figure 4.16: *Left panel:* χ^2 values for the UCM fit in the J-band (blue), H-band (green) and K-band (red). 1, 2, and 3 σ contours are coded by decreasing line thickness.*Right panel:* Final χ^2 values for the UCM fit.

4.3 Summary

UCM and GAIA models are yielding similar values for the effective temperature and the surface gravity of the GQ Lup companion that are consistent within their respective uncertainties, but clear differences in the internal consistency and fit quality are apparent.

While the GAIA models delivered a very consistent value for the effective temperature for all three bands, the surface gravity of the J-band is about 0.5 dex higher than the one obtained in from the K-band. Within the J-band the tight temperature constraint of the water vapor feature yields in turn a strong upper limit for the surface gravity when combined with the fit for the alakali metal features that are gravity sensitive. I have argued that the uncertainties in the fit of the metal lines are higher than for the water vapour, since the grid has a fixed metalicity (solar) and the alkali features are known to be not well represented in the current GAIA features (see the discussion in Reiners et al., 2007; Johnas et al., 2007).

Regardless of these uncertainties, the alkali lines in the J-band are (at the current spectral resolution) the most important gravity indicators and may only be superseded when the VO feature in the J band and the even more gravity sensitive FeH features in the H-band are better incorporated in the models. Once this is achieved, the H-band, currently delivering only extremly weak constraints could become a much better probe for the surface gravity, as indicated by low-resolution spectra of low-gravity objects. In this respect, the precision of the obtained surface gravity of the GQ Lup companion can certainly be improved, without the need of higher resolution spectra.

The UCM spectra showed a surprisingly different behavior. The J-band yielded an internally consistent fit from all features, even though the fit quality is not as good as for the GAIA models. The main reasons seems to be incomplete or outdated linelists. At lower temperatures and higher surface gravities the FeH features in the J-band are in shape much different of the ones regularly observed in L dwarfs. Aluminium and Sodium features in the J-band are also missing. Like the GAIA models, VO in the J-band and most features in the H- band are missing as well. Only the continuum shape in the H-band is well reproduced. In contrast to the GAIA models the fit from the three bands are only marginally consistent in effective temperature, with the H- and K-band yielding a higher effective temperature by almost 200 K.

Finally one should keep in mind that even though both models delivered (within the uncertainties) comparable values for the effective temperature and surface gravity of the GQ Lup companion, this is not necessarily a consistency check for the *accuracy* of these values. The concept of the effective temperature, as a measure defined over the global radiation budget and linked to the luminosty and radius of the object is hard to maintain easily for objects with high photospheric opacity, since at no part of the spectrum a true continuum can be observed and the photospheric depth at which a certain spectral feature is formed is variing strongly over the spectrum. It is thus not surprising that the first T_{eff} scales for late M and L dwarfs showed quite some spread in the predicted values for the same spectral class (see Golimowski et al., 2004, Sect. 4.4 for a review and further

references). With the availability of parallax measurements of many late M, L and T dwarfs (see e.g. Dahn et al., 2002; Vrba et al., 2004; Golimowski et al., 2004) one step towards an independent determination of effective temperatures from first principles was made. However, direcetly measured radii of late M dwarfs are scarce and for substellar objects not available at all. Thus, the improved T_{eff} scale from the forementioned authors is based on radii from the structural models.

At this point I want to emphasize that the effective temperature of the GQ Lup companion derived from spectral synthesis is well in agreement with the empircal spectral classification, done in Chapter 3.3, being M6–M8. This would translate into an effective temperature of 2850 K to 2400 K according to the scale of Golimowski et al. (2004), giving no indication for a further systematic offset of the derived effective temperature and I finally adopt $T_{\mathrm{eff}} = 2650 \pm 100$ and $\log(g) = 3.7 \pm 0.5$ as the best estimates from the spectral synthesis.

Equipped with these values, I can now derive the mass of the object, given its distance and luminosity. This will be the topic of the next chapter.

Conclusions

Science is the great antidote to the poison of enthusiasm...

Adam Smith

5.1 Physical parameters derived from spectroscopy

To determine the mass of the GQ Lup companion independently from evolutionary models, one needs its surface gravity and radius. The radius is not a direct observable, given the distance of the object and the order of magnitude of the expected value ($\sim$ one to several Jupiter radii). Thus, interferometric techniques to measure the radius directly are out of question. The only approach is to use the Stefan-Boltzmann law and resolve for the radius:

$$R = \sqrt{\frac{L}{4\pi\sigma_B T_{\text{eff}}^4}} \tag{5.1}$$

where $\sigma_B = 5.6705 \times 10^{-5}\,\text{erg}\,\text{cm}^{-2}\,\text{s}\,\text{K}^4$ is the Stefan-Boltzmann constant (in cgs units), L the luminosity and T_{eff} the effective temperature of the GQ Lup companion. The luminosity can be derived from the published K-band magnitude of $K_s = 13.1 \pm 0.2$ mag (Neuhäuser et al., 2005) and a bolometric correction. Based on the determined effective temperature, I find a bolometric correction for the K-band of $BC_{\text{K}} = 3.06 \pm 0.14$ mag using the polynomial fit from Golimowski et al. (2004, Table 4) in a range of M6 to M8. The spread in BC_{K} from the uncertainty in spectral type (or effective temperature) is only ± 0.03 mag but the rms of the fit is given as 0.13 mag The bolometric luminosity of the GQ Lup companion is thus:

$$\log\left(L/L_{\odot}\right) = \frac{BC_{\text{K}} + M_{\text{K}} - M_{\text{bol}\odot}}{2.5} \tag{5.2}$$

where BC_{K} is the previously determined bolometric correction, M_{K} is the absolute K-band magnitude and $M_{\text{bol}\odot} = 4.75$ mag is the absolute bolometric luminosity of the Sun. Adopting a distance of $d = 150 \pm 20$ pc to the GQ Lup companion (McElwain et al., 2007, and references therein), a more realistic estimate of the distance than the previously given $d = 140 \pm 50$ pc (Neuhäuser et al., 2005), the absolute K-band magnitude of the

GQ Lup companion is $M_{\rm K} = 7.22^{+0.37}_{-0.34}$ mag, where the error reflects the uncertainties in the relative magnitude and the uncertainty in distance. Thus, the luminosity according to Equ. 5.2 is

$$\log\left(L/L_\odot\right) = -2.21 \pm 0.15 \tag{5.3}$$

which is slightly different than the one given in Seifahrt et al. (2007) and takes now all error sources into account, the most dominant being still the uncertain distance[1]. Hence, the GQ Lup companion is clearly overluminous compared to average (old) field M6–M8 dwarfs, which have a luminosity of $\log\left(L/L_\odot\right) = -2.97$ to -3.40 (Golimowski et al., 2004, Table 6). This points to a larger radius for the GQ Lup companion than the ones of old field M6–M8 dwarfs. Using Equ. 5.1 I calculate a radius for the GQ Lup companion of

$$R = 3.63^{+0.75}_{-0.53} \; {\rm R_{Jup}} \tag{5.4}$$

where $L_\odot = 3.826 \times 10^{33} \, {\rm erg \, s^{-1}}$ is the luminosity of the Sun and $R_{\rm Jup} = 7.14 \times 10^9$ cm is the Jupiter radius. The uncertainty of the radius of the GQ Lup companion is calculated by formal error propagation, taking the smaller uncertainty in distance (likewise in luminosity) into account and is therefor smaller than the one given in Seifahrt et al. (2007)

Radius and surface gravity determine the mass:

$$M = \frac{g\,R^2}{G} = 26.6 \; {\rm M_{Jup}} \tag{5.5}$$

where $G = 6.674 \times 10^{-8} {\rm cm^3 \, g^{-1} \, s^{-2}}$ is the gravitational constant. Both, the surface gravity and the radius of the GQ Lup companion have unsymmetrical error margins, making a formal error propagation difficult. A worst case assessment yields constraints as low as $\sim 6 \; {\rm M_{Jup}}$ and as high as $\sim 120 \; {\rm M_{Jup}}$ for the mass of the GQ Lup companion. Note, however, that these values should not be understood as 1σ errors.

Moreover, the radius is in fact tied to the effective temperature. A higher surface gravity is usually compensated in the fit with a higher effective temperature, hence a smaller radius. Thus, this correlation yields smaller uncertainties than the worst case assessment given above. Still, the dominant source of uncertainty in the mass of the GQ Lup companion is the uncertainty in the surface gravity of ± 0.5 dex. At a fixed distance, the mass limits are 8 to 84 ${\rm M_{Jup}}$.

This approach in determining the mass of the GQ Lup companion has the advantage of being free from assumptions of evolutionary models, eventough its validity is bound to the physical assumptions of the synthetic atmospheres. At least in the case of the effective temperature we see however a good agreement with empirical relations, despite the difficulties involved when determining a spectral type from a one-dimensional scale (fixed in $\log\left(g\right)$ and [Fe/H]). The clear disadvantage is that the mass can not be pinpoint down more precisely and spans a range that is commonly attributed to planetary mass objects, brown dwarfs and even low-mass stars.

---

[1]The uncertainties in the luminosity are in fact as large $^{+0.28}_{-0.40}$ when adopting a distance of $d = 140 \pm 50$ pc as given in Neuhäuser et al. (2005).

5.2 Evolutionary models

As discussed in Point 2 and 3 of Section 1.1, the evolutionary models used in Neuhäuser et al. (2005) gave inconclusive results, lacking internal consistency when obtaining a mass from either the luminosity or the effective temperature. Since the newly derived effective temperature is significantly higher than the value of Neuhäuser et al. (2005) and also the luminosity of the GQ Lup companion had to be slightly revised, these changes might resolve the previous inconsistencies. In Fig. 5.1– 5.3 I plot the luminosity, effective temperature, radius and surface gravity of the GQ Lup companion into the models of Burrows et al. (1997)[2], Chabrier et al. (2000) and Baraffe et al. (2003)[3] and D'Antona & Mazzitelli (1997)[4]. Since the models of Wuchterl & Tscharnuter (2003) are not freely available, I use the figure from Neuhäuser et al. (2005) and overplot the new values for luminosity and effective temperature in Fig. 5.4.

Note the following remarks: The models by Burrows et al. (1997) are not complete towards young ages and low masses. Also, only the models for 'brown dwarfs' are considered here. The models of the Lyon group (Chabrier et al., 2000; Baraffe et al., 2003) are rather coarse in the time steps. The models of D'Antona & Mazzitelli (1997) are the only *hot start* models considered here that are based on grey atmospheres and the lowest mass track is for 0.020 $M_\odot$. Nonetheless, their performance is very good and their timesampling very high.

As can be seen from Fig. 5.1–5.3, luminosity and effective temperature fall on common mass tracks for all *hot start* models, hence, giving consistent values for the mass of the GQ Lup companion. The respective best fit values are $\sim$23, 31 and 26 $M_{\rm Jup}$ for the three models, respectively. These values are very close to the best value obtained independently from the evolutionary models, calculated from the radius (in turn derived from luminosity and effective temperature) and surface gravity alone.

Note, that the radius of the GQ Lup companion, plotted in the lower left panel of Fig. 5.1–5.3 is offering no additional constraint to the mass, since it is not directly measured but computed according to Equ. 5.1. However, it offers an additional check for the consistency of the measured values of luminosity and effective temperature, that are now linked by the evolutionary models. As becomes also apparent from these plots, the surface gravity is no good indicator for the mass when being combined with evolutionary models, especially when being uncertain by $\pm$0.5 dex.

---

[2]Obtained   from   the   *Brown   Dwarf   and   Extra-Solar   Giant   Planet   Calculator*   on `http://zenith.as.arizona.edu/~burrows/cgi-bin/browndwarf3.cgi`
[3]Obtained from `http://perso.ens-lyon.fr/isabelle.baraffe/`
[4]Obtained from `http://www.mporzio.astro.it/~dantona/prems.html`
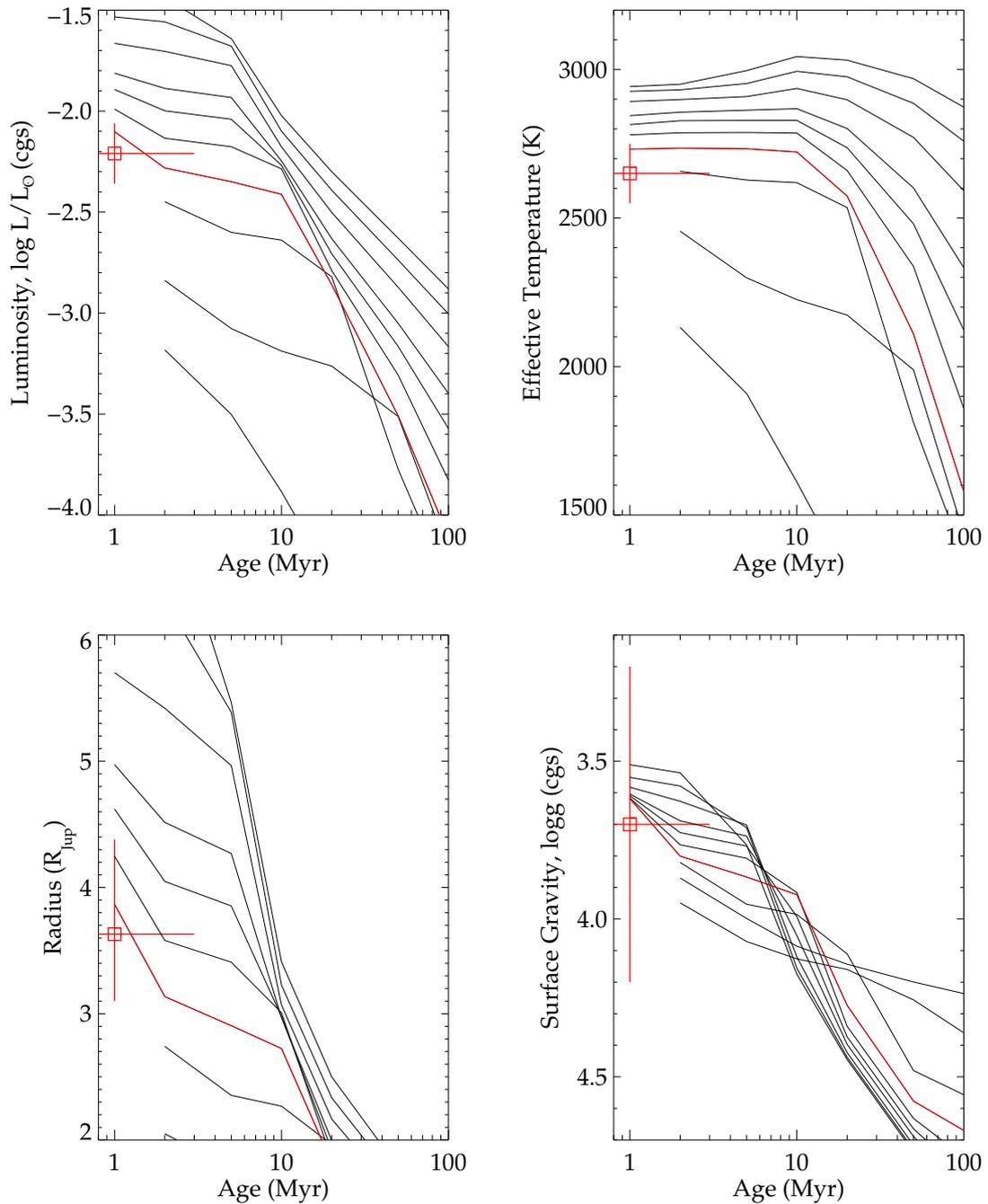
Figure 5.1: Evolutionary model by Burrows et al. (1997). Tracks for masses of 70, 60, 50, 40, 35, 30, 25, 20, 15, and 10 M_{Jup} (top to bottom) are shown. Note that lower mass tracks do not extend in age below 2 Myrs. The respective values of the GQ Lup companion are given as the red datapoint. Among the available tracks, the one for 25 M_{Jup} is fitting best and is outlined in red. Since this track is slightly too hot and luminous, a slightly lower mass should fit even better.
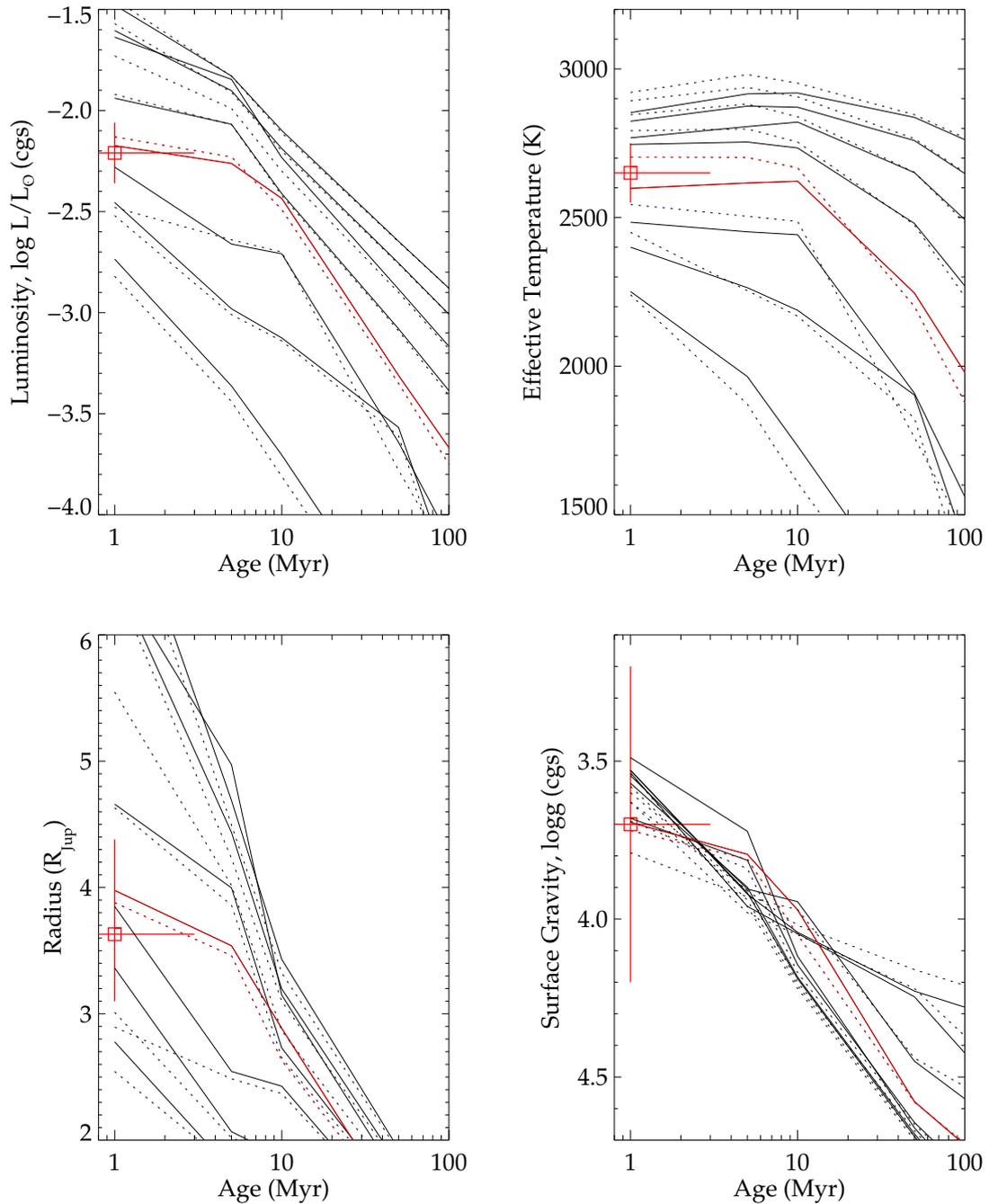
Figure 5.2: Evolutionary model by Baraffe et al. (2003) (COND, solid lines) and Chabrier et al. (2000) (DUSTY, dashed lines). Tracks for masses of 0.070, 0.060, 0.050, 0.040, 0.030, 0.020, 0.015, and 0.010 $M_\odot$ (top to bottom) are shown. The respective values of the GQ Lup companion are given as the red datapoint. Among the available tracks, the one for 0.030 $M_\odot$ ($\sim 31\ M_{\mathrm{Jup}}$) is fitting best and is outlined in red for both model classes.
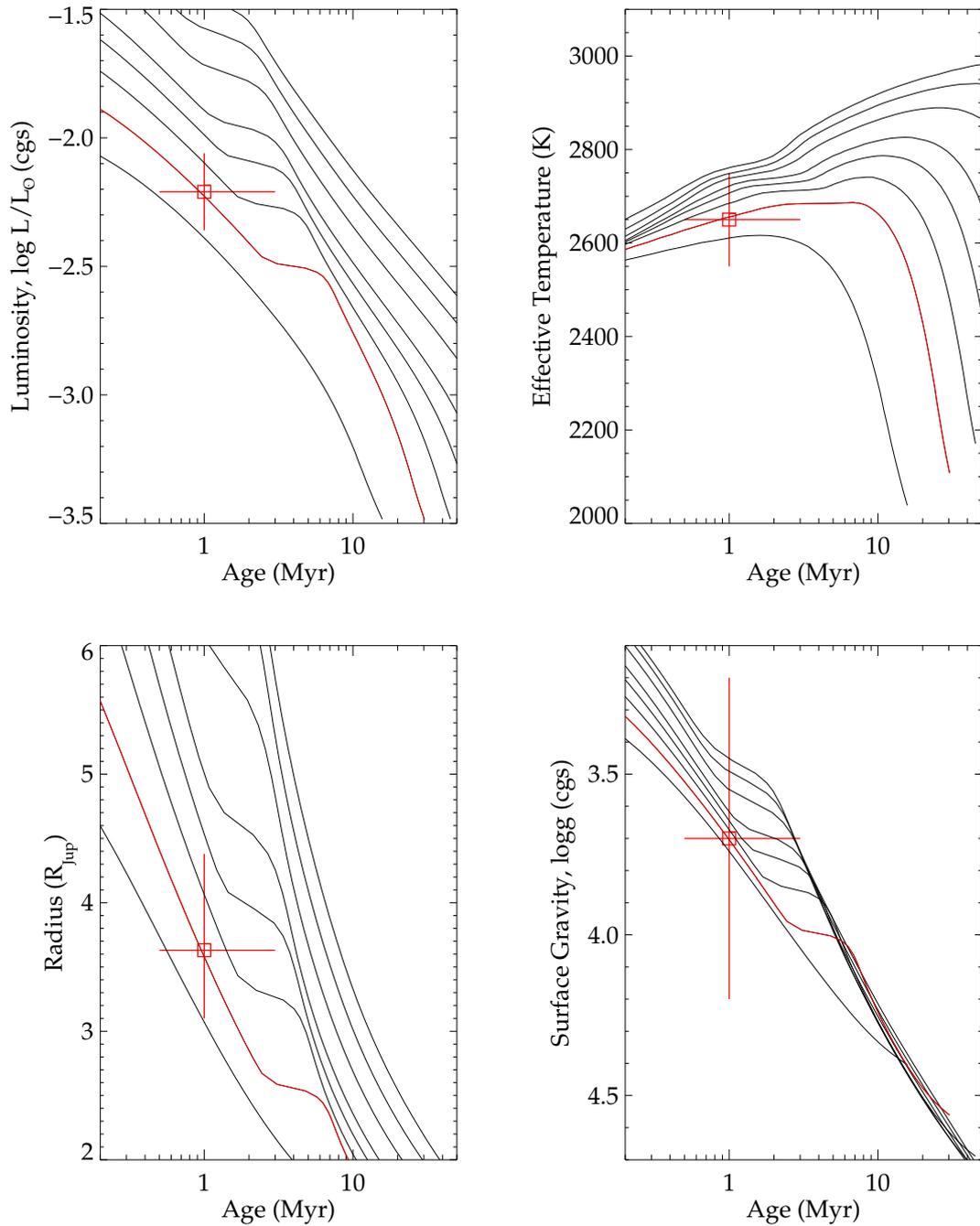
Figure 5.3: Evolutionary model by D'Antona & Mazzitelli (1997, 1998). Tracks for masses of 0.070, 0.060, 0.050, 0.040, 0.035, 0.030, 0.025, and 0.020 $M_{\odot}$ (top to bottom) are shown. Note the different scale for these plots when compares to previous two figures. The respective values of the GQ Lup companion are given as the red datapoint. Among the available tracks, the one for 0.025 $M_{\odot}$ ($\sim$ 26 M_{Jup}) is fitting best and is outlined in red.

The new values for luminosity and effective temperature of the GQ Lup companion still yield a very low mass when put in the synthetic HR diagram, taken from Neuhäuser et al. (2005, Fig. 4). The values fall right onto a mass track of 5 M_{Jup} planet. However, extrapolating from this plot the parameter space of brown dwarfs (the lowest mass track being the one for 13 M_{Jup}), the mass of the GQ Lup companion could be about 10 M_{Jup} according to these models. Taking the factor 3 into account that would be needed to bring 2M0535-05 B from its location on the 13 M_{Jup} track to its actual mass of 38 M_{Jup}, the brown dwarf tracks of Wuchterl & Tscharnuter (2003) would yield a mass of $\sim$ 30 M_{Jup} for the GQ Lup companion, comparable to the results obtained from the *hot start* models.
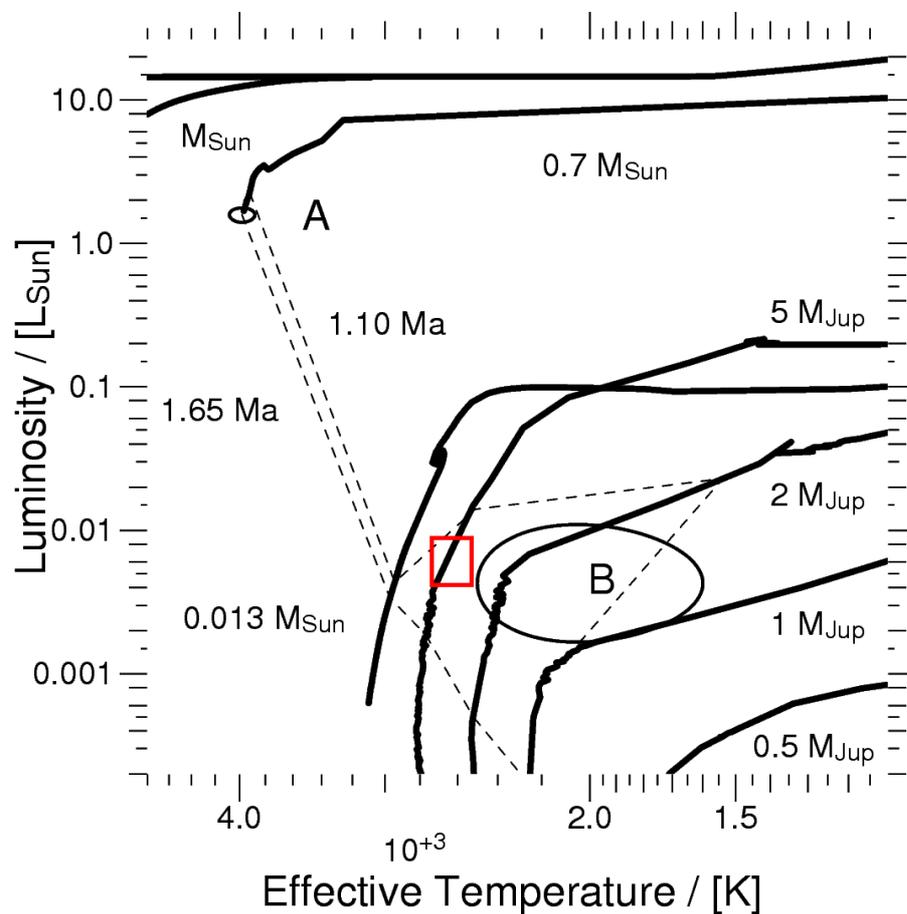
Figure 5.4: HR-Diagram from Neuhäuser et al. (2005, Fig. 4) showing tracks of Wuchterl & Tscharnuter (2003) plus additional tracks calculated by G. Wuchterl. Tracks for 1.0 and 0.7 as well as 0.013 $M_{\odot}$ (top to bottom) are from collapse calculations of initially marginally unstable Bonnor-Ebert-spheres. Planetary tracks for 5, 2, 1, and $0.5 M_{Jup}$ are models obtained in the framework of the nucleated instability hypothesis (Wuchterl, 2000). isochrones (dashed lines) for 1.10 and 1.65 Myrs are shown. The new location of the GQ Lup companion is plotted as the red box (1σ errors).

5.3 Putting the GQ Lup companion into context

Comparison to 2MASS J05352184-0546085

The recent discovery of the first brown-dwarf eclipsing binary system in the Orion Nebula Cluster, 2MASS J05352184-0546085 (hereafter 2M0535-05) by Stassun et al. (2006) set the first *lighthouse* into the regime of young low-mass objects and an anchor point for the evolutionary models. With masses of $M_1 = 60$ M_{Jup} and $M_2 = 38$ M_{Jup}, accurate to 10% and free from other physical assumptions than the laws of gravity, this object is an ideal comparison object for the GQ Lup companion. The remarking temperature reversal of 2M0535-05 (the more massive primary being cooler than the less massive secondary) is most likely an effect of a strong magnetic field on the primary. This theory was brought forth by Chabrier et al. (2007), who showed that a significant coverage by starspots originating from the magnetic field yields a smaller heat flux output, i.e. cooler T_{eff} and thus larger radii, since the total energy output (hence the luminosity) stays unaffected and the object has to compensate the smaller net- T_{eff} with a larger radius. A solution with a spot coverage of 50% for the primary and 20% for secondary of 2M0535-05 reproduces radius values within the error bars and a temperature reversal as observed by Stassun et al. (2006). Further evidence for the theory for an activity induced temperature reversal in 2M0535-05 was presented by Reiners et al. (2007) who measured a much stronger $H\alpha$ emission line in the primary than in the secondary with VLT/UVES during the respective eclipses.

Thus, when comparing both components of 2M0535-05 to the GQ Lup companion one has to keep in mind, that the primary is too cool and too large for its age and mass. According to Chabrier et al. (2007, Fig. 2) the primary of 2M0535-05 could well be ~ 500 K hotter when being spot-free (instead of the proposed coverage fraction of 50%). Given the age for 2M0535-05 of 1^{+2}_{-1} Myr (Stassun et al., 2007, see references therein) being comparable to the one of GQ Lup (Neuhäuser et al., 2005; McElwain et al., 2007), both objects should be in a very similar evolutionary stage.

Table 5.1 compares the physical parameters of 2M0535-05 obtained from the literature with the ones for the GQ Lup companion obtained in this work.

Table 5.1: Comparing the GQ Lup companion to 2M0535-05 A and B

	GQ Lup comp.	2M0535-05 A[a]	2M0535-05 B[a]
Spectral type	M7 $\pm$ 1	M6.5 $\pm$ 0.5	M6.5 $\pm$ 0.5
Effective temperature, T_{eff} (K)	2650 $\pm$ 100	2700 $\pm$ 200	2800 $\pm$ 200
Luminosity, $\log L_{bol}/L_{\odot}$	-2.21 ± 0.15	-1.65 ± 0.07	-1.83 ± 0.07
Surface gravity, $\log g$ (cgs)	3.7 $\pm$ 0.5	3.62 $\pm$ 0.1	3.54 $\pm$ 0.09
Radius, R (R_{Jup})	3.63 $^{+0.75}_{-0.53}$	6.58 $\pm$ 0.22	4.74 $\pm$ 0.18
Mass, M (M_{Jup})	$\sim$27	60 $\pm$ 5	38 $\pm$ 3

[a]All values from Stassun et al. (2007, Tab.5), except for the luminosity and effective temperature, which are taken from Stassun et al. (2007, Sect. 3.3) and Reiners et al. (2007).

From table 5.1 it becomes apparent that the GQ Lup companion has a much smaller radius than 2M0535-05 A at about the same surface gravity. Given that the effective temperature of 2M0535-05 A is diminished by about 500 K due to the beforementioned effects (as is its spectral type too late), the GQ Lup companion is also cooler and less luminous than 2M0535-05 A. Hence, it is quite certain that the GQ Lup companion is lower in mass than 2M0535-05 A. As for 2M0535-05 B, we still find a smaller radius, but similar effective temperatures and surface gravity, and consistently a smaller luminosity. Hence, at the same age, the GQ Lup companion would only be slightly less massive than 2M0535-05 B. Only if the GQ Lup companion would be older than 2M0535-05 B (more like 5-10 Myr, as argued by McElwain et al., 2007), a higher surface gravity within its present uncertainties would make the GQ Lup companion an aged twin of 2M0535-05 B with a smaller radius and likewise lower effective temperature. The other extreme, a much younger age (<1 Myr) would be the only reason to assign also a much smaller mass to the GQ Lup companion, then having indeed a surface gravity at the lower end of the proposed interval and being maybe also slightly hotter (hence, having a smaller radius in turn). Both scenarios are possible but the striking similarity of the evolutionary states of 2M0535-05 B and the GQ Lup companion rather strengthens the validity of the best guest values for radius and surface gravity obtained here. Hence, the most likely value for the mass of 27 M_{Jup} is despite its formal uncertainties a well fitting quantity when compared to 2M0535-05.

Free floating members of star forming regions

Only few other objects fall into the class of very young substellar objects. There are first a few well studied members of another closeby star forming region, the low-mass members of Upper Scorpius (hereafter USco). These objects are well studied by means of high resolution optical spectroscopy (Mohanty et al., 2004a,b). Based on spectral synthesis of alkali metal and TiO lines in the optical, effective temperatures and surface gravities, precise to ± 50 K and ± 0.25 dex have been derived by these authors. Consequently, their masses could be pinned down to a fairly high precision. The lowest mass members Usco 128 and Usco 130, had masses of 7–14 M_{Jup} based entirely on empirical methods. Since the effective temperature and surface gravity of the GQ Lup companion, as derived by Neuhäuser et al. (2005) was even lower than the respective values for the lowest mass members of USco, authors like Guenther et al. (2005) and Basri (2006) used these objects in a direct comparison to strengthen the point that the GQ Lup companion could be well below 13 M_{Jup} in mass (see Fig. 5.5), thus, favouring the mass claims based on the Wuchterl & Tscharnuter (2003) models raised in Neuhäuser et al. (2005).

While the precision of the determined physical parameters of the USco members is undoubtedly very high, the accuracy of these values is at stake. Reiners (2005) showed that the TiO-ϵ band, used for the determination of the effective temperature of the USco members by Mohanty et al. (2004a,b), has a too low band strength in the spectral models and lead to T_{eff} and $\log(g)$ fits that are systematically to low by ~ 150 K and 0.3 dex,

respectively, when compared to fits of the TiO-γ band. A preliminary revision of the derived masses showed a systematic shift towards higher masses, bringing the lowest mass members of USco back into the brown dwarf regime (see Fig. 5.6). A more precise recalculation of the parameters of the Usco members is still pending, basically postponed until a more reliable and consistent TiO linelist and partition sum is included in the spectral models. Currently, the best guess masses for USco 128 and USco 130 are around 30–40 M_{Jup} and their revised values for effective temperature, and surface gravity are about T_{eff}=2750 K and $\log{(g)}$=3.6 (Reiners, 2005), very close to the new values for the GQ Lup companion. Also the (unchanged) luminosity of USco 128 and USco130 ($\log{(L/L_\odot)}$=-2.05...-2.40) is matching the revised luminosity of the GQ Lup companion very well. Hence, there is no justification any more to assign the GQ Lup companion a lower mass in respect to USco 128 and USco 130. Eventhough the age of USco (3–5 Myr Mohanty et al., 2004a) is slightly higher than for the GQ Lup companion the mass of the GQ Lup companion, can be expected to be very similar to USco 128 and USco 130, hence about $\sim$30 M_{Jup} at the current level of accuracy.

Other young low-mass objects in USco (Preibisch & Mamajek, 2006), σ Ori (Béjar et al., 1999), Trapezium (Lucas & Roche, 2000), Taurus (Briceño et al., 2002; Luhman, 2004b), Chamaeleon (Comerón et al., 2000; Luhman, 2004) or R Corona Australis (Fernández & Comerón, 2001) have masses based on evolutionary models and their spectral type (and thus their mass) is often derived from photometry or very low resolution spectroscopy only. Even in the case of mid-resolution optical or near-infrared spectra, a reliable
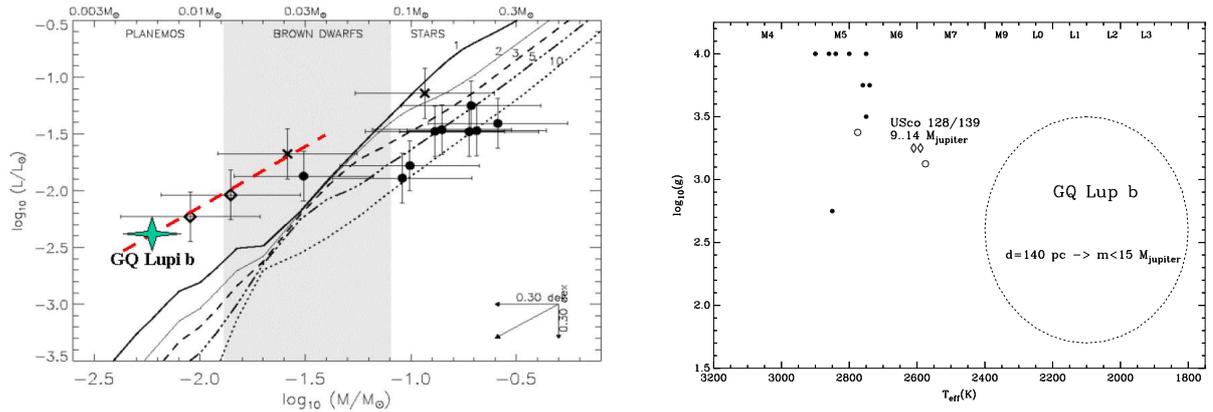
Figure 5.5: *Left:* Mass – luminosity diagram for USco objects from Basri (2006, Fig. 1). *Right:* T_{eff} – $\log{(g)}$ diagram for USco objects from Guenther et al. (2005, Fig. 6). In both plots the GQ Lup companion is shown in respect to the Usco objects with their luminosities and *uncorrected* masses, effective temperatures and surface gravities determined by Mohanty et al. (2004a,b). See also Fig. 5.6. These plots are now obsolete, because of the shifts in the properties of the USco objects (see text) and because of the new values for T_{eff}, $\log{(g)}$, and luminosity for the GQ Lup companion as published here.

spectral typing in absence of a two-dimensional spectral classification is rather uncertain. For example the ultra low mass binary Oph 162225-240515 (hereafter Oph 1622-24) was announced by the discoverers (Jayawardhana & Ivanov, 2006) to be of planetary mass (7 and 13 M_{Jup}, respectively). Subsequent studies by Luhman et al. (2007) showed that Oph 1622-2405A and B are of earlier spectral type (M7.25±0.25 and M8.75±0.25 for the A and B components, rather than M9 and M9.5-L0, respectively, as determined by Jayawardhana & Ivanov (2006)) and their masses being ∼58 and ∼20 M_{Jup}, respectively. Following the binary statistics among sunlike and low mass stars, more and more previously unresolved brown dwarfs in star forming regions appear to be double or multiple when observed with adaptive optics techniques. The latest example is the low mass double Oph 162336-240221 AB (hereafter Oph 1623-2402AB), with masses of 17^{+4}_{-5} M_{Jup} and 14^{+6}_{-5} M_{Jup} (determined from evolutionary models), respectively (Close et al., 2007).

2MASS J110913-773444 (hereafter 2M1109-77), a low-mass object with a circumstellar disk in Chamaeleon I (Luhman, 2004a) has a mass of about 8 M_{Jup} (according to evolutionary models), hence marks the current low-mass end of the known free-floating ultra low-mass population in star forming regions (Luhman et al., 2005, Fig. 2).
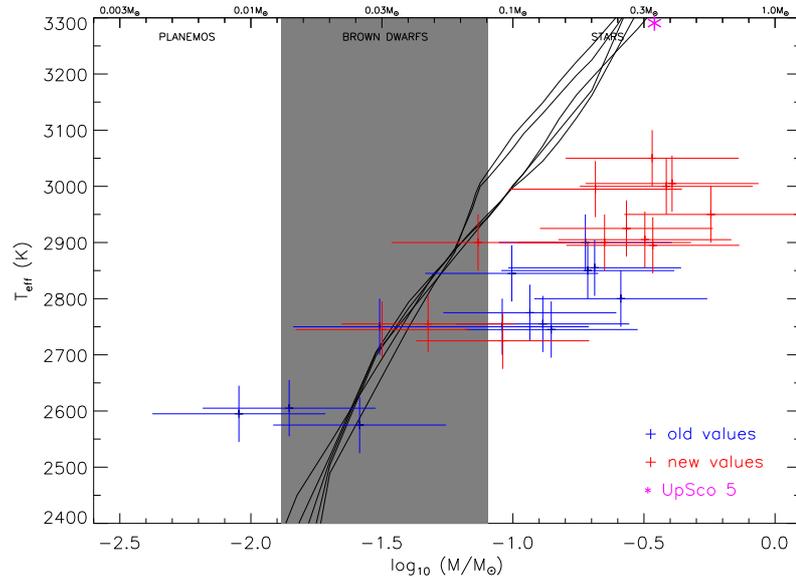
Figure 5.6: Mass − T_{eff} diagram for USco objects from Reiners (2005, Fig. 5). Temperatures and masses determined from high resolutions measurements of T_{eff}, $\log(g)$, and luminosity by Mohanty et al. (2004a,b) for young low-mass objects in USco have been revised by Reiners (2005) to be hotter and more massive. Blue crosses show old values, red crosses new values after the revision. Model isochrones (1 to 10 Myrs, top to bottom) are overplotted.

Ultra low mass companions to young stars and brown dwarfs

The second group of objects being comparable to the GQ Lup companion is a slowly growing list of low-mass companions to young stars. The list also includes now low-mass companions to brown dwarfs, such as 2MASSW J1207334-393254 (hereafter 2M1207) discovered by Chauvin et al. (2004, 2005a). The latter seems rather comparable to binary systems such as 2M0535 or Oph 1622-2405AB. However, 2M1207B holds the record for the lowest mass companion to another star or brown dwarf, being even less luminous than 2M1101-77. In a most recent study by Mohanty et al. (2007), using a new set of VLT/NACO spectra, the authors determine a mass of 8 ± 2 M_{Jup} from evolutionary models for 2M1207B, based on their new value for effective temperature of $T_{eff} = 1600 \pm 100$ K and a luminosity of $\log(L/L_\odot) = -4.72 \pm 0.14$ from Mamajek (2005). While the evolutionary models yield internal consistency for T_{eff}, $\log(L/L_\odot)$, and colours of 2M1207A, 2M1207B appears to be subluminous and Mohanty et al. (2007) suggests a grey extinction by a edge-on disk for 2M1207B. Most notably, according to Mohanty et al. (2007), 2M1207A has an effective temperature of $T_{eff} = 2550 \pm 150$ K and a luminosity of $\log(L/L_\odot) = -2.68 \pm 0.12$. At an age of 5–10 Myrs Chauvin et al. (2004) 2M1207A appears as an aged twin of the GQ Lup companion slightly cooler and less luminous but with similar mass of 24 ± 6 M_{Jup}(Mohanty et al., 2007).

The situation seems similar for the low mass companions to AB Pic (Chauvin et al., 2005b) and GSC 08047-00232 (Chauvin et al., 2005). AB Pic B is a common proper motion companion to K2V star AB Pic in the ∼30 Myr old Tucana-Horologium association. The spectral type of $L1^{+2}_{-1}$ for AB Pic B is based on a low resolution NACO K-band spectrum. The mass from evolutionary models is ∼13 M_{Jup} according to Chauvin et al. (2005b).

With a spectral type M9.5±1, GSC08047-00232B (also a proposed member of the Tucana-Horologium association) has an effective temperature of $T_{eff} = 2100 \pm 200$ K (using the temperature scale of Leggett et al., 2001) and Chauvin et al. (2005) derive a mass of 25 ± 10 M_{Jup} from evolutionary models for an adopted age of 30 Myrs. The spectral type of GSC08047-00232B is based on a NACO H-band spectrum. The masses derived for both objects heavily depend on the accuracy of the determined spectral type, the spectral type – T_{eff} relation adopted, as well as on the age and distance to the objects. As for the GQ Lup companion clear room for improvement in the determination of T_{eff} is given and a reasonable determination of the surface gravity could further bolster the mass determination from models.

Neuhäuser (2005) give a extensive overview on the effects of different distances, ages and spectral type – T_{eff} relations for the GQ Lup companion, AB Pic B and 2M1207B.

GG Tau is a young quadruple system with an age of ∼1.5 Myr (White et al., 1999; White & Basri, 2003). The lowest mass components GG Tau Ba and Bb were included

in the USco sample of Mohanty et al. (2004a,b) who determined effective temperatures of T_{eff}=2575 and 2775 K, respectively. These values and the according surface gravities and masses are prone to the underestimated TiO ϵ-band, as outlined above. Thus the lowest mass component GG Tau Bb has an effective temperature of $\sim$2700 K, a surface gravity of $\log(g)\sim$3.4 and thus a mass of about 30–40 M_{Jup} at a luminosity of $\log(L/L_{\odot})$=-1.66. The respective radius is about 7 R_{Jup}, larger than for objects of comparable mass in USco, which are at least double as old. The GQ Lup companion is less luminous and smaller at the same effective temperature than GG Tau Bb. Given the slightly higher surface gravity of the GQ Lup companion, the mass should be slightly smaller than the one for GG Tau Bb, if they are co-eval. It should be noted that the members of the GG Tau system have very different extinctions due to circum-(sub-)stellar material (see e.g. Beust & Dutrey, 2005), which could effect the accuracy of the derived luminosities.

DH Tau B is a common proper motion companion to the young T-Tauri star DH Tau, discovered by Itoh et al. (2005). The authors determine effective temperature and surface gravity from low-resolution JHK spectroscopy to T_{eff}=2700–2800 K and $\log(g)$=4.0-4.5, respectively. At an age of 0.1–4 Myr (as determined for the primary, see Itoh et al., 2005, and references therein) the mass is about 30 M_{Jup} but up to 50 M_{Jup} when adopting an age of 3–10 Myrs. The upper limit was derived from the luminosity of $\log(L/L_{\odot})$=-2.44 and effective temperature in comparison to evolutionary models. DH Tau B appears to be only marginally hotter and fainter and with a slightly higher surface gravity than the GQ Lup companion. The distance to DH Tau is not mentioned in Itoh et al. (2005). The luminosity is determined from fitting the models to the flux calibrated spectra. Luhman et al. (2006) adopt a distance of 140 pc from Wichmann et al. (1998) and calculate a luminosity of $\log(L/L_{\odot})=-2.71\pm0.12$. This results in a substantially lower mass estimate for DH Tau B of 11^{+10}_{-3} M_{Jup}.

Further substellar companion detected among young nearby associations are TWA5 B in the TW Hydrae association (spectral type: $\sim$M8, $T_{\mathrm{eff}}\sim$2600 K, mass: 15..40 M_{Jup} at d=50 pc and $\sim$10 Myr, see Lowrance et al., 1999; Neuhäuser et al., 2000), and HR7329B in the Pictoris Group (spectral type: M7–M8, $T_{\mathrm{eff}}\sim$2600 K, mass: 20..40 M_{Jup} at $d=47.6\pm1.6$ pc and and age of up to 30 Myr, see Lowrance et al., 2000; Guenther et al., 2001). Both objects are older than GQ Lup and the masses should be slightly higher than the one for the GQ Lup companion.

G 196-3 B and GJ 417 BC are substantially older than the GQ Lup companion (their age estimates range from $\sim$20–300 Myr) but their primaries are still pre-main sequence (PMS) objects. See Burgasser et al. (2005, and references therein) for for further information.

The latest addition to the list of ultra low mass companions to very young PMS objects is CHXR 73 B. According to Luhman et al. (2006), CHXR 73 B has the same M_K as DH Tau B. Adopting the same age range for both objects, the author derives a similar mass

of 12^{+8}_{-5} M_{Jup} for CHXR 73 B. The primary, CHXR 73 A, has a very low proper motion, thus the physical connection of both objects (hence common distance and age) can not be proven via common proper motion. The spectrum of CHXR 73 B is of low resolution and S/N.

Recent results about the GQ Lup companion from the literature

Two papers on the GQ Lup companion appeared during the work on this thesis that deserve futher attention.

Marois et al. (2007) fit the $RIJHKL$-band spectral energy distribution of the GQ Lup companion with a low resolution GAIA model to obtain physical parameters of the GQ Lup companion. They find a radius of 0.38 ± 0.05 $R_{\odot}$ (3.7±0.5 R_{Jup}), and an effective temperature of 2335 ± 100 K. This effective temperature is consistent with the value given in Neuhäuser et al. (2005) but inconsistent with the value derived here. This is especially noteworthy since the radius obtained by Marois et al. (2007) is fully consistent with the value given here. This is only possible since the luminosity derived by Marois et al. (2007) is lower by more than 0.2 dex due to a lower K-band magnitude obtained by these authors. Their modelfits are reported to be gravity insensitive and a $\log g$ of 3-4 is assumed. They use the evolutionary models from the Lyon group to obtain a mass of 10 to 20 M_{Jup}.

McElwain et al. (2007) obtained an integral field J and H-band spectrum with OSIRIS at Keck, which is lower in dynamic range, resolution ($R \simeq 2000$), and spectral coverage and also much lower in S/N than the SINFONI spectrum presented here. They confirm the spectral type (M6–L0) and their effective temperature of 2450^{+450}_{-150} K is consistent with the large error bars with the value from this work. Their luminosity estimate is however rather low ($\log(L/L_{\odot})= -2.46 \pm 0.15$) and a mass from evolutionary models of 10 to 40 M_{Jup} is obtained.

Summary and Outlook

6

In this thesis I demonstrate that integral field spectroscopy is a powerful tool in stellar astrophysics, eventhough it was designed for applications where a continuous two-dimensional spatial coverage is essential (hence, mostly extended objects). SINFONI, as one of the few instruments available for near infrared integral field spectroscopy, eliminates the shortcomings of conventional long slit spectroscopy and combines the advantages of high spatial resolution achievable with adaptive optics and a moderate spectral resolution, succeeding and outperforming the long slit spectrograph NACO at the VLT.

The SINFONI JHK spectrum of the GQ Lup companion offers the unique opportunity to study the spectral features of this young and ultra low mass object in unprecedented detail due to its superior spectral resolution and signal-to-noise ratio. Eventhough the NACO K-band spectrum of the GQ Lup companion is (after a most careful data reduction) fully consistent with the SINFONI spectrum, the full spatial information that is contained in the SINFONI spectrum eases the data reduction and allows a much better separation of the respective flux contributions from the primary and the companion.

Comparing the new spectrum of the GQ Lup companion with templates from existing spectral sequences for old M and L dwarfs reveals a spectral type of M6–M8 for the GQ Lup companion but also demonstrates the limitations of an one-dimensional spectral classification scheme for objects whose surface gravity is significantly lower than for old stars and brown dwarfs. Progress in empirical classification of young (ultra) low mass objects can not be achieved before a multi-dimensional spectral classification scheme has been established that takes at least the surface gravity into account, but should ideally also account for metallicity effects.

The spectrum of the GQ Lup companion was compared to updated spectral models from the Lyon group (courtesy of Peter Hauschildt, Hamburg) and the Tokyo group (courtesy of Takashi Tsuji, Tokyo). From the fitting of these synthetic model spectra an effective temperature of $T_{\text{eff}}= 2650\pm100$ K and a surface gravity of $\log{(g)}=3.7 \pm 0.5$ was derived for the GQ Lup companion. The models showed a wide consistency with

the observed spectrum but also shortcomings in the represention of some molecular and atomic species. Important gravity indicators are still missing (the FeH band in the H-band as the most prominent example). The Lyon models exhibit the highest line density and seem the more adequate, at least for the parameters of the GQ Lup companion, thus, at effective temperatures where dust is yet not forming in its atmosphere. Further progress in the precision and accuracy of the synthetic models needs and improvement of the linelists and partition sums of important species, like the alkali metals, VO and FeH.

A radius of $R = 3.63\,^{+0.75}_{-0.53}$ R$_{\text{Jup}}$ and a mass of $M \simeq 27$ M$_{\text{Jup}}$ were derived for the GQ Lup companion, using a revised value for the luminosity of $\log(L/L_\odot) = -2.21\pm0.15$, adopting a distance of $d = 150 \pm 20$ pc. These values yield fully consistent results when compared to the *hot start* models of Burrows et al. (1997); Baraffe et al. (2003) and D'Antona & Mazzitelli (1997). Eventhough this is beneficial, this finding does not add validity to the mass predictions from the evolutionary models, given the high uncertainties in the derived mass of the GQ Lup companion. However, the resolution of the apparent inconsistencies in these models reported by Neuhäuser et al. (2005) does indeed dispel the claim that the models are totally inappropriate for objects like the GQ Lup companion. Still, the oversimplified starting conditions jeopardise accurate mass predictions for the GQ Lup companion (and other objects that young and low-mass) and may only deliver by chance consistent results. Problems in describing the properties of free floating ultra low mass objects, like the well studied members of USco are still not resolved. However, the scarcity of anchor points in this part of the HR diagram is currently inhibiting a thorough test of the models.

The apparent mismatch between the mass predictions from the *hot start* models and the evolutionary models of Wuchterl & Tscharnuter (2003) is still existing, eventhough the new parameters for the GQ Lup companion are now more consistent with a 5 M$_{\text{Jup}}$ *planetary* mass track in the HR diagram of Neuhäuser et al. (2005). Eventhough not readily permitted, the new parameters could also be consistent with a (yet not calculated) 10 M$_{\text{Jup}}$ *core-collaps* mass track in these models. Given that the only available anchor point in this regime, 2M0535B has a mass underestimated by a factor of three, it seems instructive to apply this factor also for the model predictions of the GQ Lup companion. Thus, the predictions by the Wuchterl & Tscharnuter (2003) models become consistent with the *hot start* models for this case.

A final comparison with young and ultra low mass objects yields two results. First, when compared to the lower mass component of the brown dwarf eclipsing binary 2M0535, the GQ Lup companion appears to be smaller but with a higher surface gravity at comparable effective temperature. Thus, the GQ Lup companion is less luminous and most likely also slightly less massive than 2M0535B. This comparison yields a rather reliable upper mass limit of 38 M$_{\text{Jup}}$ for the GQ Lup companion, which can only be broken when one assumes a significant age difference for both objects.

Second, the GQ Lup companion is very similar in its physical properties to ultra low mass objects in USco and to companions like DH Tau B. Given the age estimate of about $\sim$1 Myr for the GQ Lup companion, it seems to be a precursor of slightly older

companions like TWA5 B, HR7329 B, or AB Pic B, the latter being substantially cooler than the GQ Lup companion.

It thus appears to be instructive to place the GQ Lup companion in the vicinity of these objects that form a class of young ultra-low mass companions and free floaters. Their mass is, as in the case of the GQ Lup companion, best constrained by evolutionary models whose accuracy has still to be proven. However, the similarity in effective temperature and luminosity (and thus radius) is striking. Only the inability to derive accurate ages of these objects inhibits an immediate contruction of an empirical mass scale. Given, that the predicted masses of these objects hold, we are faced with objects which in extreme cases have only a few Jupiter masses and contradict our current picture of brown dwarf formation as a low mass extend to stellar formation. Likewise, companions of a few to a few tens of Jupiter masses appear to be orbiting stars and suggest a re-evaluation of what we call an extra-solar planet.

What else stays to be done

Despite the advantages of the SINFONI spectrum, outlined in this thesis, it proves very hard to flux-calibrate the individual spectra and computes a continuous spectrum. The individual bands of SINFONI do not overlap and the throughput of the spectrograph depends heavily on the performance of the adaptive optics, which is highly time dependent. Still, important information is contained in the broad band flux distribution and a reconstruction of the SED would certainly improve the precision of the model fits. A major improvement of the precision in surface gravity can however not be expected before the FeH band is adequately incorporated in the models.

The Paβ emission line is an important indicator for accretion onto the GQ Lup companion. The strength of this line has proven to be time dependent (Jean-Francois Lavigne, University of Montreal, private communication). It is therefor highly interesting to examine the L, M and N-band for excess emission from (the remains of) a disk around the GQ Lup companion, driving the accretion that produces the Paβ emission. Similarly, a measurement of the Hα emission strength could contribute an estimate to the mass accretion rate via a 10% width measurement of this line.

High resolution spectra ($R \sim 50000$) with the CRIRES spectrograph could deliver much more information, given that such a measurement would actually resolve the spectral lines in the GQ Lup companion. However, such a measurement puts high demands on the performance of the synthetic model spectra, especially on the completeness of the line lists. Current fits of high resolution infrared spectra of low mass stars and brown dwarfs are very preliminary and reveal gross mismatches between the measured and modeled spectra on this level of resultion (Lyubchik et al., 2007).

Bibliography

Ackerman, A. S., & Marley, M. S. 2001, *Precipitating Condensation Clouds in Substellar Atmospheres*, ApJ, 556, 872

Abuter, R., Schreiber, J., Eisenhauer, F., Ott, T., Horrobin, M., & Gillesen, S. 2006, *SINFONI data reduction software*, New Astronomy Review, 50, 398

Allard, F., Hauschildt, P. H., & Schweitzer, A. 2000, *Spherically Symmetric Model Atmospheres for Low-Mass Pre-Main-Sequence Stars with Effective Temperatures between 2000 and 6800 K*, ApJ, 539, 366

Allard, F., Hauschildt, P. H., Alexander, D. R., Tamanai, A., & Schweitzer, A. 2001, *The Limiting Effects of Dust in Brown Dwarf Model Atmospheres*, ApJ, 556, 357

Allers, K. N., et al. 2007, *Characterizing Young Brown Dwarfs Using Low-Resolution Near-Infrared Spectra*, ApJ, 657, 511

Baraffe, I., Chabrier, G., Allard, F., & Hauschildt, P. H. 1998, *Evolutionary models for solar metallicity low-mass stars: mass-magnitude relationships and color-magnitude diagrams*, A&A, 337, 403

Baraffe, I., Chabrier, G., Allard, F., & Hauschildt, P. H. 2002, *Evolutionary models for low-mass stars and brown dwarfs: Uncertainties and limits at very young ages*, A&A, 382, 563

Baraffe, I., Chabrier, G., Barman, T. S., Allard, F., & Hauschildt, P. H. 2003, *Evolutionary models for cool brown dwarfs and extrasolar giant planets. The case of HD 209458*, A&A, 402, 701

Barber, R. J., Tennyson, J., Harris, G. J., & Tolchenov, R. N. 2006, *A high-accuracy computed water line list*, MNRAS, 368, 1087

Basri, G., Mohanty, S., Allard, F., Hauschildt, P. H., Delfosse, X., Martín, E. L., Forveille, T., & Goldman, B. 2000, *An Effective Temperature Scale for Late-M and L Dwarfs, from Resonance Absorption Lines of Cs I and Rb I*, ApJ, 538, 363

Basri, G. 2006, *Measuring physical properties of very young brown dwarfs*, Astronomische Nachrichten, 327, 3

Béjar, V. J. S., Zapatero Osorio, M. R., & Rebolo, R. 1999, *A Search for Very Low Mass Stars and Brown Dwarfs in the Young sigma Orionis Cluster*, ApJ, 521, 671

Beust, H., & Dutrey, A. 2005, *Dynamics of the young multiple system GG Tauri. I. Orbital fits and inner edge of the circumbinary disk of GG Tau A*, A&A, 439, 585

Bevington, P. R., Robinson, D. K., 2003, *Data Reduction and Error Analysis for The Physical Sciences*, McGraw-Hill Education, 3rd rev. edition

Bonnet, H., et al. 2003, *Implementation of MACAO for SINFONI at the VLT, in NGS and LGS modes*, Proc. SPIE, 4839, 329

Bonnet, H., et al. 2004, *First light of SINFONI AO-module at VLT The Messenger* , 117, 17

Borysow, A., Jorgensen, U. G., & Zheng, C. 1997, *Model atmospheres of cool, low-metallicity stars: the importance of collision-induced absorption*, A&A, 324, 185

Briceño, C., Luhman, K. L., Hartmann, L., Stauffer, J. R., & Kirkpatrick, J. D. 2002, *The Initial Mass Function in the Taurus Star-forming Region*, ApJ, 580, 317

Broeg, C., Schmidt, T. O. B., Guenther, E., Gaedke, A., Bedalov, A., Neuhäuser, R., & Walter, F. M. 2007, *Rotational period of GQ Lupi*, A&A, 468, 1039

Brott, I., & Hauschildt, P. H. 2005, *A PHOENIX Model Atmosphere Grid for Gaia*, The Three-Dimensional Universe with Gaia, 576, 565

Burgasser, A. J., Kirkpatrick, J. D., & Lowrance, P. J. 2005, *Multiplicity Amongst Wide Brown Dwarf Companions to Nearby Stars: Gliese 337CD*, AJ, 129, 2849

Burrows, A., Hubbard, W. B., Lunine, J. I., Marley, M., Guillot, T., Saumon, D., & Freedman, R. S. 1997, *Extra-Solar Giant Planet and Brown Dwarf Models*, Planets Beyond the Solar System and the Next Generation of Space Missions, 119, 9

Burrows, A., Hubbard, W. B., Lunine, J. I., & Liebert, J. 2001, *The theory of brown dwarfs and extrasolar giant planets*, Reviews of Modern Physics, 73, 719

Burrows, A., Sudarsky, D., & Hubeny, I. 2006, *L and T Dwarf Models and the L to T Transition*, ApJ, 640, 1063

Chabrier, G., & Baraffe, I. 2000, *Theory of Low-Mass Stars and Substellar Objects*, ARA&A, 38, 337

Chabrier, G., Baraffe, I., Allard, F., & Hauschildt, P. 2000, *Evolutionary Models for Very Low-Mass Stars and Brown Dwarfs with Dusty Atmospheres*, ApJ, 542, 464

Chabrier, G., Gallardo, J., & Baraffe, I. 2007, *Evolution of low-mass star and brown dwarf eclipsing binaries*, A&A, 472, L17

Chauvin, G., Lagrange, A.-M., Dumas, C., Zuckerman, B., Mouillet, D., Song, I., Beuzit, J.-L., & Lowrance, P. 2004, *A giant planet candidate near a young brown dwarf. Direct VLT/NACO observations using IR wavefront sensing*, A&A, 425, L29

Chauvin, G., et al. 2005, *Astrometric and spectroscopic confirmation of a brown dwarf companion to GSC 08047-00232. VLT/NACO deep imaging and spectroscopic observations*, A&A, 430, 1027

Chauvin, G., Lagrange, A.-M., Dumas, C., Zuckerman, B., Mouillet, D., Song, I., Beuzit, J.-L., & Lowrance, P. 2005, *Giant planet companion to 2MASSW J1207334-393254*, A&A, 438, L25

Chauvin, G., et al. 2005, *A companion to AB Pic at the planet/brown dwarf boundary*, A&A, 438, L29

Close, L. M., et al. 2007, *The Wide Brown Dwarf Binary Oph 1622-2405 and Discovery of a Wide, Low-Mass Binary in Ophiuchus (Oph 1623-2402): A New Class of Young Evaporating Wide Binaries?*, ApJ, 660, 1492

Comerón, F., Neuhäuser, R., & Kaas, A. A. 2000, *Probing the brown dwarf population of the Chamaeleon I star forming region*, A&A, 359, 269

Cushing, M. C., Rayner, J. T., Davis, S. P., & Vacca, W. D. 2003, *FeH Absorption in the Near-Infrared Spectra of Late M and L Dwarfs*, ApJ, 582, 1066

Cushing, M. C., Rayner, J. T., & Vacca, W. D. 2005, *An Infrared Spectroscopic Sequence of M, L, and T Dwarfs*, ApJ, 623, 1115

D'Antona, F., & Mazzitelli, I. 1994, *New pre-main-sequence tracks for M less than or equal to 2.5 solar mass as tests of opacities and convection model*, ApJS, 90, 467

D'Antona, F., & Mazzitelli, I. 1997, *Evolution of low mass stars*, Memorie della Societa Astronomica Italiana, 68, 807

D'Antona, F., & Mazzitelli, I. 1998, *A Role for Superadiabatic Convection in Low Mass Structures?*, Brown Dwarfs and Extrasolar Planets, 134, 442

Dahn, C. C., et al. 2002, *Astrometry and Photometry for Cool Dwarfs and Brown Dwarfs*, AJ, 124, 1170

Debes, J. H., & Sigurdsson, S. 2006, *The origins of the substellar companion to GQ Lupi*, A&A, 451, 351

Diolaiti, E., Bendinelli, O., Bonaccini, D., Close, L.M., Currie, D.G., & Parmeggiani, G. 2000, *StarFinder: an IDL GUI-based code to analyze crowded fields with isoplanatic correcting PSF fitting*, Proc. SPIE, 4007, 879

Eisenhauer, F., et al. 2003, *SINFONI - Integral field spectroscopy at 50 milli-arcsecond resolution with the ESO VLT*, Proc. SPIE, 4841, 1548

Fernández, M., & Comerón, F. 2001, *Intense accretion and mass loss of a very low mass young stellar object*, A&A, 380, 264

Gädke, Ansgar, *Eigenbewegung und Multiplizität junger Brauner Zwerge und massearmer Sterne in Chamaeleon*, Diploma Thesis, University of Jena, March 2005

Glass, I. S. , *Handbook of Infrared Astronomy*, Cambridge University Press, 1999

Golimowski, D. A., et al. 2004, *L' and M' Photometry of Ultracool Dwarfs*, AJ, 127, 3516

Gorlova, N. I., Meyer, M. R., Rieke, G. H., & Liebert, J. 2003, *Gravity Indicators in the Near-Infrared Spectra of Brown Dwarfs*, ApJ, 593, 1074

Goto, M., et al. 2003, *Spectroscopy with Adaptive Optics : Spectral Slope Variation*, Proc. SPIE, 4839, 1117

Goto, M., & The Subaru Ao/Ircs Teams 2005, *Note on Spectroscopy with Adaptive Optics*, Science with Adaptive Optics, 63

Guenther, E. W., Neuhäuser, R., Huélamo, N., Brandner, W., & Alves, J. 2001, *Infrared spectrum and proper motion of the brown dwarf companion of HR 7329 in Tucanae*, A&A, 365, 514

Guenther, E. W., Neuhäuser, R., Wuchterl, G., Mugrauer, M., Bedalov, A., & Hauschildt, P. H. 2005, *The low-mass companion of GQ Lup*, Astronomische Nachrichten, 326, 958

Guieu, S., et al. 2007, *On the circum(sub)stellar environment of brown dwarfs in Taurus*, A&A, 465, 855

Hauschildt, P. H., and Baron, E., 1999, *Numerical solution of the expanding stellar atmosphere problem*, J. Comp. Applied Math. 109, 41

Homeier, D., Allard, F., Hauschildt, P. H., Barman, T. S., Schweitzer, A., & Baron, E. A. 2005, *Spectral Properties of Brown Dwarfs and Hot Jupiters*, High Resolution Infrared Spectroscopy in Astronomy, 465

Horne, K. 1986, *An optimal extraction algorithm for CCD spectroscopy*, PASP, 98, 609

Itoh, Y., et al. 2005, *A Young Brown Dwarf Companion to DH Tauri*, ApJ, 620, 984

Jayawardhana, R., & Ivanov, V. D. 2006, *Discovery of a Young Planetary-Mass Binary*, Science, 313, 1279

Janson, M., Brandner, W., Henning, T., & Zinnecker, H. 2006, *Early ComeOn+ adaptive optics observation of GQ Lupi and its substellar companion*, A&A, 453, 609

Johnas, C. M. S., Hauschildt, P. H., Schweitzer, A., Mullamphy, D. F. T., Peach, G., & Whittingham, I. B. 2007, *The effects of new Na I D line profiles in cool atmospheres* A&A, 475, 1039

Jung, Y., Lundin, L. K., Modigliani, A., Dobrzycka, D., & Hummel, W. 2006, *New data reduction challenges on the VLT with SINFONI and VISIR*, Astronomical Society of the Pacific Conference Series, 351, 295

Kirkpatrick, J. D., Dahn, C. C., Monet, D. G., Reid, I. N., Gizis, J. E., Liebert, J., & Burgasser, A. J. 2001, *Brown Dwarf Companions to G-Type Stars. I. Gliese 417B and Gliese 584C* , AJ, 121, 3235

Kirkpatrick, J. D. 2005, *New Spectral Types L and T*, ARA&A, 43, 195

Kirkpatrick, J. D., Barman, T. S., Burgasser, A. J., McGovern, M. R., McLean, I. S., Tinney, C. G., & Lowrance, P. J. 2006, *Discovery of a Very Young Field L Dwarf, 2MASS J01415823-4633574*, ApJ, 639, 1120

Kirkpatrick, J. D. 2007, *Outstanding Issues in Our Understanding of L, T, and Y Dwarfs*, ArXiv e-prints, 704, arXiv:0704.1522

Kleinmann, S. G., & Hall, D. N. B. 1986, *Spectra of late-type standard stars in the region 2.0-2.5 microns* ApJS, 62, 501

Leggett, S. K., Allard, F., Geballe, T. R., Hauschildt, P. H., & Schweitzer, A. 2001, *Infrared Spectra and Spectral Energy Distributions of Late M and L Dwarfs*, ApJ, 548, 908

Lowrance, P. J., et al. 1999, *A Candidate Substellar Companion to CD -33° 7795 (TWA 5)*, ApJ, 512, L69

Lowrance, P. J., et al. 2000, *A Candidate Substellar Companion to HR 7329*, ApJ, 541, 390

Lyubchik, Y., Jones, H. R. A., Pavlenko, Y. V., Martin, E., McLean, I. S., Prato, L., Barber, R. J., & Tennyson, J. 2007, *Spectral analysis of high resolution near-infrared spectra of ultra cool dwarfs*, A&A, 473, 25

Lucas, P. W., & Roche, P. F. 2000, *A population of very young brown dwarfs and free-floating planets in Orion*, MNRAS, 314, 858

Luhman, K. L. 2004, *A Census of the Chamaeleon I Star-forming Region* ApJ, 602, 816

Luhman, K. L. 2004, *The First Discovery of a Wide Binary Brown Dwarf*, ApJ, 614, 398

Luhman, K. L. 2004, *New Brown Dwarfs and an Updated Initial Mass Function in Taurus*, ApJ, 617, 1216

Luhman, K. L., Adame, L., D'Alessio, P., Calvet, N., Hartmann, L., Megeath, S. T., & Fazio, G. G. 2005, *Discovery of a Planetary-Mass Brown Dwarf with a Circumstellar Disk*, ApJ, 635, L93

Luhman, K. L., et al. 2006, *Discovery of a Young Substellar Companion in Chamaeleon*, ApJ, 649, 894

Luhman, K. L., Allers, K. N., Jaffe, D. T., Cushing, M. C., Williams, K. A., Slesnick, C. L., & Vacca, W. D. 2007, *Ophiuchus 1622-2405: Not a Planetary-Mass Binary*, ApJ, 659, 1629

Lyubchik, Y., Jones, H. R. A., Pavlenko, Y. V., Viti, S., Pickering, J. C., & Blackwell-Whitehead, R. 2004, *Atomic lines in infrared spectra for ultracool dwarfs* A&A, 416, 655

Marley, M. S., Seager, S., Saumon, D., Lodders, K., Ackerman, A. S., Freedman, R. S., & Fan, X. 2002, *Clouds and Chemistry: Ultracool Dwarf Atmospheric Properties from Optical and Infrared Colors*, ApJ, 568, 335

Mamajek, E. E. 2005, *A Moving Cluster Distance to the Exoplanet 2M1207b in the TW Hydrae Association*, ApJ, 634, 1385

Marois, C., Macintosh, B., & Barman, T. 2007, *GQ Lup B Visible and Near-Infrared Photometric Analysis*, ApJ, 654, L151

Meyer, M. R., Edwards, S., Hinkle, K. H., & Strom, S. E. 1998, *Near-Infrared Classification Spectroscopy: H-Band Spectra of Fundamental MK Standards*, ApJ, 508, 397

McElwain, M. W., et al. 2007, *First High-Contrast Science with an Integral Field Spectrograph: The Substellar Companion to GQ Lupi*, ApJ, 656, 505

McGovern, M. R., Kirkpatrick, J. D., McLean, I. S., Burgasser, A. J., Prato, L., & Lowrance, P. J. 2004, *Identifying Young Brown Dwarfs Using Gravity-Sensitive Spectral Features*, ApJ, 600, 1020

McLean, I. S., Prato, L., McGovern, M. R., Burgasser, A. J., Kirkpatrick, J. D., Rice, E. L., & Kim, S. S. 2007, *The NIRSPEC Brown Dwarf Spectroscopic Survey. II. High-Resolution J-Band Spectra of M, L, and T Dwarfs*, ApJ, 658, 1217

McLean, I. S., McGovern, M. R., Burgasser, A. J., Kirkpatrick, J. D., Prato, L., & Kim, S. S. 2003, *The NIRSPEC Brown Dwarf Spectroscopic Survey. I. Low-Resolution Near-Infrared Spectra*, ApJ, 596, 561

Modigliani, A., et al. 2007, *The SINFONI pipeline*, Proceedings ADA IV 2006, arXiv:astro-ph/0701297

Mohanty, S., Basri, G., Jayawardhana, R., Allard, F., Hauschildt, P., & Ardila, D. 2004, *Measuring Fundamental Parameters of Substellar Objects. I. Surface Gravities*, ApJ, 609, 854

Mohanty, S., Jayawardhana, R., & Basri, G. 2004, *Measuring Fundamental Parameters of Substellar Objects. II. Masses and Radii*, ApJ, 609, 885

Mohanty, S., Jayawardhana, R., Huélamo, N., & Mamajek, E. 2007, *The Planetary Mass Companion 2MASS 1207-3932B: Temperature, Mass, and Evidence for an Edge-on Disk*, ApJ, 657, 1064

Moon, T. T., & Dworetsky, M. M. 1985, *Grids for the determination of effective temperature and surface gravity of B, A and F stars using uvby-beta photometry*, MNRAS, 217, 305

Mugrauer, M., & Neuhäuser, R. 2005, *GQ Lup and its common proper motion companion*, Astronomische Nachrichten, 326, 701

Muzerolle, J., Hillenbrand, L., Calvet, N., Briceño, C., & Hartmann, L. 2003, *Accretion in Young Stellar/Substellar Objects*, ApJ, 592, 266

Natta, A., Testi, L., Muzerolle, J., Randich, S., Comerón, F., & Persi, P. 2004, *Accretion in brown dwarfs: An infrared view*, A&A, 424, 603

Neuhäuser, R., Guenther, E. W., Petr, M. G., Brandner, W., Huélamo, N., & Alves, J. 2000, *Spectrum and proper motion of a brown dwarf companion of the T Tauri star CoD-337795*, A&A, 360, L39

Neuhäuser, R., Guenther, E. W., Wuchterl, G., Mugrauer, M., Bedalov, A., & Hauschildt, P. H. 2005, *Evidence for a co-moving sub-stellar companion of GQ Lup*, A&A, 435, L13

Neuhäuser, R. 2005, *Homogeneous comparison of directly detected planet candidates: GQ Lup, 2M1207, AB Pic*, in Multiple Stars across the H-R Diagram: ESO Astrophysics Symposia, Hubrig, S., Petr-Gotzens, M., Tokovinin, A.(Eds.), also at Astrophysics e-prints, arXiv:astro-ph/0509906

Preibisch T., & Mamajek, E. 2006, *Handbook of Star Forming Regions*, ASP Conference Series, submitted

Press, W. H., Teukolsky, S. A., Vetterling, W. T., & Flannery, B. P. 1992, *Numerical recipes in C. The art of scientific computing*, Cambridge: University Press, c1992, 2nd ed.

Ralchenko, Yu., Jou, F.-C., Kelleher, D.E., Kramida, A.E., Musgrove, A., Reader, J., Wiese, W.L., and Olsen, K., 2007, *NIST Atomic Spectra Database* (version 3.1.2, on-line resource), National Institute of Standards and Technology, Gaithersburg, MD. Available: `http://physics.nist.gov/asd3`

Rebolo, R., Zapatero Osorio, M. R., Madruga, S., Bejar, V. J. S., Arribas, S., & Licandro, J. 1998, *Discovery of a Low-Mass Brown Dwarf Companion of the Young Nearby Star G 196-3*, Science, 282, 1309

Reiners, A., Basri, G., & Mohanty, S. 2005, *Discovery of an M4 Spectroscopic Binary in Upper Scorpius: A Calibration Point for Young Low-Mass Evolutionary Models*, ApJ, 634, 1346

Reiners, A. 2005, *Calibrating models of ultralow-mass stars*, Astronomische Nachrichten, 326, 930

Reiners, A., Homeier, D., Hauschildt, P. H., & Allard, F. 2007, *A high resolution spectral atlas of brown dwarfs*, aap, 473, 245

Reiners, A., Seifahrt, A., Stassun, K. G., Melo, C., & Mathieu, R. D. 2007, *Detection of strong activity in the eclipsing binary brown dwarf 2MASSJ05352184-0546085 - A possible explanation for the temperature reversal*, ApJ Letters accepted, ArXiv e-prints, 711, arXiv:0711.0536

Roe, H. G. 2002, *Implications of Atmospheric Differential Refraction for Adaptive Optics Observations*, PASP, 114, 450

Schmidt, T.O.B., et al. 2007, *in preparation*

Schreiber, J., Thatte, N., Eisenhauer, F., Tecza, M., Abuter, R., & Horrobin, M. 2004, *Data Reduction Software for the VLT Integral Field Spectrometer SPIFFI*, Astronomical Data Analysis Software and Systems (ADASS) XIII, 314, 380

Seifahrt, A., Neuhäuser, R., & Hauschildt, P. H. 2007, *Near-infrared integral-field spectroscopy of the companion to GQ Lupi*, A&A, 463, 309

Sparks, W. B., & Ford, H. C. 2002, *Imaging Spectroscopy for Extrasolar Planet Detection*, ApJ, 578, 543

Stassun, K. G., Mathieu, R. D., & Valenti, J. A. 2006, *Discovery of two young brown dwarfs in an eclipsing binary system*, Nature, 440, 311

Stassun, K. G., Mathieu, R. D., & Valenti, J. A. 2007, *A Surprising Reversal of Temperatures in the Brown Dwarf Eclipsing Binary 2MASS J05352184-0546085*, ApJ, 664, 1154

Thatte, N., Abuter, R., Tecza, M., Nielsen, E. L., Clarke, F. J., & Close, L. M. 2007, *Very high contrast integral field spectroscopy of AB Doradus C: 9-mag contrast at 0.2arcsec without a coronagraph using spectral deconvolution*, MNRAS, 378, 1229

Tsuji, T., & Ohnaka, K. 1995, *Opacities of Very Cool and Dense Gaseous Mixtures - an Extension of Stellar Opacities to the Substellar Regime*, Astrophysical Applications of Powerful New Databases, 78, 69

Tsuji, T., Ohnaka, K., Aoki, W., & Nakajima, T. 1996, *Evolution of dusty photospheres through red to brown dwarfs: how dust forms in very low mass objects* A&A, 308, L29

Tsuji, T., Ohnaka, K., & Aoki, W. 1997, *Model atmospheres of late-type stars: New possibilities with the new space data*, in Diffuse Infrared Radiation and the IRTS, 124, 91

Tsuji, T. 2000, *in Very Low-Mass Stars and Brown Dwarfs, ed. R. Rebolo & M. R. Zapatero Osorio (New York: Cambridge Univ. Press)*, 156

Tsuji, T. 2001, *in Ultracool Dwarfs: New Spectral Types L and T, ed. H. R. A. Jones & I. A. Steele (Berlin: Springer)*, 9

Tsuji, T. 2002, *Dust in the Photospheric Environment: Unified Cloudy Models of M, L, and T Dwarfs*, ApJ, 575, 264

Vrba, F. J., et al. 2004, *Preliminary Parallaxes of 40 L and T Dwarfs from the US Naval Observatory Infrared Astrometry Program*, AJ, 127, 2948

White, R. J., Ghez, A. M., Reid, I. N., & Schultz, G. 1999, *A Test of Pre-Main-Sequence Evolutionary Models across the Stellar/Substellar Boundary Based on Spectra of the Young Quadruple GG Tauri*, ApJ, 520, 811

White, R. J., & Basri, G. 2003, *Very Low Mass Stars and Brown Dwarfs in Taurus-Auriga*, ApJ, 582, 1109

Wichmann, R., Bastian, U., Krautter, J., Jankovics, I., & Rucinski, S. M. 1998, *HIP-PARCOS observations of pre-main-sequence stars*, MNRAS, 301, L39

Woitke, P., & Helling, C. 2003, *Dust in brown dwarfs. II. The coupled problem of dust formation and sedimentation*, A&A, 399, 297

Woitke, P., & Helling, C. 2004, *Dust in brown dwarfs. III. Formation and structure of quasi-static cloud layers*, A&A, 414, 335

Wuchterl, G. 2000, *Extrasolar Giant Planets: Masses and Luminosities from In-Situ Formation Theories*, From Extrasolar Planets to Cosmology: The VLT Opening Symposium, Springer, 408

Wuchterl, G., & Tscharnuter, W. M. 2003, *From clouds to stars. Protostellar collapse and the evolution to the pre-main sequence I. Equations and evolution in the Hertzsprung-Russell diagram*, A&A, 398, 1081

Wuchterl, G. 2005, *Convective radiation fluid-dynamics: formation and early evolution of ultra low-mass objects*, Astronomische Nachrichten, 326, 905

Zapatero Osorio, M. R., Béjar, V. J. S., Martín, E. L., Rebolo, R., Barrado y Navascués, D., Bailer-Jones, C. A. L., & Mundt, R. 2000, *Discovery of Young, Isolated Planetary Mass Objects in the σ Orionis Star Cluster* , Science, 290, 103

Zapatero Osorio, M. R., Lane, B. F., Pavlenko, Y., Martín, E. L., Britton, M., & Kulkarni, S. R. 2004, *Dynamical Masses of the Binary Brown Dwarf GJ 569 Bab*, ApJ, 615, 958

Appendices

GAIA cond synthetic model fits for the J-band
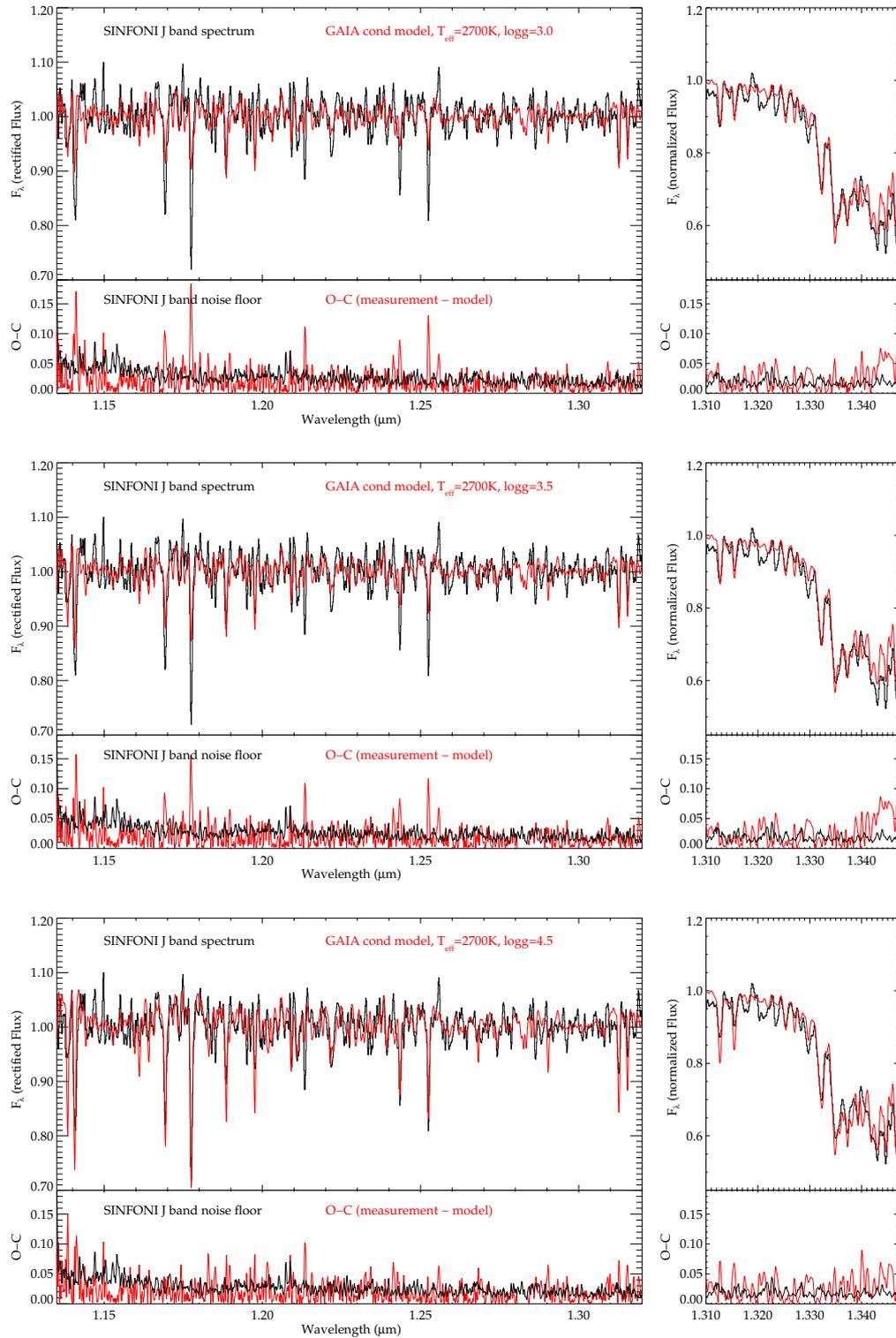
Figure 1: GAIA model fits to the SINFONI J band spectrum of the GQ Lup companion.
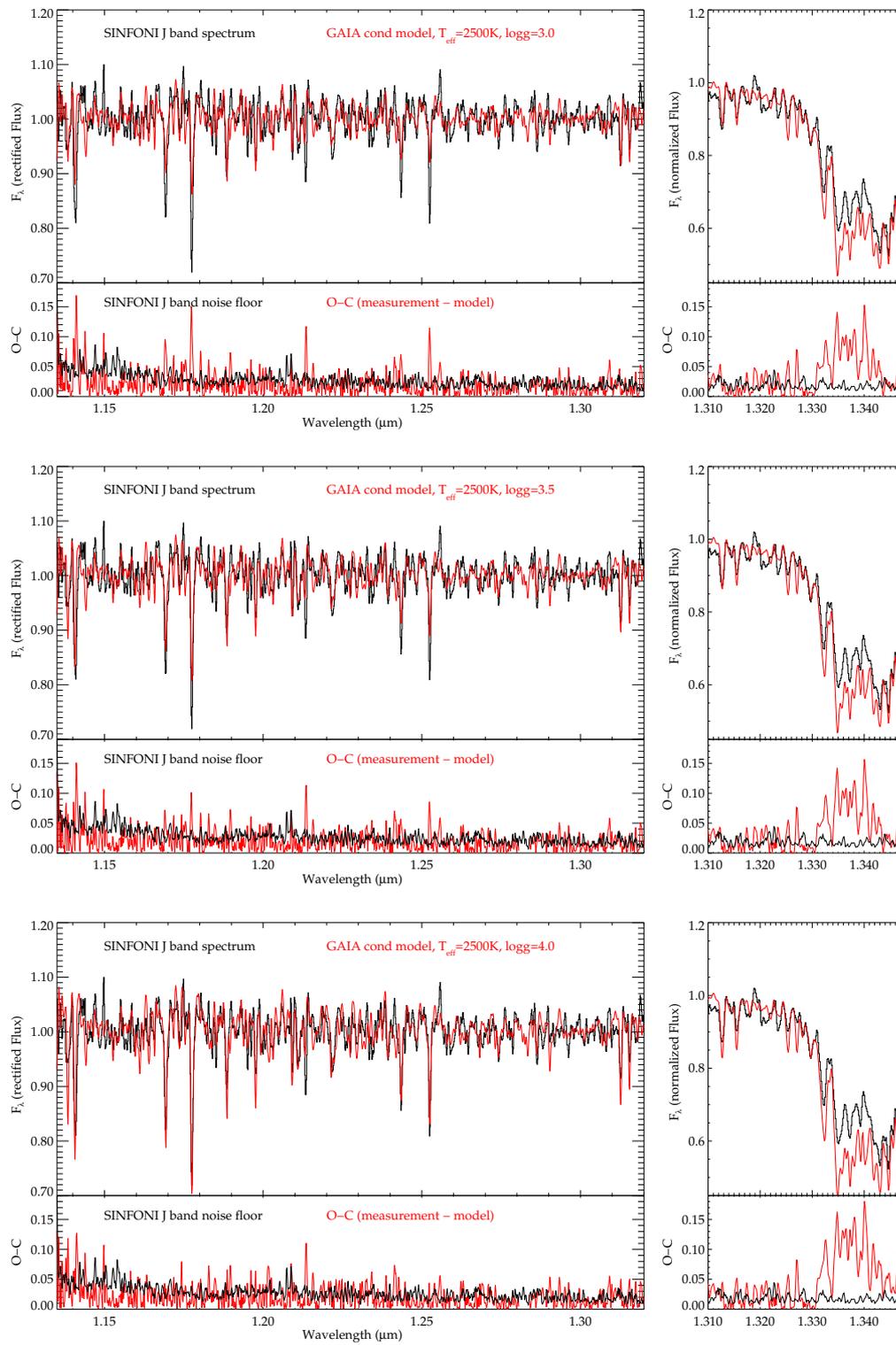
Figure 2: GAIA model fits to the SINFONI J band spectrum of the GQ Lup companion.
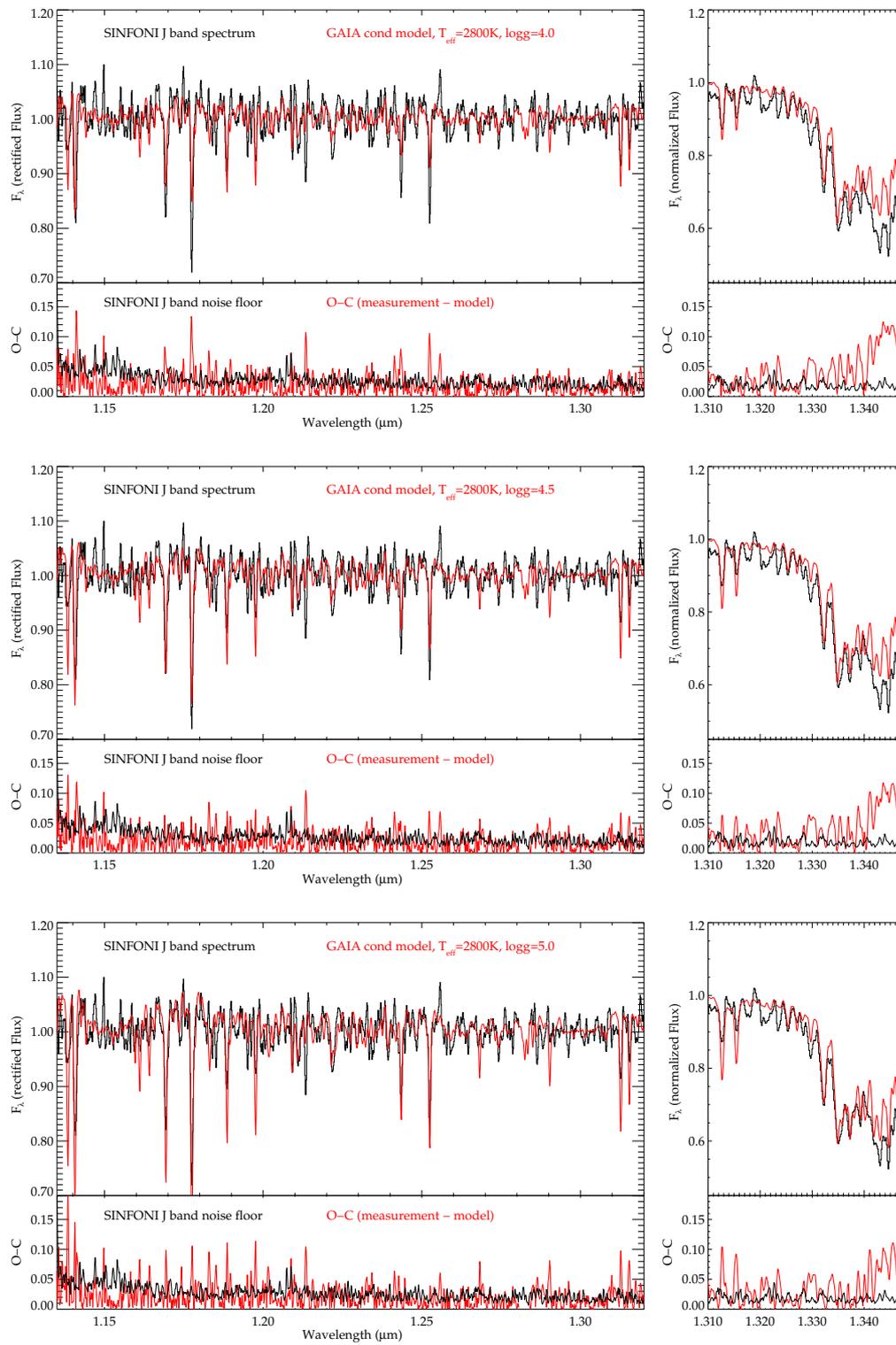
Figure 3: GAIA model fits to the SINFONI J band spectrum of the GQ Lup companion.

GAIA cond synthetic model fits for the H-band
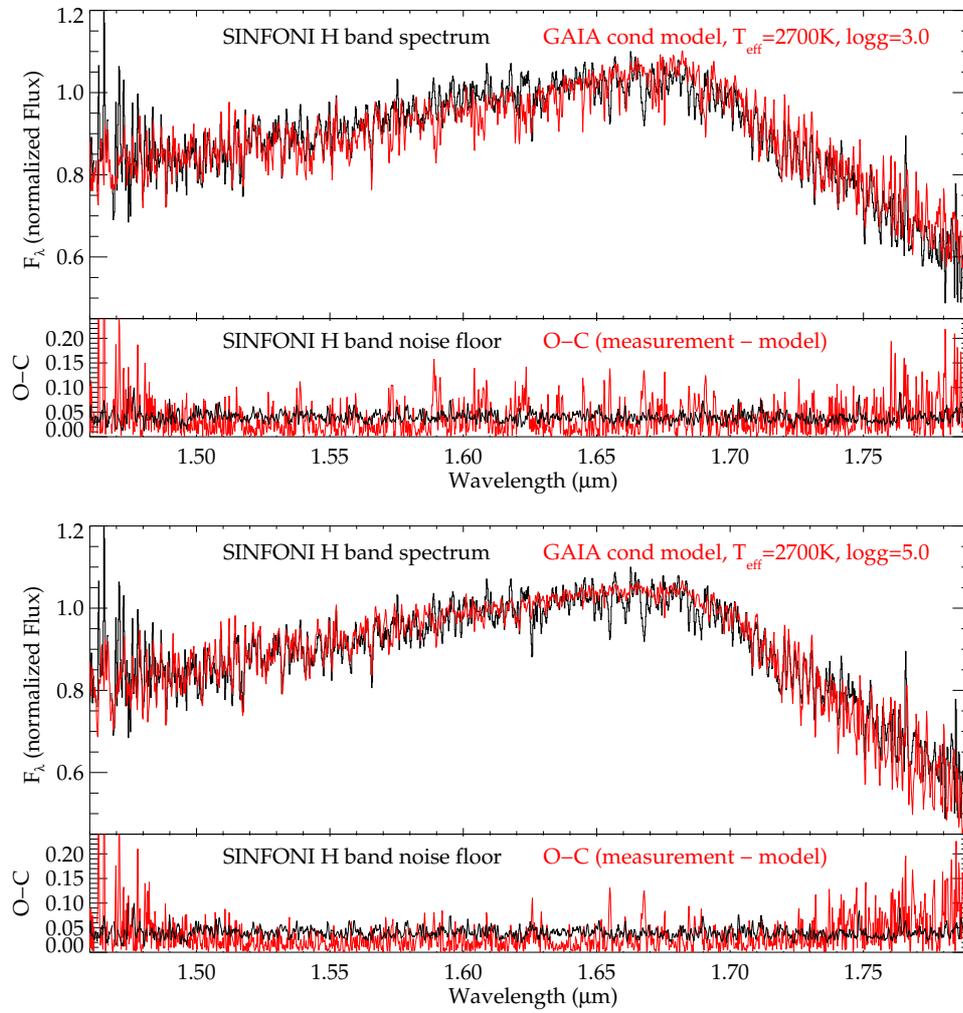
Figure 4: GAIA model fits to the SINFONI H band spectrum of the GQ Lup companion.
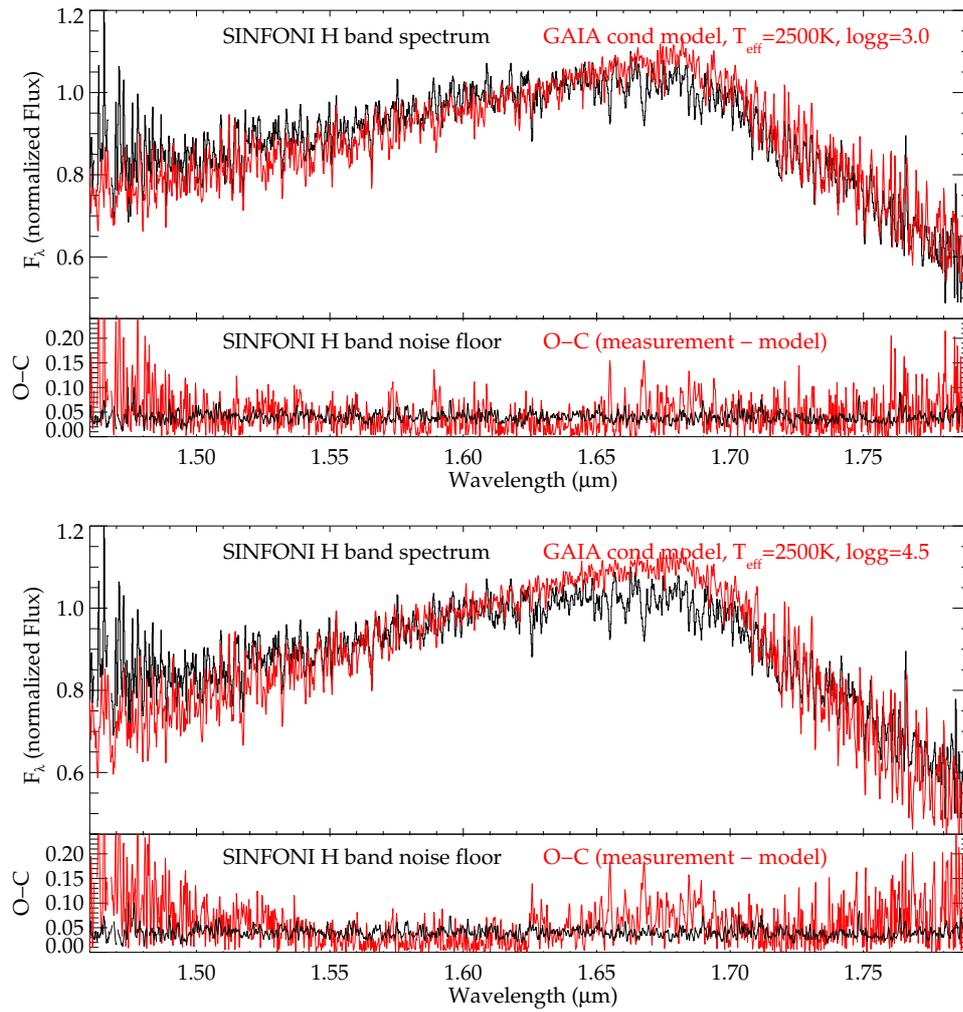
Figure 5: GAIA model fits to the SINFONI H band spectrum of the GQ Lup companion.
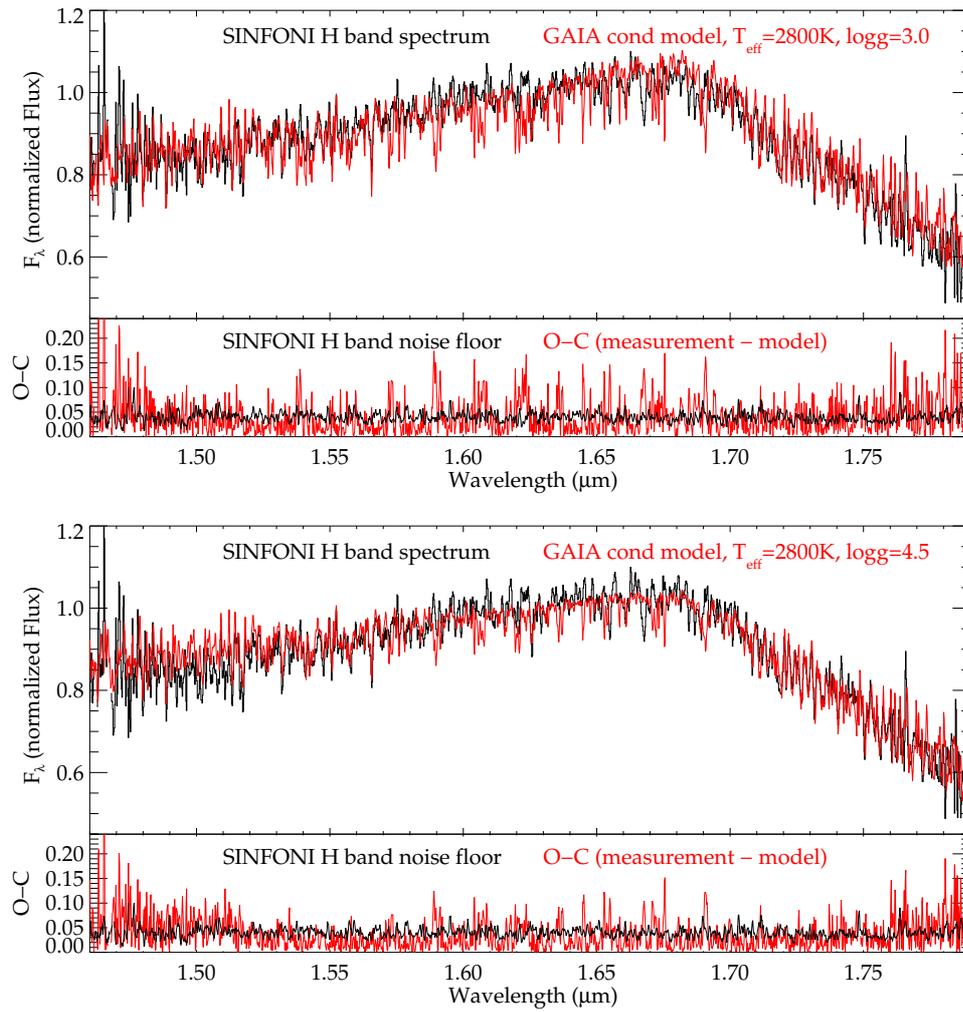
Figure 6: GAIA model fits to the SINFONI H band spectrum of the GQ Lup companion.

GAIA cond synthetic model fits for the K-band
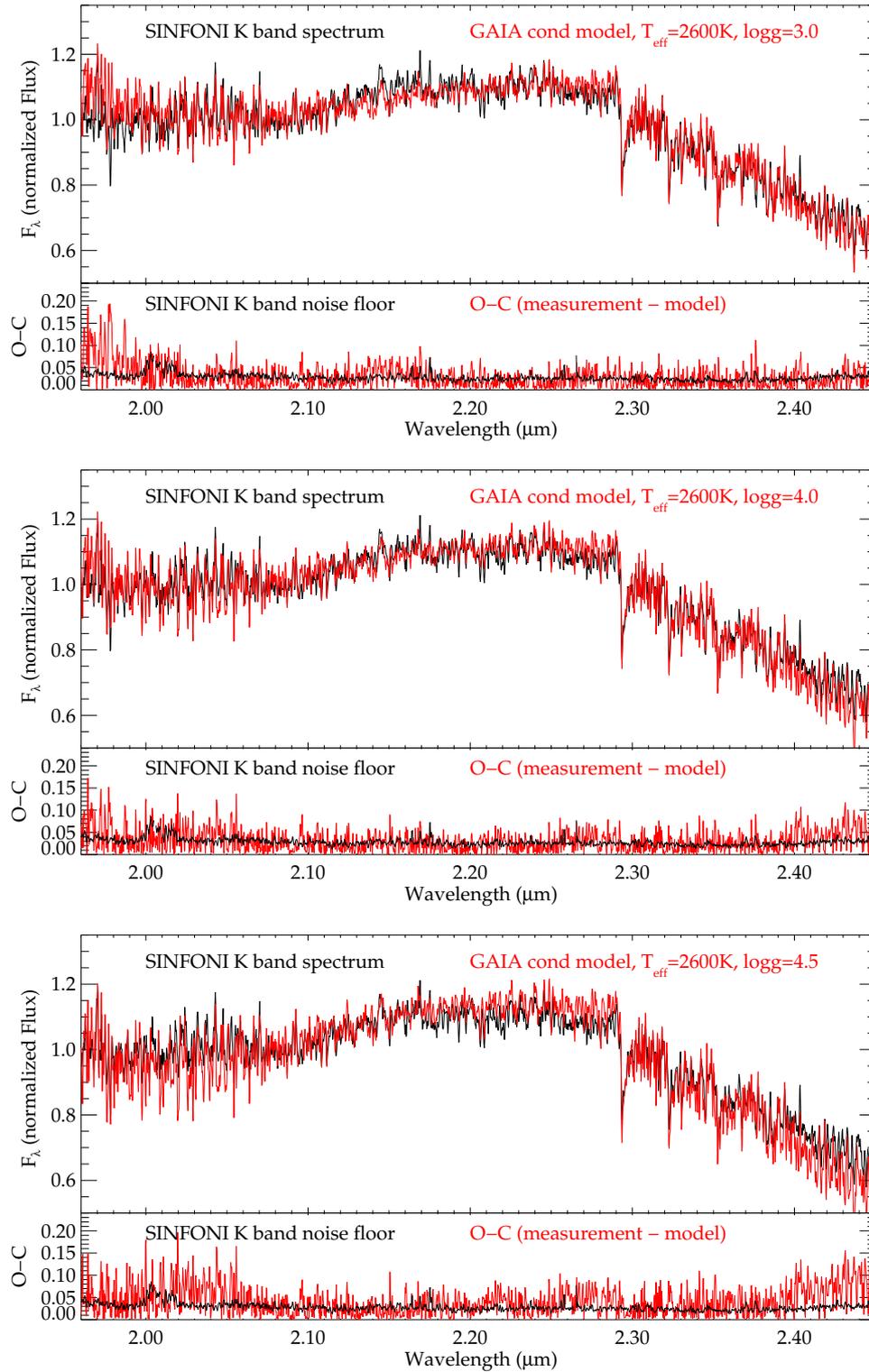
Figure 7: GAIA model fits to the SINFONI K band spectrum of the GQ Lup companion.
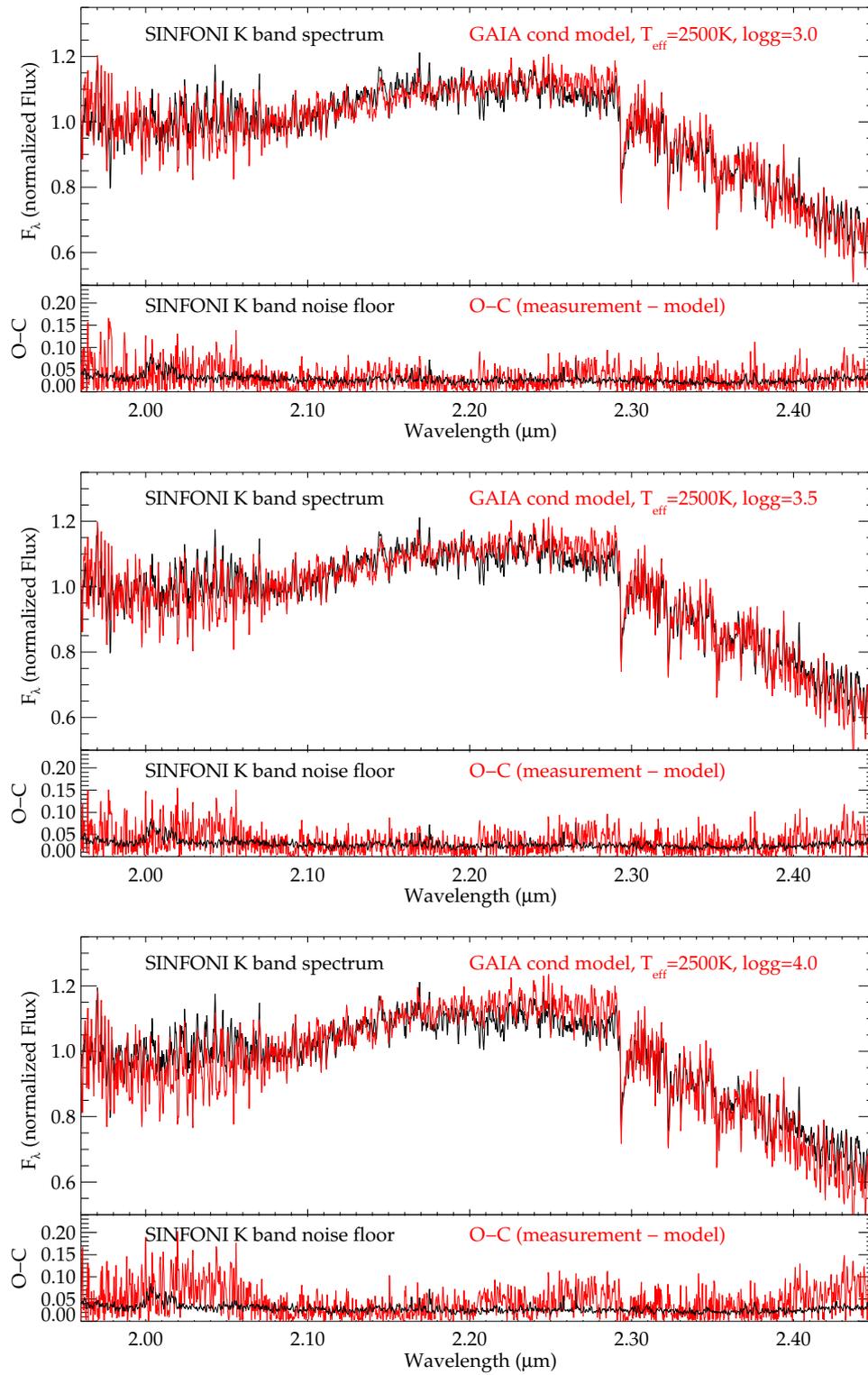
Figure 8: GAIA model fits to the SINFONI K band spectrum of the GQ Lup companion.
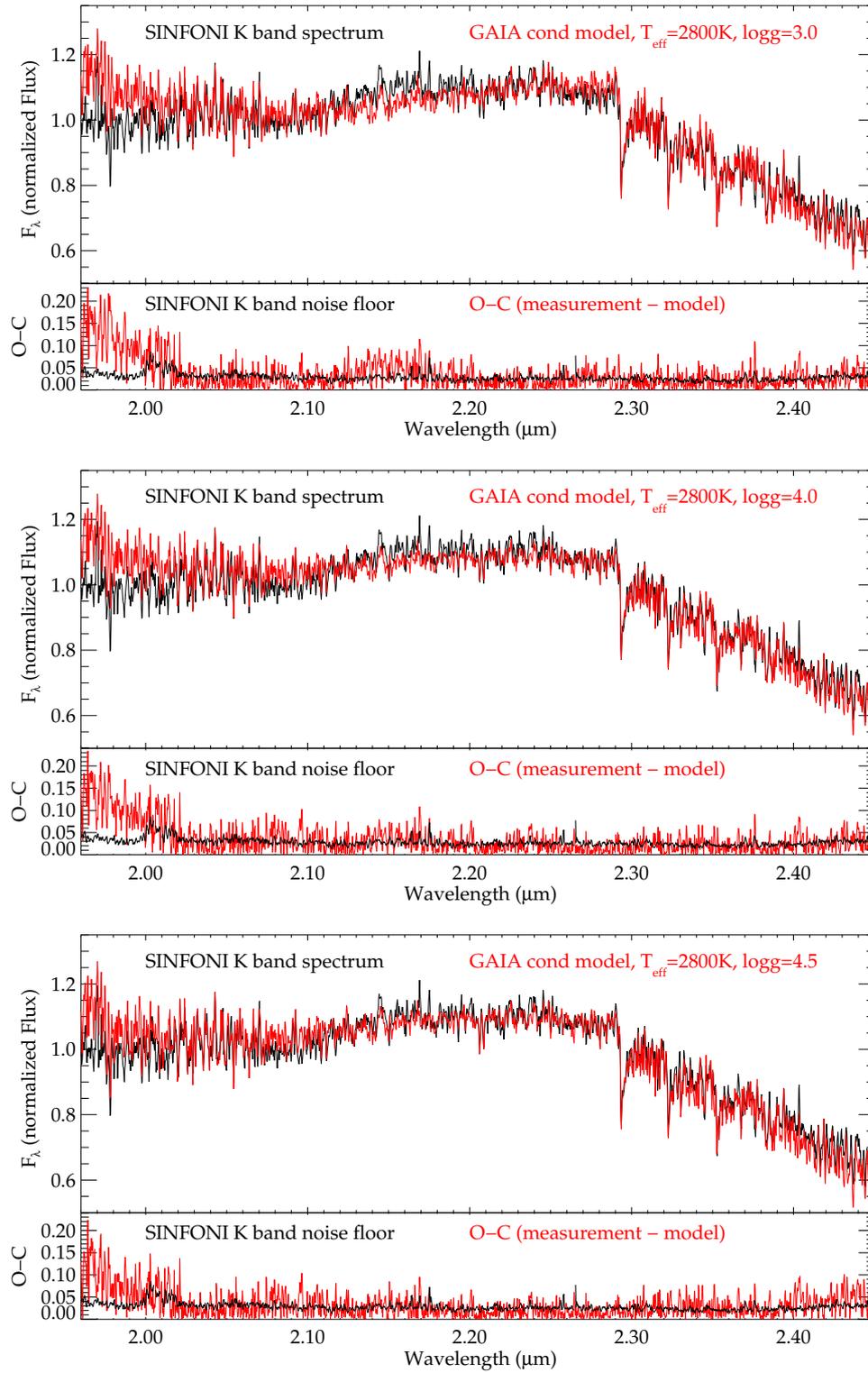
Figure 9: GAIA model fits to the SINFONI K band spectrum of the GQ Lup companion.

Unified cloudy model (UCM) fits for the *J*-band
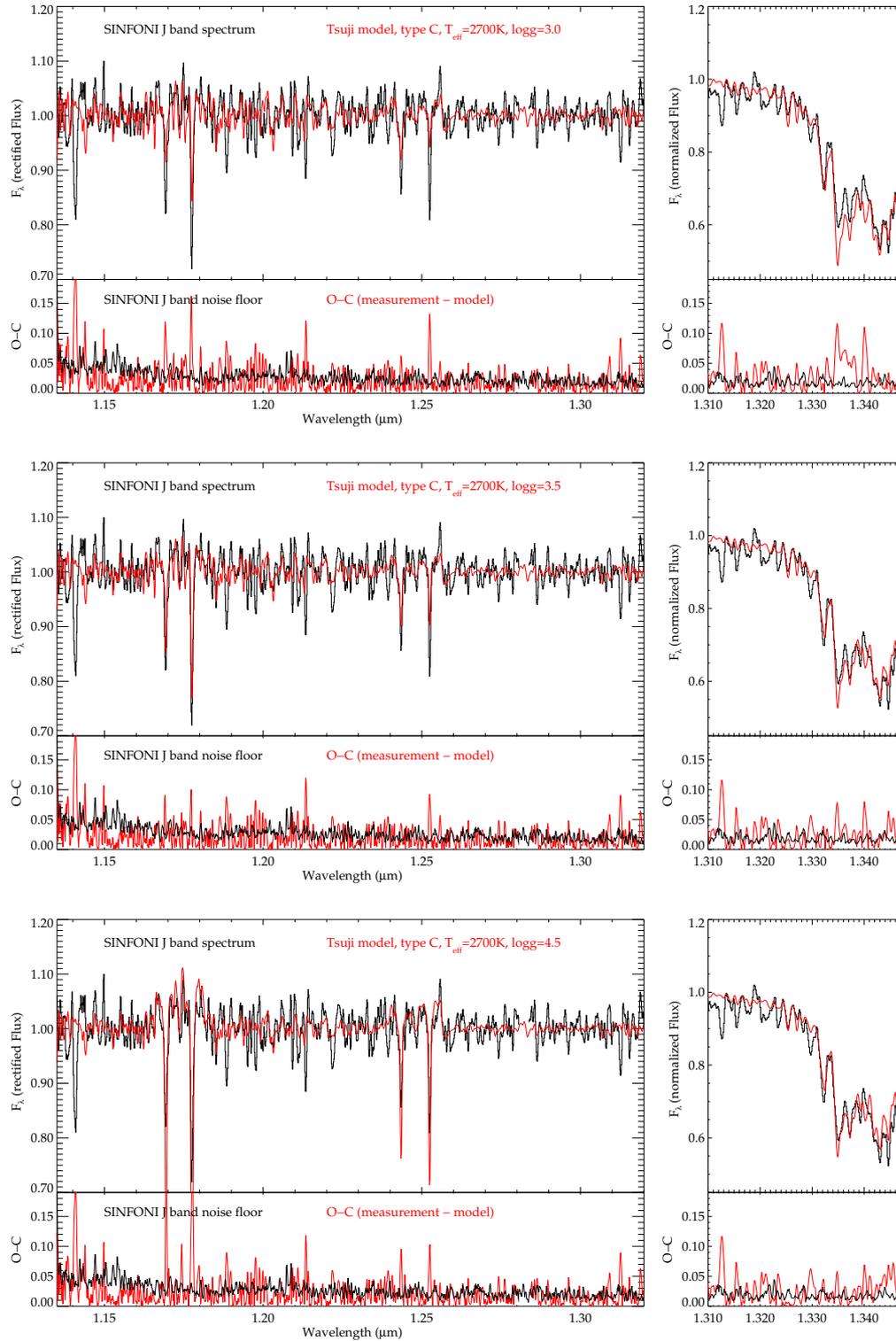
Figure 10: UCM fits to the SINFONI *J* band spectrum of the GQ Lup companion.
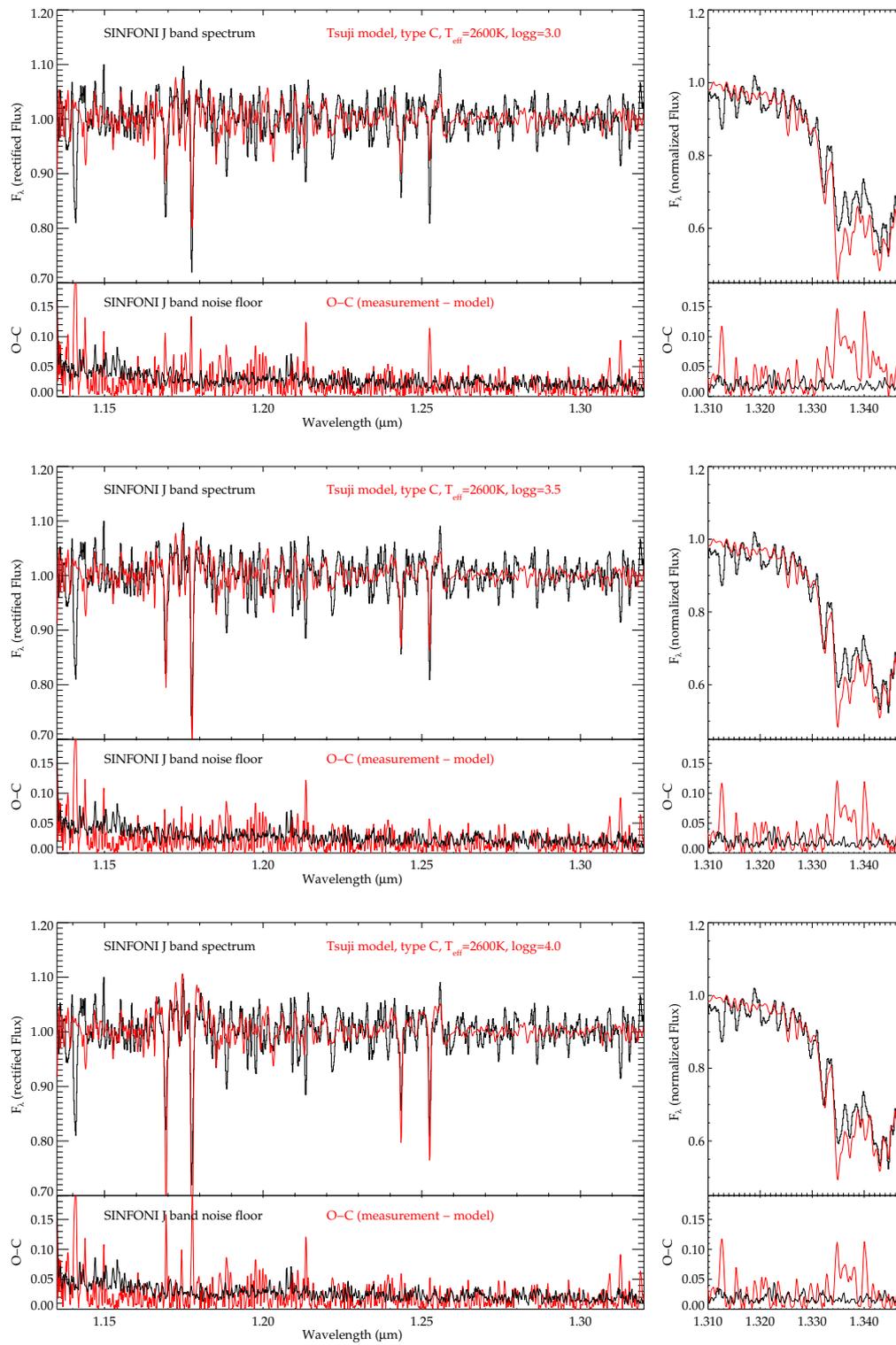
Figure 11: UCM fits to the SINFONI J band spectrum of the GQ Lup companion.
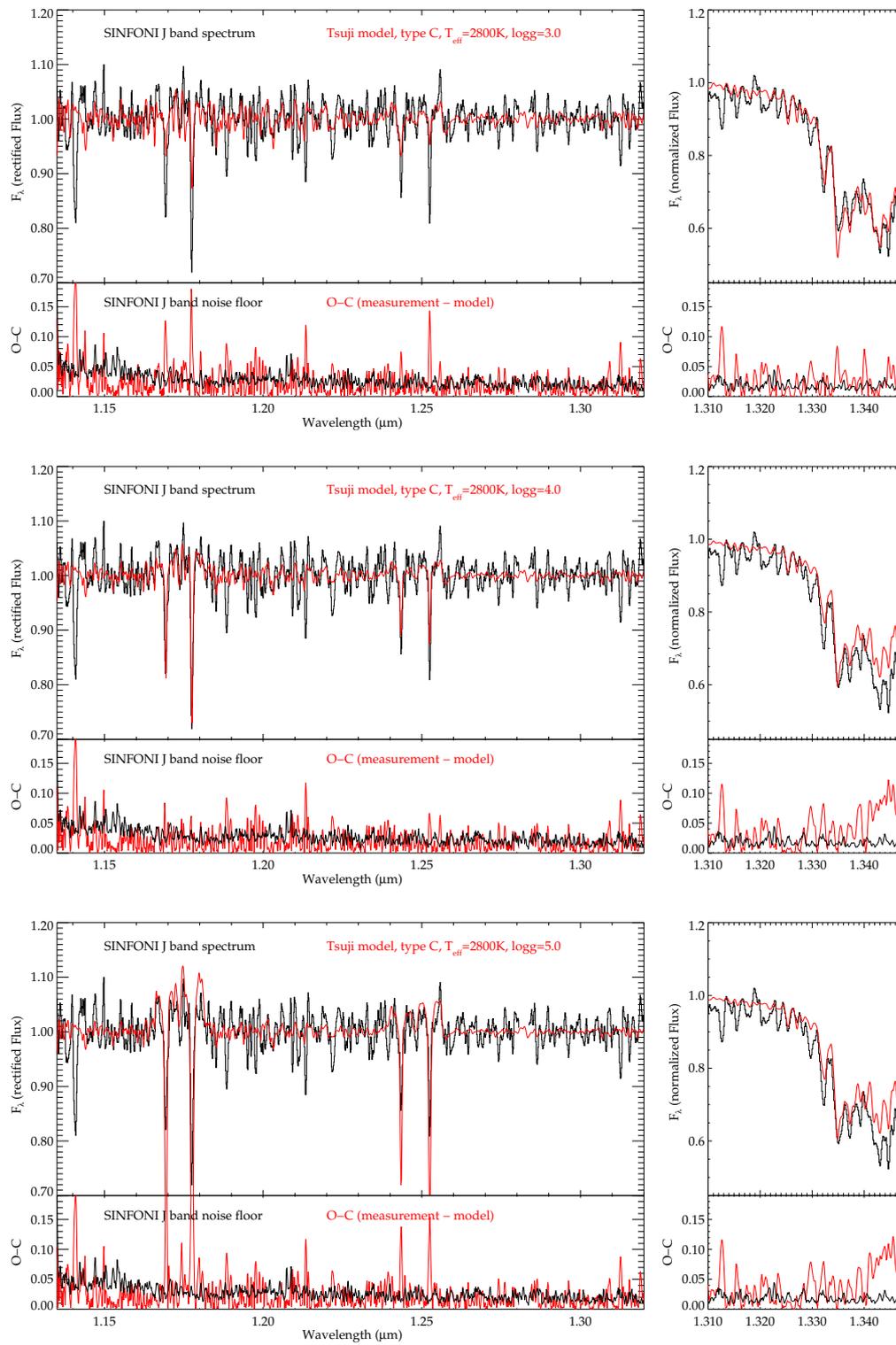
Figure 12: UCM fits to the SINFONI J band spectrum of the GQ Lup companion.

Unified cloudy model (UCM) fits for the H-band
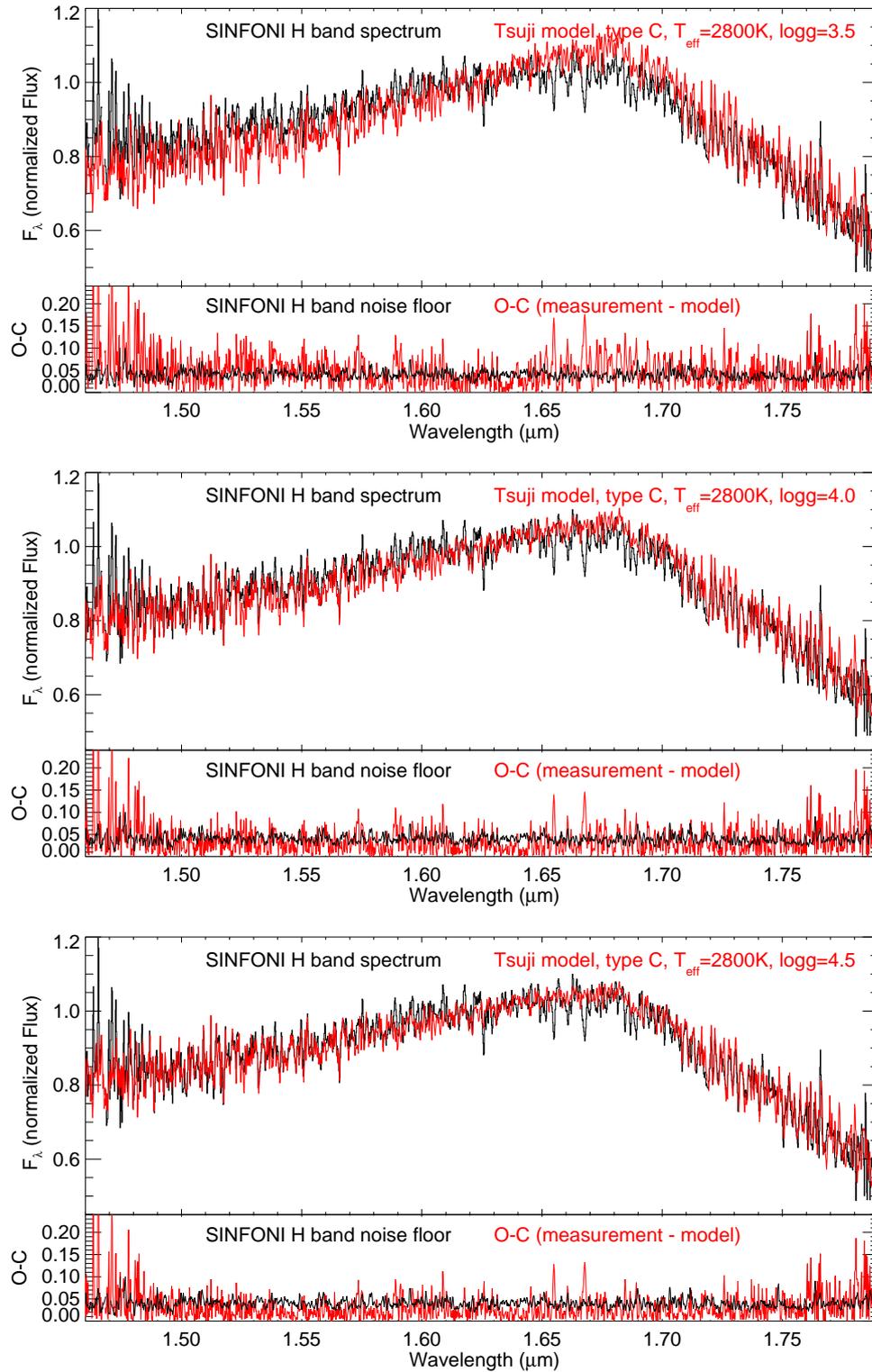
Figure 13: UCM fits to the SINFONI H band spectrum of the GQ Lup companion.
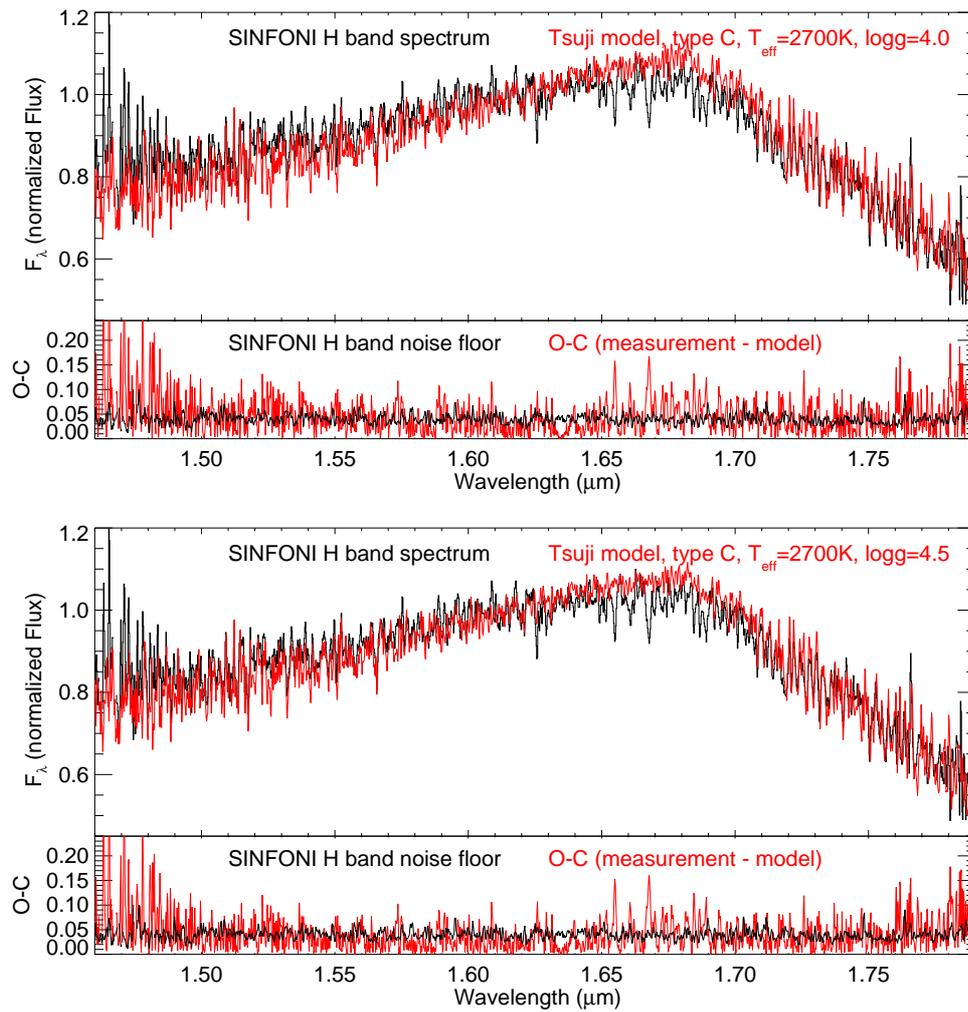
Figure 14: UCM fits to the SINFONI H band spectrum of the GQ Lup companion.
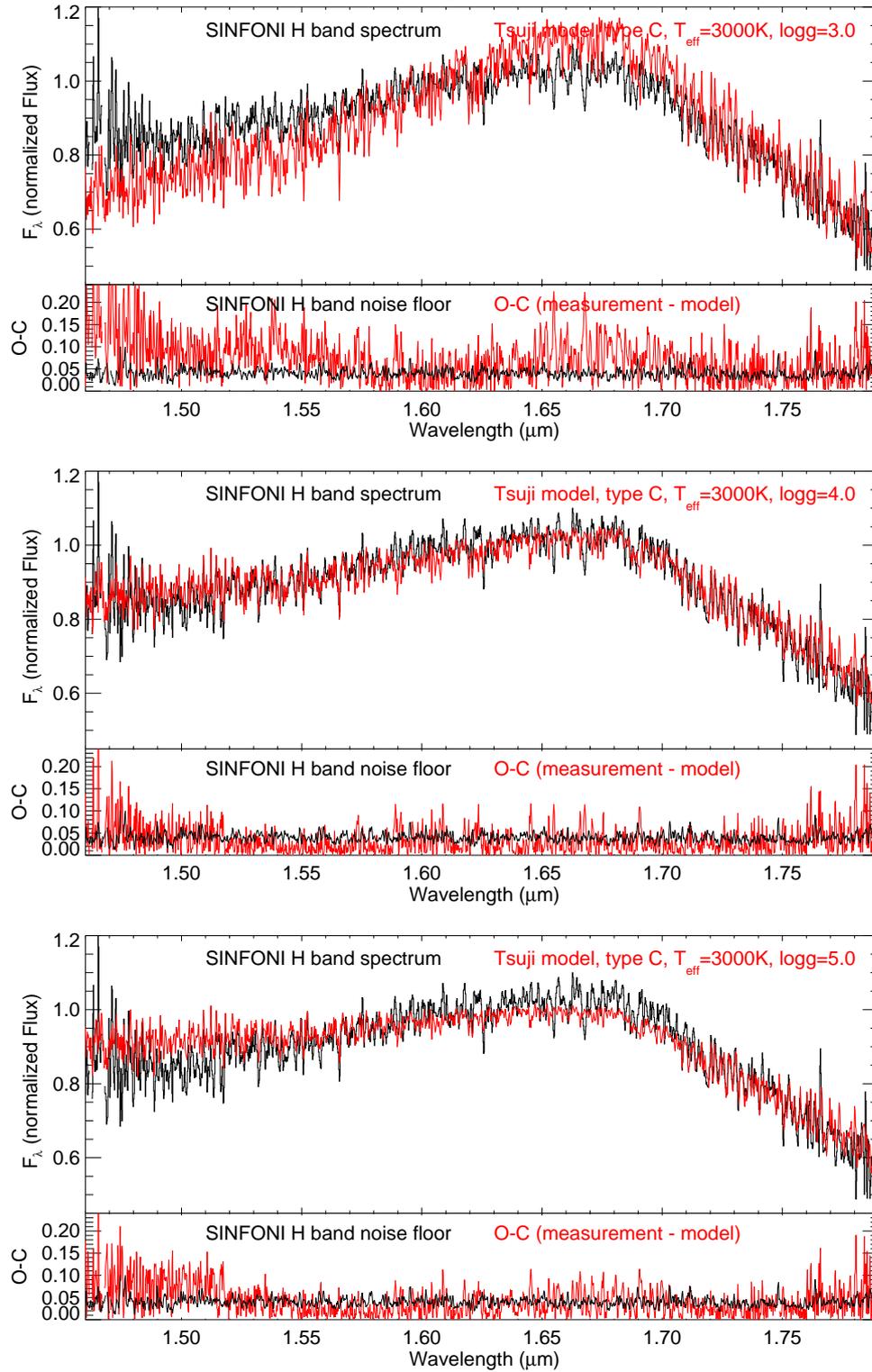
Figure 15: UCM fits to the SINFONI H band spectrum of the GQ Lup companion.

Unified cloudy model (UCM) fits for the K-band
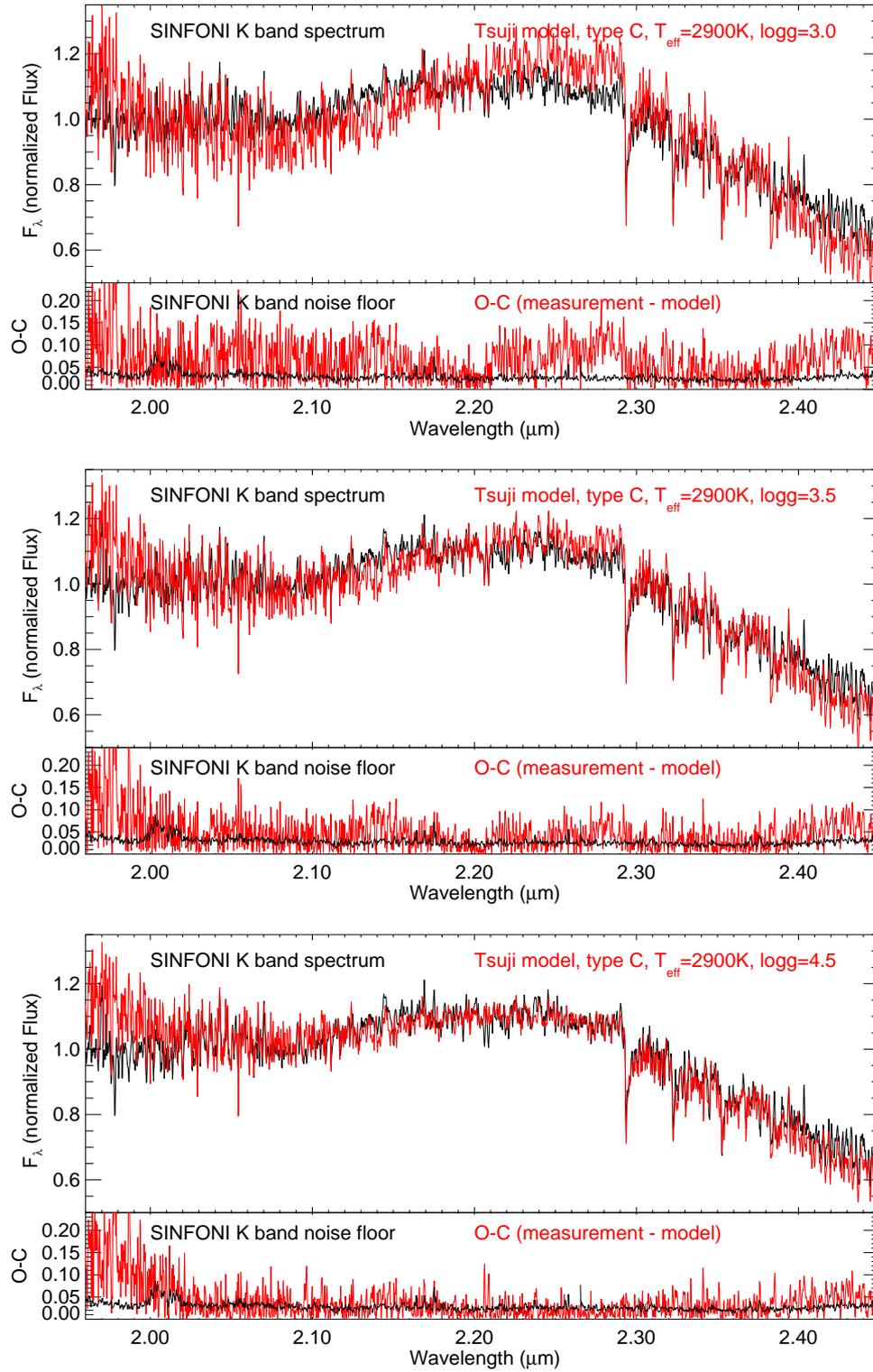
Figure 16: UCM fits to the SINFONI K band spectrum of the GQ Lup companion.
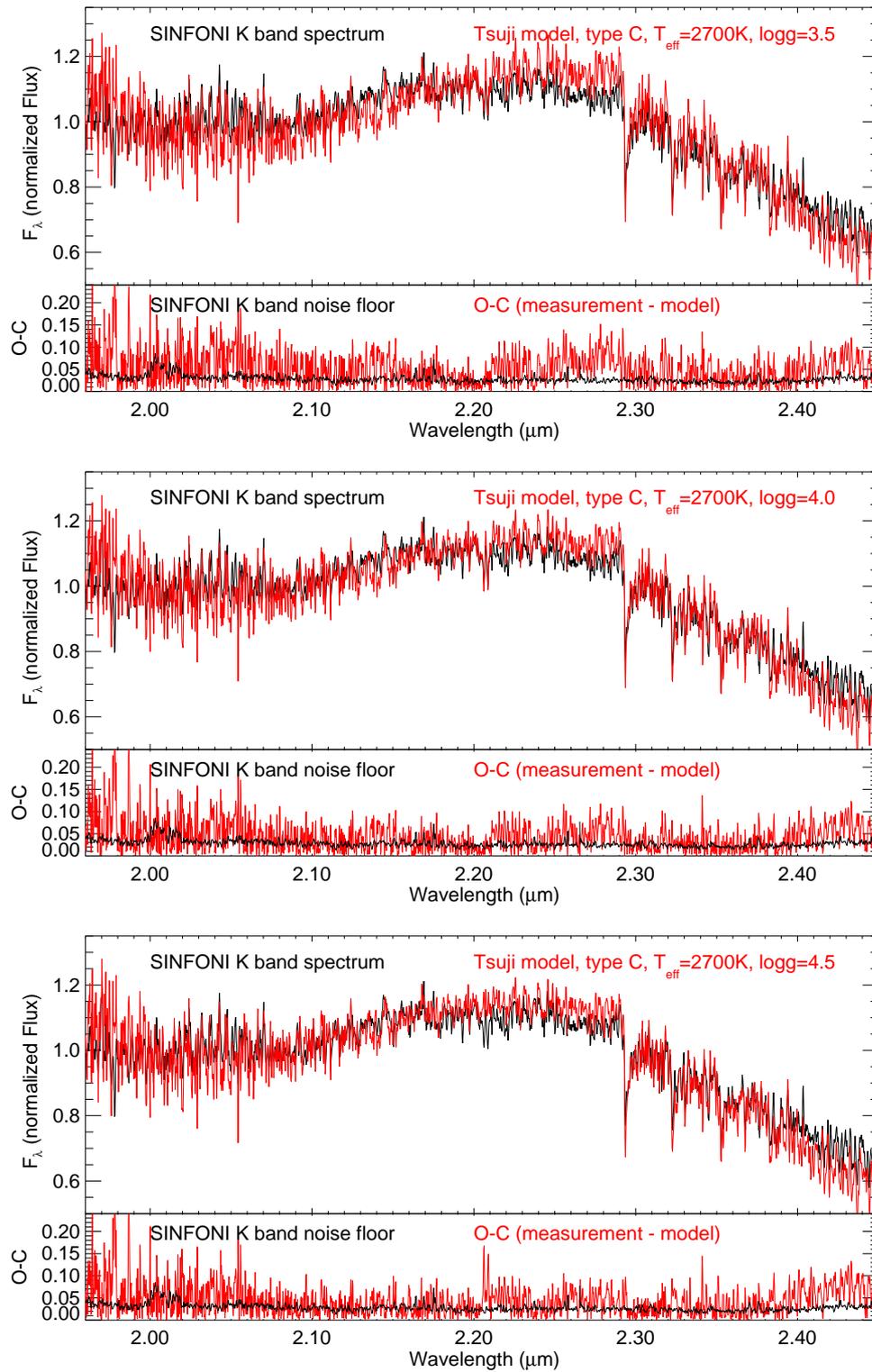
Figure 17: UCM fits to the SINFONI K band spectrum of the GQ Lup companion.

Figure 18: UCM fits to the SINFONI K band spectrum of the GQ Lup companion.

List of Figures

Acknowledgements – Danksagungen